2019-04-29

Describing Seasonal Marine Carbon System Processes in Cambridge Bay Nunavut using an Innovative Sensor Platform

Duke, Patrick James

UNIVERSITY OF CALGARY

Describing Seasonal Marine Carbon System Processes in Cambridge Bay Nunavut using an Innovative Sensor Platform

by

Patrick James Duke

A THESIS

SUBMITTED TO THE FACULTY OF GRADUATE STUDIES

IN PARTIAL FULFILMENT OF THE REQUIREMENTS FOR THE

DEGREE OF MASTERS OF SCIENCE

GRADUATE PROGRAM IN GEOGRAPHY

CALGARY, ALBERTA

APRIL, 2019

Abstract

The marine carbonate system is a critical component of global biogeochemical cycles. It determines a given marine region's status as a source or sink for atmospheric CO_2, and long term changes (i.e. ocean acidification) that can affect key ecosystem functions. Carbonate system processes are highly variable through space and time, which makes it difficult to fully characterize a region without either intensive sampling, or long-term deployment of high-precision instruments. Both of these are difficult in the Arctic, where challenging logistics limit sampling opportunities, and instruments must endure extreme conditions. In this work, we present the first high-resolution marine carbon system dataset covering a full Arctic cycle of sea ice growth and melt. We deployed a Satlantic SeaFET Ocean pH Sensor and a Pro-Oceanus CO2-Pro CV sensor for consecutive nearly yearlong deployments onboard the Cambridge Bay Ocean Networks Canada Undersea Community Observatory from September 2015 – June 2018. The sensors measurements were compared to discrete sample references, and determined to require multipoint *in situ* calibration, but were representative of the greater sea surface mixed layer inside the bay through most of the year. Using a diagnostic box model approach, seasonal influencing processes on the marine carbon system at the platform were quantitatively determined. Air-sea gas exchange and biologic respiration/ remineralization were dominant in the fall, whereas following sea ice freeze up brine rejection drove pCO_2 to seasonal supersaturation with respect to the atmosphere, and the aragonite saturation state to become undersaturated. Shortly after the sun rose under the ice in the late winter, the ecosystem at the

platform became net autotrophic at very low light levels, driving pCO_2 to undersaturation. As sea ice melted, an under-ice phytoplankton bloom drew down a significant amount of carbon before the open water season, returning the aragonite saturation state to supersaturation at the platform. These observations show a dynamic system, where biological processes occur at times and rates previously unknown to the literature. These processes will need to be included in future biogeochemical modeling efforts, if we are to properly resolve the current, and future, role of the Arctic Ocean basin in global biogeochemical cycles.

Keywords: Arctic, Oceanography, Biogeochemistry, Ocean Acidification, Gas Exchange

Preface

Figure 1 Schematic illustration of the seawater carbonate system. Adapted from Figure 1.1.3 in Zeebe & Wolf-Gladrow (2001) © 2001 Elsevier Science, with permission from Elsevier.

Figure 2 Summary schematic of Yager et al. (1995) proposed model of annual marine $pCO_{2(sw)}$ cycle in the Arctic. Adapted from Figure 9 in Else et al. (2012) © 2012 American Geophysical Union (AGU). AGU operates under an open access policy, which allows use of materials for republication in academic work as long as credit is attributed to the author. The source has been referenced within the figure caption and is listed in the References section.

Figure 3 Weekly average sea ice concentration, $pCO_{2(air)}$, $pCO_{2(sw)}$, and sea-surface temperature, measurements in Amundsen Gulf from October 2007 to August 2008. Adapted from Figure 3 in Else et al. (2012) © 2012 American Geophysical Union (AGU). AGU operates under an open access policy, which allows use of materials for republication in academic work as long as credit is attributed to the author. The source has been referenced within the figure caption and is listed in the References section.

Figure 11 Schematic representation of a diagnostic box model used to compute changes in DIC. Adapted from Figure 2 in Gruber et al. (1998) © 1998 Elsevier Science, with permission from Elsevier.

Acknowledgements

So much love for my family for everything. Huge thanks to Dr. Brent Else for the mentorship and guidance he provided through my time as an undergrad and as my graduate supervisor. Special thanks to my lab mates and buddies Vishnu Nandan, Mohamed Ahmed, Sam Jones, Brian Butterworth, Kristina Miller, and Stephen Gonski for their support and assistance all the way through my program. Thanks to Shawn Marriot for his tireless work in the field and for making me feel at home during my time up north along with my friends Patty Kamoayok, and Mitchell Kamoayok. Thanks to the Hamlet and residence of Cambridge Bay for allowing me to conduct research on the traditional territory of the Inuit people. Thanks to the Hunters and Trappers Organization and all the guides that helped in the field, particularly Colin Amegainik for becoming a friend after our work together. This work would not have been possible without the guidance from collaborators Lisa Miller and Akash Sastri. Funding for the project comes from the Marine Environmental Observation Prediction and Response Network, Ocean Networks Canada, Polar Knowledge Canada, and Helmuth Thomas at Dalhousie University. Thanks to Polar Knowledge Canada staff at the Canadian High Arctic Research Station for all the field support. Finally, thanks to the Department of Geography at the University of Calgary for hosting me for the last seven years.

Table of Contents

List of Tables

List of Figures

Definitions and Abbreviations

CO_2	Carbon Dioxide
pCO_2	Partial pressure of carbon dioxide
Ω	Calcium carbonate saturation state
DIC	Dissolved Inorganic Carbon
TA	Total Alkalinity
CTD	Conductivity-Temperature-Depth
ISFET	Ion Sensitive Field Effect Transistor
FET|EXT	External Reference Electrode
FET|INT	Internal Reference Electrode
CB	Marine Region of Cambridge Bay Nunavut
ONC	Ocean Networks Canada
O_2	Oxygen
PAR	Photosythetically Active Radiation
RMSE	Root Mean Square Error
C_0	Model II Least Squares Fit Intercept
C_1	Model II Least Squares Fit Slope

1.0. Introduction

Recently, within the context of geologic time, humans have become the primary driver of planetary scale climate change (Coombs, 2014). The consequence of anthropogenic changes to Earth's systems has led to the current state of rising carbon dioxide gas concentrations in the atmosphere, primarily due to fossil fuel burning, leading to global warming (IPCC, 2013; King et al., 2015). Continued global temperature increases will have major implications for both ecological and human systems (IPCC, 2014). Climate change is a global issue of immediate importance. Rapid and far-reaching transitions in all sectors (e.g. energy, land, infrastructure, and industry) are required on an unprecedented scale to limit global warming to 1.5°C (Hoegh-Guldberg et al., 2018; Rogelj et al., 2018). One particular area of scientific interest lies in understanding the oceanic response to climate change. Investigating marine carbon sequestration processes can enhance our modeling capabilities in projecting potential oceanic climate change mitigation.

Arrhenius (1897) concluded that greenhouse gases (such as CO_2), trap radiative energy in Earth's atmosphere. This trapped energy leads to increased surface air temperatures. Naturally, CO_2 concentration in the atmosphere is governed by the exchange of CO_2 with the oceanic and terrestrial reservoirs. The global oceans and the terrestrial biosphere (including biota and soil) contain significantly more CO_2 compared to the atmosphere, approximately 50 and three times as much respectively (Sundquist, 1985). The ongoing accumulation of anthropogenic greenhouse gases in the atmosphere will have reaching implications for the two adjunct, dynamic reservoirs of carbon on Earth. It is estimated that about 25-50% of anthropogenic CO_2

emissions to the atmosphere are absorbed annually by the ocean (Sabine, 2004; Le Quéré et al., 2010). This sequestration potential is shifting as the impacts of climate change trickle through the Earth's systems.

The Arctic is particularly sensitive to climate change. Some observed impacts in the Arctic attributed to CO_2 emissions include: significant shrinking of sea ice cover in summer (Perovich et al., 2007), delayed sea ice freeze-up (Maslanik et al., 2007), a net thinning of the sea ice pack and a decrease in perennial ice cover (Laxon et al., 2013), sea surface water freshening and warming (Yamamoto-Kawai et al. (2009); Steele et al., (2008)), thawing permafrost (Vonk & Gustafsson, 2013), increased terrestrial runoff (Nummelin et al., 2016), changes in the magnitude and timing of primary production (Kevin R. Arrigo & van Dijken, 2015), and changing ocean mixed layer dynamics (Toole et al., 2010). The aforementioned changes and associated feedbacks could have profound and long lasting impacts on carbon cycling in the Arctic Ocean and its shelf seas. The global implications associated with the changes in the Arctic marine environment are related to how the Arctic Ocean and its shelf seas typically act as net sinks for atmospheric CO_2 (Bates & Mathis, 2009). With datasets that extend through the polar night, we can gain insight into how changing sea ice conditions – which provide a variable cover over the ocean — might enhance or inhibit the ability of seasonally ice-covered seas to capture CO_2 (Yager et al., 1995).

Under-sampling is the largest problem in our ability to predict and understand the implications of climate change in the Arctic. Much uncertainty still remains with regard to the Arctic annual marine carbon cycle. The overall scarcity of measurements temporally, presents a significant

challenge for accurately constraining net carbon exchange behavior in the Arctic Ocean and its shelf seas. The dominant constraint on datasets in the Arctic can be attributed to our use of large research vessels. These vessels are restricted to near ice-free conditions, biasing sampling programs towards the summer months.

One means tin addressing the temporal coverage issue is the establishment of long duration time-series spearheaded by new autonomous sensor technology. Longer duration studies could expand on our understanding of the seasonal and inter-annual variability of the carbon system in the Arctic marine environment. This is particularly important in exploring ocean–sea ice–atmosphere gas exchange processes which are not clear in the literature (Semiletov et al., 2007), and monitoring decreasing ocean pH spatially and seasonally (Qi et al., 2017). With datasets that extend through the less sampled seasons of fall and winter, we can progress marine carbon system understanding, supporting both flexible and generalized representations in models of the Arctic climate system. Coupled system processes in the Arctic marine carbon system evolve over the course of the year in response to seasonal cycles and episodic events. In order to fully understand the current seasonal state of any system, prior states need to be understood and how they evolve on seasonal scales. With this sentiment in mind, it becomes essential that new observing activities set out to be conducted for at least a full annual cycle.

1.1. Carbonate Chemistry

In order to understand the biogeochemical processes affecting inorganic carbon in the ocean, a basic comprehension of seawater carbonate chemistry is required. Carbon dioxide

does not simply dissolve in seawater like other gases such as oxygen and nitrogen; instead it reacts with water and is partitioned among four different chemical species. Equations 1A – 3A below describe the partitioning reactions (where brackets denote total concentrations) and their associated equilibrium constants (the solubility constant is denoted by K_0, and dissociation constants are denoted by K_1, K_2).

Eq. 1A $$CO_{2(gas)} + H_2O \rightleftharpoons \mathrm{H_2CO_3}^*, K_0 = \frac{[\mathrm{H_2CO_3}^*]}{[pCO_{2(air)}]}$$

Eq. 2A $$\mathrm{H_2CO_3}^* \rightleftharpoons H^+ + \mathrm{HCO_3}^-, K_1 = \frac{[H^+][\mathrm{HCO_3}^-]}{[\mathrm{H_2CO_3}^*]}$$

Eq. 3A $$\mathrm{HCO_3}^- \rightleftharpoons \mathrm{H}^+ + {CO_3}^{2-}, K_2 = \frac{[H^+][{CO_3}^{2-}]}{[\mathrm{HCO_3}^-]}$$

When gaseous CO_2 ($CO_{2(gas)}$) first dissolves in seawater it gets hydrated to the form aqueous CO_2 ($CO_{2(aq)}$), which reacts with water to form carbonic acid (H_2CO_3) (Eq. 1A). These two species ($CO_{2(aq)}$ and H_2CO_3) are chemically indistinguishable so they are often combined and denoted as a hypothetical species $H_2CO_3^*$. $pCO_{2(air)}$ in Eq. 1A refers to the partial pressure of CO_2 in the atmosphere. $H_2CO_3^*$ dissociates in two steps to form bicarbonate (HCO_3^-) and carbonate ions (CO_3^{2-}) (Eq. 2A, 3A).

Typically studies focus on the four directly observable inorganic carbon system parameters: partial pressure of CO_2 in seawater ($pCO_{2(sw)}$), pH, dissolved inorganic carbon (DIC), and total alkalinity (TA) (Dickson et al., 2007). The observation of any two parameters can be used to solve for the remaining two. The measurement of DIC, TA, temperature and salinity will suffice to completely characterize the marine carbonate system (Zeebe & Wolf-Gladrow, 2001).

However, it is also possible to use pCO_2, and pH measurements to derive DIC and TA. The computation of unobserved variables takes place through the use of CO2SYS, a computer program developed to describe the marine carbonate system (Lewis et al., 1998; Pierrot et al., 2006; Van Heuven et al., 2011).

Of the four directly observable carbon system parameters, $pCO_{2(sw)}$ is most commonly utilized in scientific studies concerned with oceanic uptake of atmospheric carbon dioxide or outgassing to the atmosphere. The measurement of pH is often tied to scientific inquiries into ocean acidification and assessing the impact of carbon dioxide concentrations on calcium carbonate shell forming organisms. DIC and TA are widely measured parameters as both are preserved when bottled and can be analyzed at a later date (Dickson et al., 2007). DIC and TA are important parameters for interpreting biogeochemical processes influencing the marine carbonate system, and are typically the centerpiece of budgeting studies.

1.1.1. Air-Sea Gas Exchange

Air-sea gas exchange is denoted through the use of Eq. 4A, the bulk parametrization including ΔpCO_2 (Eq. 5A), solubility ($\propto$) and gas transfer velocity (k). Air-sea gas exchange along a gradient is always working towards achieving equilibrium. A positive ΔpCO_2, means that the seawater is supersaturated with respect to the atmosphere and acts as a source for CO_2. A negative ΔpCO_2, relates to undersaturated seawater capable of acting as a sink for CO_2.

Eq. 4A $$F_{CO_2} = \propto k \Delta pCO_2$$

Eq. 5A $$\Delta pCO_2 = pCO_{2(sw)} - pCO_{2(air)}$$

At regional, seasonal, and inter-annual scales, ΔpCO_2 is largely driven by variability in $pCO_{2(sw)}$, which is much higher than variability in $pCO_{2(air)}$. $pCO_{2(sw)}$ is determined by Eq. 6A.

Eq. 6A $$pCO_{2(sw)} = \frac{K_2}{K_0 \cdot K_1} \frac{[\mathrm{HCO_3}^-]^2}{[{CO_3}^{2-}]}$$

The first control on $pCO_{2(sw)}$ consists of the ratio of equilibrium constants, K_2 / [(K_0)(K_1)] (Eq. 6A). All equilibrium constants are dependent on temperature, salinity and pressure. Sea surface temperature exerts a thermodynamic control on the seawater carbonate system and thus changes $pCO_{2(sw)}$ by about 4% per °C (Takahashi et al., 1993). This means that colder water is capable of carrying more dissolved CO_2 than warmer water. An increase (decrease) in temperature will decrease (increase) the solubility of CO_2, increasing (decreasing) $pCO_{2(sw)}$ (Weiss, 1974). Salinity also affects the carbonate chemistry and hence $pCO_{2(sw)}$. If DIC and TA are held constant, an increase (decrease) in salinity would cause a decrease (increase) in solubility of CO_2, increasing (decreasing) $pCO_{2(sw)}$ (Weiss, 1974). The factors of salinity and temperature do not affect $pCO_{2(sw)}$ to the same degree. $pCO_{2(sw)}$ has a much greater sensitivity to temperature than to salinity variations. Approximately two-thirds of the temperature sensitivity of $pCO_{2(sw)}$ is a result of the strong temperature dependence of the solubility constant K_0, while the contribution of the ratio of the dissociation constants K_2/K_1 explains the remaining third (Sarmiento & Gruber, 2006). Within the global open ocean, surface seawater temperature varies by about 30°C whereas salinity varies by about 7 PSU. With a larger variability globally and seasonally, temperature is regarded as the greater physical control on $pCO_{2(sw)}$ (Sarmiento & Gruber, 2006).

The second control on $pCO_{2(sw)}$ is the concentration of bicarbonate and carbonate ions. These marine carbon species are discussed in the following section on dissolved inorganic carbon and total alkalinity.

1.1.2. pH and Ocean Acidification

pH is related to the concentration of protons (H^+) in a solution (Eq. 7A). The logarithmic term means a ten-fold increase in the concentration of hydrogen ions causes a change of one pH unit. In seawater, describing pH is not as simple as the activity of single hydrogen ions as they are not the only contributor to acidity. Hydrogen sulphate (HSO^{4-}) and hydrogen fluoride (HF) also contribute to seawater acidity (Dickson, 1984; Hansson, 1973). This requires additional pH scales being used to determine the pH of seawater (Zeebe & Wolf-Gladrow, 2001).

Eq. 7A $$pH = -log_{10}[\mathrm{H}^+]$$

Eq. 8A $$pH_T = -log_{10}([H^+]_F + [HSO^{4-}]) = -log_{10}[H^+]_T$$

The much larger concentrations of HSO^{4-} compared to HF in seawater combined with the poor constraints on HSO^{4-} dissociation constants means that the total scale (Eq. 8A), is more widely used (Hansson, 1973). H^+_F is representative of "free" hydrogen ions including hydrated molecules also present in seawater. pH in the total scale is universally used as it is one of the simpler pH scales as reflected in similarities to Eq. 7A. The importance of pH as a universal environmental indicator is without doubt, as the parameter provides information on the equilibrium processes within the marine CO_2 system. pH is also a key monitoring parameter as

atmospheric CO_2 concentrations increase, and more CO_2 diffuses into the oceans altering seawater chemistry, lowering pH in a process known as ocean acidification.

Eq. 9A $$\Omega = \frac{[\mathrm{Ca}^{2+}][\mathrm{CO}_3^{2-}]}{K_{sp}^{'}}$$

The saturation states of aragonite (ΩAr) and calcite (ΩCa) are commonly used to interpret the status of ocean acidification. Aragonite and calcite are relatively soluble forms of calcium carbonate found in marine plankton and invertebrates. Saturation state refers to the potential a mineral to form (Ω > 1) or dissolve (Ω < 1) (Eq. 9A). When Ω > 1, seawater is supersaturated with respect to the mineral $CaCO_3$; conversely, when Ω < 1, seawater is undersaturated. In the global ocean the saturation horizon separates waters at depth that are supersaturated in $CaCO_3$ from those that are undersaturated. Above the saturation horizon $CaCO_3$ does not readily dissolve therefore most calcifying organisms live in waters closer to the surface.

1.1.3. Dissolved Inorganic Carbon and Total Alkalinity

DIC is simply a measure of all the carbonate species concentrations present in seawater (Eq. 10A). TA is a measurement of excess bases (proton acceptors) over acids (proton donors) (Eq. 11A).

Eq. 10A $$DIC = [\mathrm{H_2CO_3}^{*}] + [\mathrm{HCO_3}^{-}] + [{CO_3}^{2-}]$$

Eq. 11A $$TA = [\mathrm{HCO_2}^{-}] + 2\left[{CO_3}^{2-}\right] + [B(OH)_4{}^{-}] + [OH^{-}] + \left[{HPO_4}^{2-}\right] + 2\left[{PO_4}^{3-}\right] + [SiO(OH)_3{}^{-}] + [HS^{-}] + [NH_3] - [H^{+}] - [HSO_4{}^{-}] - [HF] - [H_3PO_4] - minor\ bases$$

TA is affected by biological activity, such as photosynthesis, remineralization, precipitation/dissolution of $CaCO_3$, and mixing (Figure 1). DIC is affected by all the aforementioned processes as well as air-sea gas exchange as it includes the concentration of $H_2CO_3^*$ and TA does not (Eq. 1A).

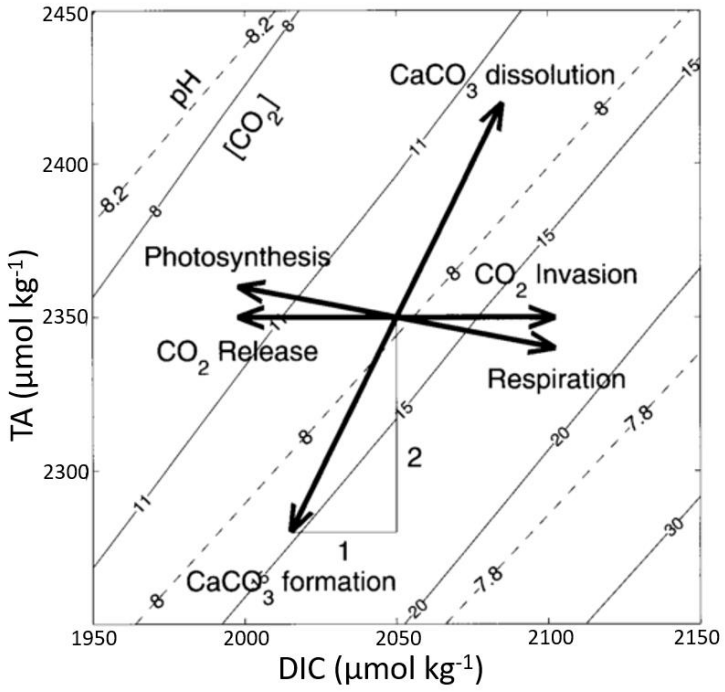

Figure 1 Effect of various processes on DIC and TA (arrows) adapted from Zeebe & Wolf-Gladrow (2001) with permission from Elsevier. Solid and dashed lines indicate levels of constant dissolved CO_2 (in µmol kg^{-1}) and pH, respectively, as a function of DIC and TA.

DIC and TA include both bicarbonate and carbonate ion concentrations which are a primary control on seawater pCO_2 (Eq. 6A; Eq. 10-11A,). If DIC is increased (decreased), $pCO_{2(sw)}$ increases (decreases). On the other hand, if TA is increased (decreases), $pCO_{2(sw)}$ decreases (increases).

Dependent on the marine environment, the dominant controlling factor of surface water DIC/ TA is biological activity, including photosynthetic uptake of CO_2 to form organic matter, and the reverse processes of respiration/ remineralization (Eq. 12A). Photosynthesis decreases DIC and the concentration of free protons (H^+), therefore increasing TA (Figure 1). Photosynthesis results in a net transfer of inorganic carbon from the surface into the deep ocean, often referred to as the "biological pump" (Volk & Hoffert, 1985). The process of photosynthesis is limited by the availability of light and nutrients. Large seasonal phytoplankton blooms often deplete nutrients within the surface layer if there are no other external sources to replenish the local supply. A major source of nutrients comes from either the deep ocean or riverine input, and therefore productivity tends to be higher in regions of upwelling and river discharge.

Eq. 12A $$106CO_2 + 16NO_3^- + HPO_4^{2-} + 78H_2O + 18H^+ \rightleftharpoons \mathrm{C_{106}H_{175}O_{42}N_{16}P} + 150O_2$$

Remineralization is the process of heterotrophic organisms consuming organic material and returning it to an inorganic state. This process adds DIC, and removes TA from seawater. This process is not limited by light and can occur within the surface layer and as organic matter sinks into the deep ocean. In the deep ocean the waters tend to be enriched in nutrients and DIC, due to high respiration rates. The upwelling of these enriched waters drive regional phytoplankton booms.

Eq. 13A $$Ca^{2+} + 2HCO_3^- \rightleftharpoons \mathrm{CaCO_3} + H_2O + CO_{2(aq)}$$

The biogenic formation and dissolution of calcium carbonates also plays an important role in marine carbon cycling. Some marine organism such as coccolithophorids (phytoplankton), and

foraminifera, and pteropods (zooplankton) form calcite or aragonite shells. The formation of these shells consumes CO_3^{2-} (Eq. 13A), lowering DIC and decreasing TA by twice as much due to the charge of carbonate ions (Figure 1). The net effect of forming (dissolving) calcium carbonate is to slightly increase (decrease) $pCO_{2(sw)}$. This biogenic process is also referred to as the "carbonate pump", due to the downward transport of DIC/ TA from the surface (where $CaCO_3$ shells are formed) into the deep ocean (where $CaCO_3$ shells dissolve).

Upwelling and vertical mixing can also have a significant impact on DIC/ TA by modifying the surface water properties and carbonate chemistry (Chierici et al., 2011). The same goes for horizontal advection in regions where strong lateral DIC/ TA gradients exist in conjunction with surface currents.

1.2. Arctic Marine Carbon System

The Arctic Ocean and its shelf seas exhibit a unique marine biogeochemical setting unlike any other on the planet. The Arctic basin is geographically unique in that it is continentally enclosed compared to other basins, limiting exchange with the Pacific and Atlantic Oceans through the Bering and Fram Strait respectively. The Arctic Ocean is dominated by the presence of multi-year sea ice at a significantly larger extent compared to the Southern Ocean due to relatively limited circulation. There is also a disproportionate amount of continental terrestrial discharge into the Arctic basin compared to other global oceans. The Arctic basin receives ~11% of global river discharge, yet makes up only 2.8% of global ocean basin area, containing only 1% of the global ocean seawater volume (Lewis & Jones, 2000).

The prominent factors influencing marine carbon cycling at high northern latitudes include: sea ice, fresh water input, solubility changes from temperature and salinity, the biological pump, the carbonate pump, and air-sea gas exchange (AMAP, 2013). Unlike other global oceans with extensive carbon system observations, the Arctic Ocean and associated Arctic shelf seas lack necessary monitoring to give conclusive carbon budgets, or definitive inter-annual, annual, seasonal or daily cycles at the same spatial scale documented elsewhere. The overall scarcity of measurements temporally presents a significant challenge for accurately constraining net carbon exchange behavior in the Arctic basin. The largest gap in published observations occurs through the polar night, as much of the Arctic supports seasonal sea ice cover inaccessible to cruise expeditions. Past summer-heavy sampling plans prove insufficient in describing the total carbon system, which is needed in order to understand the processes that govern the exchange of CO_2 between the ocean and the atmosphere, and key ecosystem processes (i.e. ocean acidification). In order to effectively understand these processes in a changing climate, the complete annual marine carbon cycle in the Arctic requires further investigation. Building a deeper understanding of how the Arctic marine carbonate system is currently influenced by biogeochemical processes can better inform modelling studies to help us further understand how the Arctic Ocean and its shelf seas will respond to climate change impacts attributed to anthropogenic CO_2 emissions. Currently, we are at a period in the literature where we are building foundational knowledge of annual Arctic marine under-ice carbon cycling. Proposed projects such as the Multidisciplinary drifting Observatory for the Study of Arctic Climate (MOSAiC, September 2019), are looking to make major strides in achieving a deeper more

holistic understanding of the annual Arctic marine carbon cycle to support representation in models.

1.2.1. Seasonal Rectification Hypothesis

In the absence of high resolution *in situ* observations, conceptual models have been proposed based on limited datasets to describe annual Arctic marine carbon cycling. An important conceptual model for predicting air-sea exchange of CO_2 in Arctic seas was presented by Yager et al. (1995) (Figure 2). The Yager model looked at annual carbon cycling in the Northeast Water Polynya in northern Baffin Sea. The conceptual model described these polynya regions in the Arctic as strong annual sinks for atmospheric CO_2, because the seasonal cycle of $pCO_{2(sw)}$ is in-phase with the seasonal cycle of sea ice formation/ melt.

The model starts in the fall where $pCO_{2(sw)}$ is undersaturated with respect to the atmosphere but air-sea gas flux is limited by calm winds. Yager predicted replenishment of DIC could be achieved by a few weeks of strong winds preceding sea ice formation, increasing $pCO_{2(sw)}$ going into the winter. From the end of the fall through the polar night, biological respiration exceeds carbon fixation increasing DIC, contributing to the gradual rise in $pCO_{2(sw)}$. During this time the ice cover provides a barrier for gas exchange with the atmosphere leading to supersaturation. Once light penetration permits, primary production in ice algae provides a mechanism for the initial reduction of accumulated respiratory DIC in near-surface layers, reducing $pCO_{2(sw)}$. Once the ice melts in early summer, the meltwater creates a thin highly stratified layer in the near surface. This stratified layer acts to isolate the water column below from air-sea gas exchange. Through the summer months phytoplankton blooms transform significant amounts of DIC to

organic carbon reducing $pCO_{2(sw)}$, allowing the continued undersaturation and subsequent drawdown of CO_2.

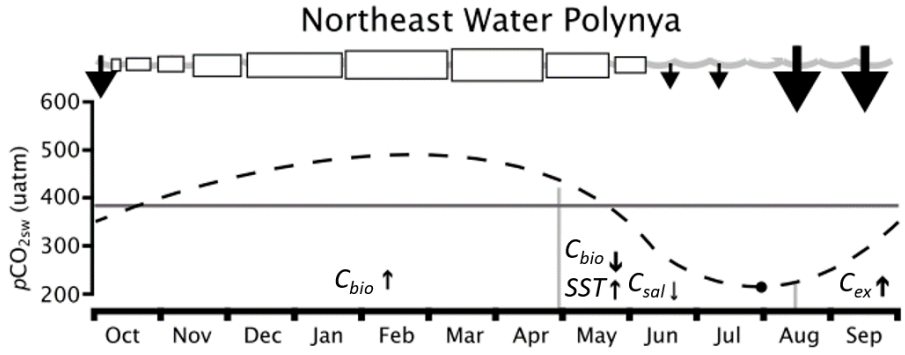

Figure 2 Summary schematic of Yager et al. (1995) proposed model of annual marine $pCO_{2(sw)}$ cycle in the Arctic adapted from Else et al. (2012). The solid line represents the atmospheric pCO_2 reference value, where the dashed line is proposed $pCO_{2(sw)}$. The black boxes on top denote relative sea ice concentration. Black arrows on top give the direction and relative magnitude of air-sea gas exchange. The annotations below indicate processes dominant in controlling $pCO_{2(sw)}$ throughout the year abbreviated as: C_{bio}, biology; SST, sea-surface temperature; C_{sal}, salinity; C_{ex}, air-sea gas exchange. These processes are accompanied by arrows indicating increasing (up) or decreasing (down) $pCO_{2(sw)}$, with the relative importance being the size of the arrow.

In the proposed model from Yager et al. (1995) there is no duration throughout the polynya's annual cycle when the Arctic surface water acts as a source of CO_2 to the atmosphere, although there is a period of pCO_2 supersaturation. Yager dubbed this theoretical cancellation of one half of the typical air-sea exchange cycle (Brix, Gruber, & Keeling, 2004) in the Arctic as the "*seasonal rectification hypothesis*." A key component of the hypothesis is the preconditioning of surface water pCO_2 to undersaturation with respect to the atmosphere while there is still ice cover in the spring. Preconditioning would therefore have the potential to impact the magnitude and even direction of air-sea gas exchange following ice breakup into the summer open water season. The theory describes the annual marine carbon cycle in the Arctic's seasonally ice free regions as net sinks for atmospheric CO_2.

1.2.2. Annual Arctic Marine pCO_2 Cycle

The shortcomings of the Yager et al. (1995) proposed "*seasonal rectification hypothesis*" are founded in the lack of continuous annual data. The dataset used to put forward such a hypothesis was collected aboard the United States Coast Guard Cutter Polar Sea cruise from July-August 1992. The intention of such data collection was not to give complete temporal or spatial coverage for the Northeast Water Polynya (Yager et al., 1995). The most recent study to publish a near complete annual dataset of Arctic $pCO_{2(sw)}$ was conducted onboard the Canadian Coast Guard Service Amundsen from October 2007 to August 2008. The expedition took place in the southeastern Beaufort Sea, overwintering in a mobile ice pack in the Amundsen Gulf (Else et al., 2012; Shadwick et al., 2011; Shadwick et al., 2013).

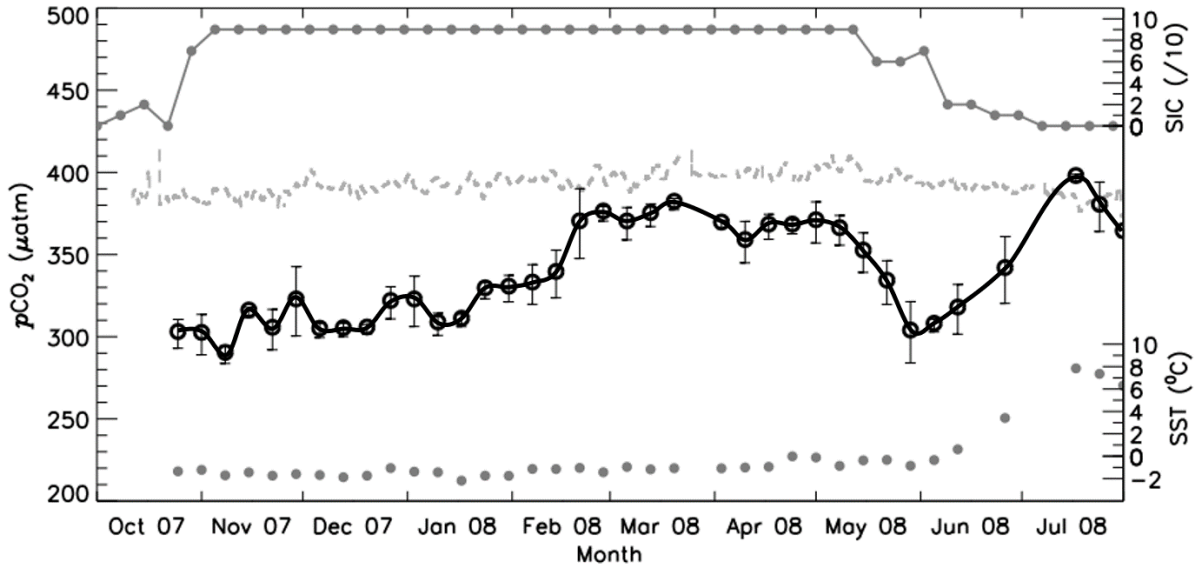

Figure 3 Weekly average $pCO_{2(sw)}$ measurements in Amundsen Gulf from October 2007 to August 2008 (open circles); error bars are 1 standard deviation. Also shown is sea-surface temperature from the equilibration system (solid circles), atmospheric $pCO_{2(air)}$ from the meteorological tower (gray dashed line), and sea ice concentration from weekly Canadian Ice Service charts (solid line). Figure adapted from Else et al. (2012).

Else et al. (2012), and Shadwick et al. (2011) published interpretations of this dataset which included seasonal $pCO_{2(sw)}$ observations in Amundsen Gulf, Banks Island Shelf, and the Mackenzie Shelf. Based on the Amundsen Gulf study in Figure 3, the seasonal marine carbon cycle was described in detail. Starting in the fall (October/ November) the surface mixed layer in Amundsen Gulf was consistently undersaturated. Sea ice began forming before air-sea exchange had reached an equilibrium in sea surface pCO_2 (Else et al., 2012).

Through the winter months from October to early March, they observed a gradual increase in $pCO_{2(sw)}$ to a maximum of ~380 µatm (Figure 3). This maximum was still undersaturated compared to boundary layer atmospheric levels (~395 µatm) despite the partial replenishment of $pCO_{2(sw)}$ by respiration of organic matter increasing DIC (Shadwick et al., 2011). The winter increase was concurrent with an increase in sea surface salinity attributed primarily to brine rejection by sea ice formation. This brine rejection is also thought to have played an important role in the overall $pCO_{2(sw)}$ increase. The sea ice carbon phenomenon has been explained in other works as the "sea ice pump" exporting CO_2 to depth (Loose et al., 2011; Rysgaard et al., 2011). When sea ice forms and grows throughout the winter, impurities including salts and carbonates in the seawater, are rejected from the ice lattice structure and concentrate in brines. When brine is rejected below sea ice, the brine facilitates mixing in the underlying water-column. When high DIC brines are rejected below the ice they increase concentrations in the surface waters (Chierici et al., 2011). Rysgaard et al. (2011) reported an increase in the TA:DIC ratio within sea ice as it grew though the winter months with $CaCO_3$ crystal formation in brine. The observation suggests that sea ice more efficiently rejects DIC through brine as

compared to TA, which would contribute to an increase in $pCO_{2(sw)}$ as the TA:DIC ratio in the underlying water column would decrease.

The cover of sea ice through the winter does not act as an absolute barrier to gas exchange, as the ice is porous. Brine channels allow for the exchange of salt and gases between the ice and the atmosphere, and ice with the underlying seawater (Papakyriakou & Miller, 2011). Brine channels in very cold conditions can have very high pCO_2 values (Loose et al., 2011). Gas fluxes through the winter months with the atmosphere are distinctly between the atmosphere and the ice, and not the underlying water. The sea ice carbon pool is therefore unique from the underlying water carbon pool in early and mid-winter with solid, cold ice present. During full ice cover, gas fluxes are near zero, but into spring as sea ice warms, fluxes are downward from the atmosphere into the ice (Butterworth & Else, 2018). At sites with either incomplete or broken ice cover through the winter months (i.e. Banks Island Shelf, a flaw-lead polynya), CO_2 fluxes can be much higher than in open, ice-free waters (Else et al., 2012). High CO_2 fluxes in the presence of a broken and mobile ice cover increases the net CO_2 sink through boundary-layer turbulence and frazil ice formation (Anderson et al., 2004; McPhee & Stanton, 1996).

Beginning in early spring, $pCO_{2(sw)}$ began a sustained decrease through the end of May (Figure 3) almost entirely driven by biological production (Else et al., 2012). The initial draw down was attributed to ice algae in Shadwick et al. (2011) and Else et al. (2012). Both studies were however working with a dataset at only monthly resolution. The region of Amundsen Gulf is also heavily fractured and the impact of a rapid-onset under-ice phytoplankton bloom could have been misattributed to an ice algae bloom (Else et al., 2019).

Although sea ice reduces light transmission to the underlying ecosystem, under-ice biological communities appear to be well-adapted (Mundy et al., 2009). Primary production starts with extensive springtime blooms of ice algal communities acting as important contributors to Arctic primary production and possible seeding populations (Arrigo et al., 2010). Ice algae are thought to be the first autotrophic organisms that can impact DIC and in turn $pCO_{2(sw)}$, taking advantage of returning spring sunlight following winter darkness (Leu et al., 2015). Primary productivity from ice algae is significant during spring and early summer as it is up to two orders of magnitude greater than water column productivity (Gradinger, 2009). However, it has been shown that ice algae production does not appear to affect mixed layer DIC concentrations to an extent that would significantly impact air-sea exchange of CO_2 in the ice-free season (Else et al., 2019). Past studies have concluded that the total biomass of ice algae is not enough to reduce DIC significantly, although this could vary regionally.

Following ice algal blooms are under-ice phytoplankton booms, which typically occur only after sea ice has reached an advanced state of melt significantly increasing light transmission to underlying water (Arrigo et al., 2012; Fortier et al., 2002; Mundy et al., 2009, 2014). It has also been shown that an under-ice phytoplankton bloom can have an immediate and significant impact on DIC in the water column (Else et al., 2019). The under-ice phytoplankton is apparent in Figure 3 as the steep drawdown of pCO_2 occurring through May as sea ice starts to melt and breakup.

To date within the literature, the timing of DIC drawdown in the Arctic, and the biological community first responsible for it, is subject to considerable uncertainty. Although given the

uncertainty, the commonality between multiple reports is the undersaturation of $pCO_{2(sw)}$ in Arctic surface waters at the winter-spring transition. Measurements made under sea-ice prior to sea-ice melt and consequential phytoplankton blooms are dominantly undersaturated with respect to the atmosphere (Bates et al., 2006; Else et al., 2012; Miller, et al., 2011; Papakyriakou et al., 2011). These studies appear to validate a key point of the Yager et al. (1995) "*seasonal rectification hypothesis.*" Capturing an annual dataset with improved temporal resolution compared to Else et al. (2012), Shadwick et al. (2011), and Yager et al. (1995), able to capture the initiation of the spring drawdown missed in Else et al. (2019) could: effectively evaluate the "*seasonal rectification hypothesis*", draw conclusions on the role of under-ice pCO_2 preconditioning going into the open water season, and identify gaps for further scientific inquiry.

1.3. Arctic Ocean Acidification

As anthropogenic emissions increase atmospheric pCO_2, sea surface pCO_2 trends increase roughly in parallel as the ocean works to achieve air-sea equilibrium (IPCC, 2013). The main implication of increasing surface ocean pCO_2 is ocean acidification, characterized by a decrease in seawater pH and carbonate saturations states. Currently the Arctic basin is thought be more vulnerable to acidification than any other ocean basin (Steinacher et al., 2008). Acidification is intensified in the Arctic due to environmental conditions including: low sea surface temperatures, large fresh water supply (river runoff and ice melt), inflow of Pacific water with low pH (AMAP, 2018), low TA surface water, and strong seasonal warming preventing summer primary production from increasing pH (Shadwick et al., 2013). The highest

surface ocean pH values are found in the Arctic and are associated with a high oceanic carbon buffer capacity, meaning it is easier to move $CO_{2(aq)}$ through the equilibrium reactions (Eq. 1-3A) to form other species so that more CO_2 gas can enter the ocean (Fassbender et al., 2017).

Seasonal undersaturation of aragonite in surface and shallow subsurface waters in the Arctic Ocean and associated shelf seas caused by sea ice meltwater and river runoff has been reported during spring and early summer (Bates & Mathis, 2009). Trends in the western Arctic suggest that within a few decades it is likely the entire upper water column may become undersaturated with respect to aragonite due to sea ice meltwater and atmospheric uptake (Qi et al., 2017). In the western Arctic the percentage of vertical area in the water column experiencing aragonite undersaturation (0–250 m depth, between 70◦ and 90◦ N) increased by a factor of six from 5% in 1994 to 31% in 2010, with an average rate of increase of 1.5% per year (Qi et al., 2017). It appears that we are heading for what some would suggest could be called an "aragonite tipping point" (AMAP, 2013). Future sea ice melt could potentially enhance the air-sea CO_2 flux in the Arctic by ~ 28% per decade (Bates et al., 2006), pushing through the suggested "tipping point". Projected model simulations depict that when atmospheric CO_2 concentrations increase to 552 ppm, occurring in the year 2054 under the older A2 "business-as-usual" emissions scenario, 50% of the Arctic's marine surface area is projected to become undersaturated with respect to aragonite throughout the year (Steinacher et al., 2009). Extensive ecological impacts from the stress of acidification include local or regional extinction of sensitive calcareous species, opportunity for invasive species, and food insecurity further up the food chain into larger fish and marine mammal species.

There is an evolution in saturation state as waters transit from the North Pacific to the North Atlantic via the Canadian Arctic Archipelago (Yamamoto-Kawai et al., 2013). Pacific waters have low pH and calcium carbonate saturation states due to high concentrations of re-mineralized carbon from global circulation history. As the waters transit the Arctic, calcium carbonate saturation states are further decreased following the addition of fresh water from rivers and sea-ice melt low in Ca^{2+} (AMAP, 2013). As waters outflow over the Canadian Arctic Archipelago into the northern Atlantic they have a much lower saturation state, forming a strong ΩAr, and ΩCa front between Arctic and Atlantic waters above Davis Strait (Yamamoto-Kawai et al., 2013). The central Arctic, Canadian Basin, and Baffin Bay display the greatest rates of acidification and pH decline as a result of melting sea ice (AMAP, 2018). However shallow, nearshore waters that are seasonally covered by continuous landfast sea ice show the largest vulnerability (AMAP, 2013). These environments effectively shut down CO_2 evasion during the winter while still permitting metabolism of terrigenous and marine organic carbon through respiration decreasing pH, ΩAr, and ΩCa (Garneau et al., 2006).

The seasonal cycle of calcium carbonate saturation states in the Amundsen Gulf were explored in Shadwick et al. (2011), Chierici et al. (2011). The changes in ΩAr and ΩCa seasonally are due to biological processes (photosynthesis and respiration), physical mixing, sea ice melt, and salinity and temperature changes. Through the winter ΩAr and ΩCa in the surface waters decreased as respiration, and mixing with subsurface waters increased DIC (Chierici et al., 2011). In the early spring and summer biological production drew down pCO_2, increasing ΩAr and ΩCa. Between spring and summer, below a depth of roughly 50 m, Shadwick et al. 2011

observed an increase in DIC, with both pH and ΩAr decreased. Bates et al. (2009) referred to this process as the seasonal ‘‘*phytoplankton-carbonate saturation state*’’ interaction. In it, Bates et al. (2009) states that biological processes drive divergent trajectories for carbonate chemistry in surface and subsurface waters of Arctic shelves seasonally. Shadwick et al. 2011 reported that between summer and autumn the largest decrease in surface DIC was observed, coincident with the largest decrease in surface salinity. In the fall a minimum in pCO_2 resulting from the dilution of the mixed-layer by sea ice melt and cooling, results in a decreased ΩAr (Bates et al., 2009; Chierici & Fransson, 2009). Shadwick et al. (2011) and Chierici et al. (2011) did not observe prolonged periods of seasonal aragonite undersaturation in the surface, with the only observed undersaturation occurring in the winter attributed to upwelling of Pacific origin waters (Azetsu-Scott et al., 2010).

The large scale and rapid rate of chemical changes being observed now in the Arctic and its shelf seas, offers researchers the opportunity to investigate the physiological processes and action mechanisms of acidification, as well as assess potential ecosystem acclimation and adaptation, and model future impacts at various temporal and spatial scales (Fabry, McClintock, Mathis, & Grebmeier, 2009). A high resolution dataset spanning the complete cycle of sea ice formation and melt could provide insight into seasonal patterns in $CaCO_3$ saturation states, quantitatively differentiate influencing seasonal processes, and offer a means of describing the strong influence of biological activity.

1.4. Carbon System Sensors

Under-sampling is the largest inhibiter in our ability to predict and understand the implications of climate change and acidification in the Arctic Ocean and its shelf seas. One means to address the lack of temporal coverage is through the deployment of new autonomous sensor technology to establishing long duration time-series.

Innovative sensor platforms have made substantial gains in recent years, increasing in both accuracy and precision, while lowering costs. Continuous monitoring platforms contribute to our understanding of long term ocean change, offering increased temporal resolution and the ability to resolve variability compared to occasional field measurements. In order to be easily installed on modern observation platforms, new sensors need to cope with more stringent requirements (e.g. payload capacity, power availability, response time). Currently, autonomous pH and pCO_2 sensors are the furthest along in carbon sensor development, being widely deployed by oceanographers interested in the marine carbon system.

1.4.1. pH Sensors

The most widely recognized and accurate measurement of pH is made using a hydrogen gas electrode, also known as a Harned Cell. Solutions analyzed using a Harned Cell are generally considered primary standards (Buck et al., 2002). Due to impracticalities of the Harned Cell for field use, there are three main commercially available techniques for measuring pH *in situ* in the ocean: use of a glass electrode, a liquid junction electrode, or spectrophotometry (Ulfsbo et al., 2017).

The glass electrode method measures the electrical potential of a solution between two electrodes, with the glass electrode referenced against a solution of stable pH (usually 7). The YSI EXO sonde is a commercially available sensor using the glass electrode principle. The EXO is capable of operating within a wide range of salinity (0-40 PSU) and pH values (0-14), but lacks comparable quoted accuracy (uncertainty of 0.2 pH units) (Ulfsbo et al., 2017).

The liquid (gel) junction and/or junctionless external reference electrode method uses an ion-selective field effect transistor, or ISFET (Martz et al. 2010). Commercially available sensors implementing ISFET technology include SeaFET sensors by Sea-Bird Scientific (Satlantic). The sensors require long conditioning periods (~1 week) to minimize drift during *in situ* ocean deployments (Martz et al., 2010). Each sensor also requires a full individual calibration at varying temperature and salinity prior to deployment (Bresnahan et al., 2014). Following the tedious pre-deployment procedures these sensors are capable of relatively high sampling rates (1 second frequency).

The spectrophotometric method uses an appropriately selected sulfonephtalein indicator dye depending on expected sample pH. Each indicator dye form has distinctive absorption characteristics (Aßmann et al., 2011; Clayton & Byrne, 1993). Meta cresol purple is a common indicator dye used for seawater pH measurements, with purified meta cresol purple characterized for a temperature range of 5-35°C and a salinity range of 20-40 PSU (Liu et al., 2011). Spectrophotometric methods require sample filtration as bubbles and particulate matter can lead to poor quality measurements (DeGrandpre et al., 1995). Setbacks of wet chemistry spectrophotometry include the requirement for indicator storage, as well as valves and pumps

to propel sample and indicator solutions through the sensor. The reagents may have limited lifetimes (~1 year) and specific storage requirements (e.g. exclusion of ultra-violet radiation). Immobilization of the pH indicator into a solid porous matrix provides a promising alternative to wet spectrophotometry. The spectrophotometric method is available commercially through Sunburst Sensors as the SAMI-pH, and have some of the highest quoted sensor accuracies (uncertainty of 0.003 pH units).

1.4.2. pCO_2 Sensors

Seawater *in situ* pCO_2 measurements are based on the equilibration of a medium in a sensor detector with a seawater sample, and subsequent determination of the CO_2 in the medium (Körtzinger et al., 1996). What varies between pCO_2 instruments are (1) the means of equilibration of the gases' partial pressures, and (2) the type of detector (Pereira et al., 2017). Three different equilibration principles exist: liquid-gas, liquid-liquid, and liquid-solid.

In the liquid-gas principle, CO_2 in surrounding seawater equilibrates with gas contained in a chamber directly, or through a gas-permeable membrane (Pereira et al., 2017). CO_2 concentrations measured optically using non-dispersive infrared absorption spectroscopy are a widespread design using the liquid-gas principle. Examples of commercially available instruments that use this technology include the CONTROS model HydroC CO2, and the Pro-Oceanus CO2-Pro instruments. The technique allows for deep deployments (up to 6000 m), and a wide range of observable pCO_2 values (0-2000 µatm).

Using the liquid-liquid principle, pCO_2 is measured indirectly through spectrophotometric pH determination. Spectrophotometric pCO_2 systems pump a colorimetric pH indicator (e.g. meta cresol blue) through a CO_2 permeable membrane where it equilibrates with the seawater sample. Subsequently in a detection cell, the solution absorption is measured at wavelengths that correspond to the absorbance frequencies of the acidic and conjugate base forms of the indicator, and a reference wavelength that is independent (DeGrandpre et al., 1995). A shift in the pH indicator solution color is due to pCO_2 (DeGrandpre et al., 1995). Examples of instruments that use colorimetric technology include the Sunburst model SAMI pCO2. The method does result in a relatively slow sensor response rate (~5 minutes).

In the liquid-solid principle, a dye-embedded sensing foil is in equilibrium with seawater CO_2. Optode sensors measuring pCO_2 consist of an analyte-sensitive indicator (i.e. dye) immobilized in a gas-permeable membrane, referred to as the sensor foil. A light emitting diode is directed to the sensor foil, exciting the indicator, which emits photons and these are subsequently detected with a photodetector. A comparison of the phase shift between the sensing foil and the reference luminophore provides estimates of pCO_2 (Atamanchuk et al., 2014). Optical sensors are not yet commercially available, but advanced prototypes are being tested including the Aanderaa pCO_2 Optode (Atamanchuk et al., 2014; Fritzsche et al., 2017, 2018). Benefits of the optical method include the ability to make profiling measurements due to the relatively fast response rates (45 seconds in 40°C).

1.4.3. Sensor Precision, Accuracy and Reliability

A key goal for observational scientists includes ensuring that measurements made in the field are of appropriate quality for their intended purpose, and that they are comparable with one another. In an ocean observing network this is particularly important as measurements are made at different times, in different places, and in many cases by different instruments, maintained by different groups (Newton et al., 2015). Currently, best practices and quality assurance/ control protocols for more mature oceanographic sensor measurements, such as salinity and oxygen, are relatively established and have been broadly adopted. Established, universal protocols are particularly lacking in new sensor technology including carbon system sensors of pH and pCO_2. Practical suggestions for ISFET pH sensor type use and quality controls have recently been published (Bresnahan et al., 2014; Kapsenberg et al., 2017; McLaughlin et al., 2017; Rérolle et al., 2016), but there is significantly less information available regarding pCO_2 sensors. Without standardized protocols it leaves decisions on quality assurance/ control, data archiving and metadata up to the individual user or manufacturer. As carbon system sensors become more commercially available it requires a community effort to develop and document calibration protocols. In the interest of traceability and reproducibility, any data reprocessing needs to be reported by users.

The real goal of collecting sensor data is scientific evaluation of changing ocean chemistry, not simply to measure pH or pCO_2. This mean there needs to be assurance of data quality. Depending on the scientific application, data quality for monitoring the marine carbon system falls into two categories: climate and weather level data. Climate level data refers to

measurements of a sufficient quality to assess long-term trends with a defined level of confidence. Climate level data implies an uncertainty of approximately 0.003 in pH; of 2 µmol/kg in measurements of DIC and TA; and a relative uncertainty of 0.5% in pCO_2. This quality of data is to support detection of long-term anthropogenically-driven changes in hydrographic conditions and carbon chemistry over multi-decadal timescales (Newton et al., 2015). Such precision is only currently achievable by a very limited number of laboratories and is not typically achievable for all parameters by even the best autonomous sensors (Newton et al., 2015). Climate level carbon data reporting is only common at long duration world class ocean observing sites including the two US stations: the Bermuda Atlantic Time-Series Study and the Hawaii Ocean Time-Series, both creating unparalleled datasets.

Weather level data refers to measurements of sufficient quality to identify relative spatial patterns and short-term variation. This implies an uncertainty of approximately 0.02 in pH; of 10 µmol/kg in measurements of DIC and TA; and a relative uncertainty of 2.5% in pCO_2. Weather level data could support mechanistic interpretation of an ecosystems response to, and impact on, local immediate ocean acidification dynamics (Newton et al., 2015). Weather level data can be useful in identifying regional seasonal or sub-seasonal patterns in carbonate system parameters, and identifying influencing biogeochemical processes. Such precision should be achievable in most laboratories, and with the best autonomous sensors (Newton et al., 2015).

For oceanographic sensors to approach very high deployment confidence it can take up to 20 years of development and testing, as was the case with salinity, and oxygen technologies. Carbon system sensors are still in an early phase of development, with most instruments being

developed and tested in temperate oceanic waters with moderate temperatures and relatively constant salinities. However, the potential application of autonomous sensors goes far beyond these test conditions, including high-latitude waters. In the Arctic marine setting temperatures are much lower and salinities much more variable. Deployment of sensors in a variety of novel conditions globally, while carefully documenting their responses, helps build the community effort towards maturing the technology.

2.0. Study Objectives

The overarching objective of this project is to describe the seasonal marine carbon cycle on an Arctic continental shelf sea impacted by many of the processes common to such regions (i.e., sea ice growth and decay, river runoff, biological production). This was done utilizing *in situ* pCO_2 and pH data collected by an innovative autonomous sensor platform (the Ocean Networks Canada Undersea Community Observatory in Cambridge Bay, Nunavut), in combination with ancillary field data. The evaluation of a high-resolution marine carbon time-series in the Canadian Arctic Archipelago is the first of its kind to our knowledge. In pursuit of the primary objective utilizing the underwater observatory, the following sub objectives are also addressed:

(1) Validation of pH/ pCO_2 sensor measurements using discrete samples, and providing a post-deployment data correction method to produce final sensor time-series data products.

(2) Describing the oceanographic context of which the Ocean Networks Canada undersea platform is capable of capturing, at its deployment depth and location within Cambridge Bay.

(3) Quantitatively describing the influencing factors on the marine carbon system seasonally through a complete cycle of sea ice growth and melt in Cambridge Bay, using a diagnostic box model.

This study contributes to validating the methodology of long duration autonomous sensor deployments in harsh Arctic marine conditions as a means of increasing temporal data coverage. We directly test and validate new innovative autonomous carbon system sensor technology for nearly yearlong Arctic deployments in seasonal sea ice covered waters. This study also contributes to addressing the knowledge gap in understanding processes critically influencing the Arctic marine carbon cycle through the polar night, providing a more complete and detailed picture of Arctic marine carbon cycling. The final sensor derived time-series dataset produced also provides a significant base monitoring dataset for high latitude ocean acidification in the future.

3.0. Materials & Methods

3.1. Field Site

Cambridge Bay is the experimental Arctic estuary site for this study. Herein, we refer to the marine region of Cambridge Bay as "CB", to avoid confusion with the Hamlet of Cambridge Bay (also known as known as Iqaluktuttiaq in the local language of Inuinnaqtun, meaning "good fishing place" (ᐃᖃᓗᖅᑐᑎᐊᖅ in Inuktitut)). CB is located on the Southern shore of Victoria Island in the Province of Nunavut, Canada (69.1149°N, 105.0548°W). CB is located within the Southwestern Kitikmeot region of the Canadian Arctic Archipelago, called Qitirmiut. The greatest depth in CB is 86 m. The wide entranceway is extremely shallow with two sills restricting flow between the bay and the Northwest Passage connection of Dease Strait (Figure 4).

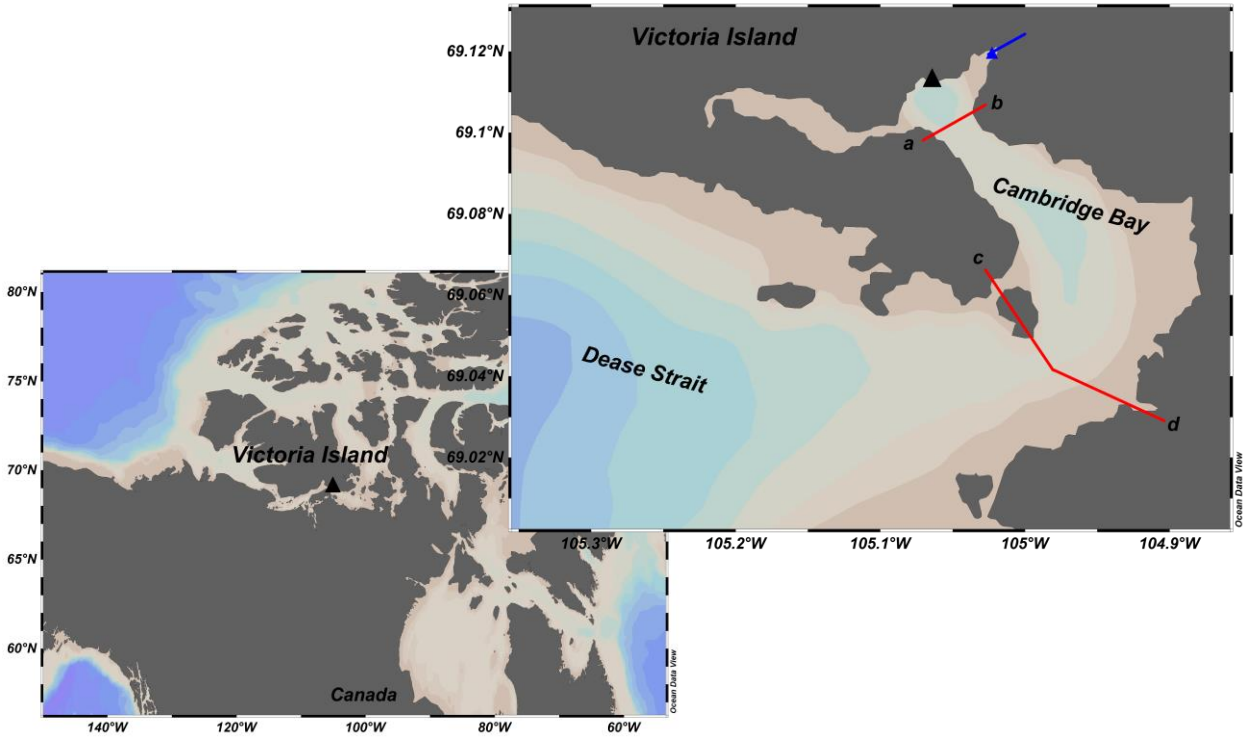

Figure 4 Map of Cambridge Bay, Nunavut, Canada (Iqaluktuttiaq in Inuinnaqtun, or ᐃᖃᓗᒃᑑᑎᐊᖅ in Inuktitut). Our sampling platform is denoted by a black triangle. Where Freshwater Creek discharges into CB is marked by a blue arrow. A bay sill runs from a-b, approximately along the red line at a maximum depth of 20 m, and from c-d at a maximum depth of 11 m.

CB is characteristic of an Arctic Estuary system, being a near-shore environment with seasonal variations in terrestrial runoff, and a river-to-shelf salinity gradient. CB is an outlet for a fairly large watershed (1490 km^2) flowing in from Freshwater Creek (Figure 4). Freshwater Creek typically starts flowing in early June, peaks in discharge around late June/ early July during freshet, and stops flowing in early November (Environment and Natural Resources Canada, 2019).

CB is classified as being within the Canadian Arctic Archipelago seasonal sea ice zone, with sea ice forming annually. Complete ice cover in the bay as reported by the Canadian Ice Service, has a mean of around early October. Sea ice thickness increases through the polar winter reaching a maximum in May, with an average maximum thickness being about ~1.5 m (Ocean Networks

Canada, Oceans 2.0). Sea ice melt commences around June as reported by the Canadian Ice Service, and by the second half of July, CB is typically completely ice free. The seasonal dynamics of sea ice add complexity to wind mixing, buoyancy, and circulation within CB (Carmack, 1986). During much of the winter the sea ice is covered by snow to variable depths depending on the year, but usually less than 0.3 m.

Lewis & Walker's (1970) work in CB highlights changes in the water column throughout the year. In early winter following sea ice freeze-up, salt released by the growth of sea ice causes an increase in the salinity of the upper layer, which becomes isohaline and isothermal early in the winter. Brine induced salinity-driven convection causes downward mixing throughout the winter. It is predicted that by spring this process may produce a condition approaching neutral static stability through the full water column in CB (Lewis & Walker, 1970). The early summer water column differs greatly with a pronounced two-step stratification, forced by a thin (<2m) spring freshet surface layer and freshening in the upper 20-30 m from Freshwater Creek run-off and sea ice melt (Lewis & Walker, 1970). Following an approximate three week period of two step stratification, wind-forced mixing produces a familiar two layer isocline separated structure in CB. Annually we see salinity ranging from 16 – 30 PSU, and temperature ranging from -1.5°C – 10°C at the location and depth of our site in CB discussed in the following section (Ocean Networks Canada, Oceans 2.0).

CB does experience moderate tidal influence semi-diurnally. The daily range of heights at highest tides is 0.6 m while the average daily range is 0.4 m. The bay does exhibit stable density stratification annually which combined with the shallow sill depths, suggests that much of the

water movement caused by tides occurs in the surface layers (Gade et al., 1974). However, in the wintertime under the cover of sea ice CB is reported as having very minimal water movement (Lewis & Walker, 1970).

3.2. Platform Deployment History

This study utilized the Ocean Networks Canada (ONC) Undersea Community Observatory in CB, Nunavut (Figure 5). The platform is situated on the ocean floor at a depth of seven meters below the sea surface, just off shore. First installed in September of 2011, it is the first such instrument system capable of year-round, 24/7 monitoring in Canada's high Arctic marine ecosystem (Ocean Networks Canada, 2011). CB was chosen by ONC for several factors including: the existing community and infrastructure (e.g. power, airstrip and accessible wharf), the protected location in the bay, and the outreach potential both to the local community and seasonal visitors (Ocean Networks Canada, 2011). The cabled capability of the platform offers continuous near real-time monitoring throughout the year, including under sea ice though the polar night. The platform offers a continuous presence in the Arctic to establish a baseline for marine environmental information within the Canadian Arctic Archipelago. The data collected from the community observatory is streamed live over the open access ONC Ocean 2.0 data outlet. Marine carbon sensor deployment onboard the platform started in 2015. Table 1 details deployment intervals and onboard marine carbon system sensors, and ancillary sensor ID’s for the 2015, 2016, and 2017 deployments.

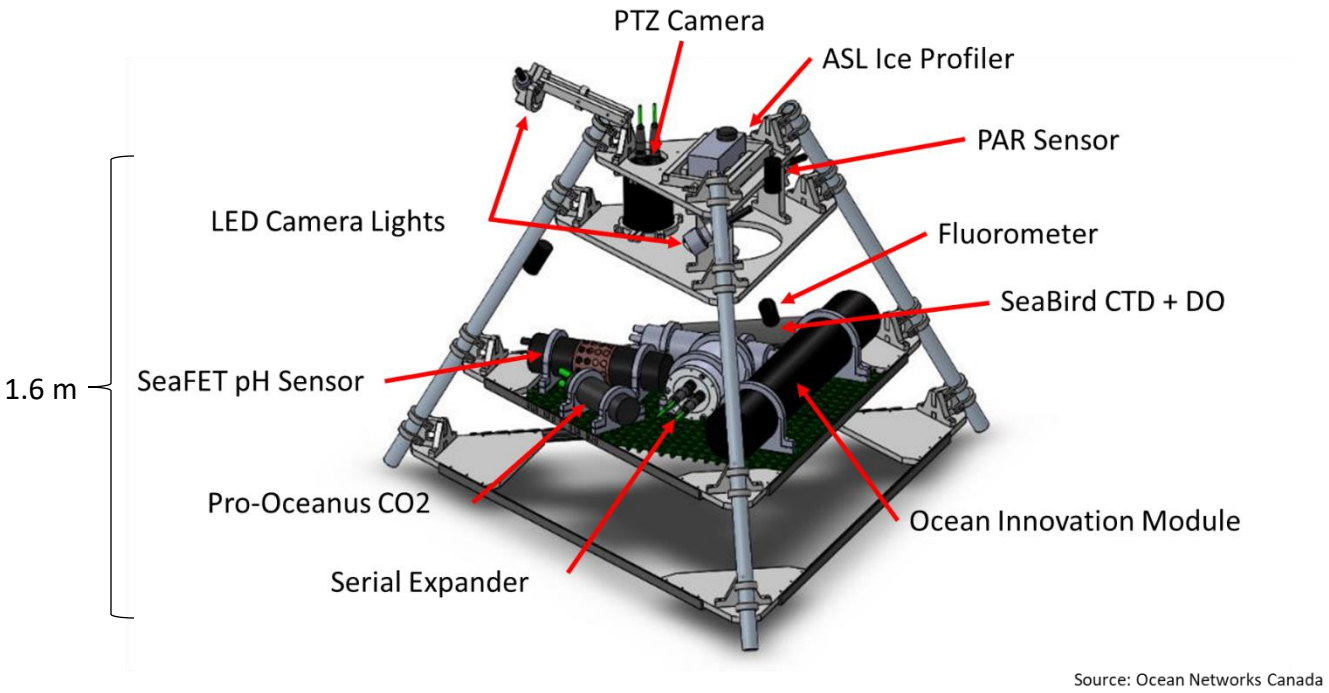

Figure 5 Ocean Networks Canada Undersea Community Observatory schematic of onboard sensors and relative sensor locations for 2016 deployment in Cambridge Bay, Nunavut.

Table 1 Onboard sensor details for the 2015, 2016, and 2017 ONC platform deployments.

	2015	**2016**	**2017**
Deployment Date	2015-08-27 20:05:40	2016-08-25 22:24:00	2017-09-14 23:22:00
Recovery Date	2016-08-24 03:21:00	2017-09-02 16:50:00	2018-07-24 22:06:00
Carbon system sensors	Pro-Oceanus CO2-Pro CV (SN 35-250-75) Sunburst SAMI pH sensor (P0073)	Pro-Oceanus CO2-Pro CV (SN 36-314-75) Satlantic SeaFET Ocean pH Sensor (SN 246)	Pro-Oceanus CO2-Pro CV (SN 35-250-75) Satlantic SeaFET Ocean pH Sensor (SN 452)
Ancillary sensors	Sea-Bird SBE 63 Dissolved Oxygen Sensor (630834) ASL Shallow Water Ice (53029) Sea-Bird SeaCAT SBE19plus V2 (7589) WET Labs ECO-PARS (S/N 459)	Sea-Bird SBE 63 Dissolved Oxygen Sensor (630834) ASL Shallow Water Ice (53029) Sea-Bird SeaCAT SBE19plus V2 (7518) WET Labs ECO-PARS (S/N 440)	Sea-Bird SBE 63 Dissolved Oxygen Sensor (631008) ASL Shallow Water Ice Profiler (53038) Sea-Bird SeaCAT SBE19plus V2 (7589) WET Labs ECO-PARS (S/N 459)

3.3. Sensor Operation / Principle

3.3.1. Satlantic SeaFET Ocean pH Sensor

A Satlantic SeaFET Ocean pH Sensor was first deployed in CB on the ONC platform in 2016. The SeaFET uses ISFET technology (Martz et al., 2010). An ISFET is housed within both the internal (FET|INT) and external (FET|EXT) potentiometric cells. FET|INT uses the ISFET as the working electrode and an Ag/AgCl electrode bathed in 4.5 M KCl gel as the internal reference electrode. FET|EXT also uses an ISFET as the working electrode and a chloride ion sensitive pseudo-reference electrode, making it salinity dependent. Using internal and external cell voltage readings and sample temperature, two independent pH measurements can be derived by the SeaFET. Both pH electrodes demonstrate exceptional stability over a range of salinities (9–36 PSU) and temperatures (−1 to 35 ◦C) (Bresnahan et al., 2014; Gonski et al., 2018;

Kapsenberg et al., 2017; Martz et al., 2010; Miller et al., 2018). For a more detailed discussion on ISFET pH sensor technology see Bresnahan et al. (2014), or Martz et al. (2010).

The SeaFET instrument is calibrated at Satlantic prior to field deployment. The Canadian Department of Fisheries and Oceans, Institute for Ocean Sciences runs a spectral pH analysis to ensure accuracy, and ONC performs data streaming compatibility tests in separate test tanks in Victoria, BC, Canada also prior to deployment. Satlantic maintains that SeaFET accuracy is within 0.05 pH, with precision better than 0.001 pH, a sensor precision of 0.0001 pH, and stability of 0.005 pH/month.

3.3.2. Pro-Oceanus CO2-Pro CV

A Pro-Oceanus CO2-Pro CV sensor was first deployed onboard the ONC platform in 2015. The CO2-Pro measures the partial pressure of CO_2 gas dissolved in seawater using non-dispersive infrared detection. When the CO2-Pro is turned on, the non-dispersive infrared detector warms up and stabilizes at the set optical cell temperature of 30°C. The sensor then carries out a zero point calibration by circulating internal gas through a CO_2 absorption chamber containing Ascarite, removing all CO_2 from the detection cell allowing for a zero CO_2 baseline measurement. This zero point measurement is subsequently carried out every 12 hours. Next the CO2-Pro circulates the internal gas around a closed circuit connecting the equilibrator and detector. The sensor is fitted with an equilibrator composed of a gas permeable poly-dimethylsiloxane membrane. An associated Sea-Bird Electronics SBE 5M submersible pump flows water at 35 mL/s past the outer surface of the equilibrator membrane to accelerate the equilibration. Once the internal gas is fully equilibrated with the surrounding seawater (typically

10-15 min after a zero point calibration) the inferred signal of the internal gas, taken at a wavelength of 4.26 µm, is measured to calculate the absorbance and seawater CO_2 concentration. The CO2-Pro also records gas stream water vapor partial pressure, total pressure, as well as gas analyzer detector and source temperature. For a more detailed discussion on the operating principle of the CO2-Pro see Jiang et al. (2014).

The CO2-Pro instrument is calibrated by Pro-Oceanus using National Institute of Standards and Technology traceable CO_2 calibration gases prior to field deployment. ONC preforms data streaming compatibility tests in their test tank in Victoria, BC, Canada also prior to deployment. Pro-Oceanus maintains that accuracy stays within 0.5% over the calibrated range (0-1000 µatm), and drift is restricted to less than 10 µatm per year while measuring pCO_2 concentration with a precision of 0.01 ppm.

3.3.3. Preliminary Sensor Data Inspection

Before any sensor calibration could be completed we inspected pH and pCO_2 measurements through all deployments for five conditions (McLaughlin et al., 2017): (1) erratic values that appeared as unreasonable spikes in the data record, (2) sensor instability at the start of deployment (i.e. sensor conditioning), (3) sensor failure that manifested as drift, (4) sensor offset throughout deployment, and (5) sensor mechanical failure resulting in the abrupt end of data collection. Potentially errant pH_{raw}^{sensor} and $pCO_{2_{raw}}^{sensor}$ measurements were flagged using a third-order one-dimensional median filter $[y(k) = x(k-1{:}\,k+1)]$, to find values occurring as isolated anomalous spikes. The filter ensured that values around the flagged measurement which occurred in a series of similarly high or low values were maintained.

Across all deployments the third-order one-dimensional median filter was applied to $pCO_{2_{raw}}^{sensor}$, in order to find lower than expected data spikes occurring along a regular interval of 12 hours. This regular interval of errant measurements coincided with the CO2-Pro SN 35-250-75 scheduled zero point calibration. Throughout both deployments for the SN 35-250-75 sensor (Table 1; 2015-2016, 2017-2018 deployments) this behavior remained consistent. It appears that the immediate measurement following a zero point calibration did not equilibrate quickly enough with the surrounding seawater to make an accurate measurement in this sensor. This did not occur for SN 36-314-75 (Table 1; 2016-2017 deployment).

Throughout the first deployment in particular, CO2-Pro sensor behavior following a power outage to the platform measured significantly lower than expected pCO_2 values. A power outage caused the zero point calibration count to reset, negating the regular calibration offset the sensor was designed to account for leading to lower values (Section 3.3.2.). A second filter was applied to flag measurements made coinciding with anomalies in the zero point calibration count which occurred following every power outage. This was a regular phenomenon following a blackout and data was discarded from before the sensor could perform another zero point calibration.

SeaFET sensor instability at the start of deployment is due to reconditioning of the sensor in a new environment (Bresnahan et al., 2014). Highly variable pH_{raw}^{sensor} values were flagged at the beginning of the deployment that were not otherwise associated with similar variability in temperature or salinity over the same time interval. Table 2 shows pH_{raw}^{sensor} and physical parameter variability in factory single point calibrated values for FET|INT, and FET|EXT during

the conditioning period of 10 days following deployment. It is clear that during the 2016-2017 deployment environmental variability was higher causing a greater variability in observed pH values compared to 2017-2018. Such variability within the sensor conditioning period can lead to sensor offset throughout deployment. The most extreme conditioning variability potentially went unrecorded as the SeaFET experienced a delay in receiving power from time of deployment by 22 hours, and 103 hours over the 2016-2017 and 2017-2018 deployments respectively.

Table 2 Observed range in raw SeaFET sensor pH, and SeaBird CTD temperature and salinity within the first 10 days during the 2016-2017 and 2017-2018 deployments.

Year	Δ pH FET|INT	Δ pH FET|EXT	Δ Temperature (°C)	Δ Salinity (PSU)
2016-2017	0.1139	0.0453	3.17	1.97
2017-2018	0.0268	0.0155	1.09	0.30

Sensor mechanical failure resulting in the abrupt end of data collection did occur. The SeaFET deployments were unaffected but unfortunately two CO2-Pro deployments ended prematurely. The infrared gas analyzer source lamp in SN 36-314-75 failed on 2017-06-27, before platform recovery on 2017-09-02. SN 35-250-75 had a mechanical failure on 2018-06-09 before ONC platform recovery on 2018-07-24. Unaddressed in this study is the Sunburst SAMI pH sensor which failed very early into the 2015-2016 deployment (Table 1).

3.4. Field Measurements

3.4.1 Sensor Evaluation Sampling

In order to evaluate and calibrate the deployed *in situ* carbon system sensors onboard the platform we needed to determine the sensor accuracy relative to a reference. Sources of reference carbon data could include: a secondary carbon system sensor instrument, modeled carbon data from regional climatology, pre-deployment and post deployment factory calibrations, or discrete water samples. An independent reference point at deployment can be used to infer drift or offset from storage, transportation, and conditioning. An independent reference at recovery can infer drift during deployment. Ideally, independent references should be collected periodically throughout deployment to correct if the rate of drift varies with time. Our study made use of a discrete reference water sampling approach. Relying on a discrete sampling approach, the primary control on the quality of the final carbon system sensor time series data is directly related to the number and quality of discrete samples collected over the sensor deployment interval (McLaughlin et al., 2017). As described by Rivest et al. (2016), the optimal discrete sampling scheme is characterized by > 10 usable discrete bottle samples for sensor deployments of several months or more. Rivest et al. (2016) stresses that the remoteness of most open-ocean sensor deployments limit opportunities to maintain, calibrate, and verify the performance of the sensors. However, this is also true for deployments in harsh environmental conditions. CB experiences air temperature lows of -40°C, with wind chill lows of -60°C regularly from December through March. These temperatures make winter water sampling extremely difficult and required adapted sampling protocols.

Table 3 Discrete sampling dates for onboard carbon system sensor validation and correction over the 2015, 2016, and 2017 ONC platform deployments.

	2015	**2016**	**2017**
ONC Discrete Sampling Dates (*) denotes discarded samples (+) denotes unavailable carbon sensor data	2015-08-28+ 2016-02-16 2016-03-13 2016-05-15 2016-05-22 2016-05-28 2016-06-08 2016-08-25+	2017-01-28 2017-02-02 2017-02-27* 2017-03-04* 2017-03-11* 2017-03-18 2017-03-28* 2017-04-01 2017-04-14 2017-04-24* 2017-04-30 2017-05-03* 2017-05-16 2017-05-24* 2017-06-03* 2017-06-09 2017-06-12 2017-06-17 2017-06-24 2017-07-03* 2017-07-10 2017-07-20 2017-08-01+	2017-09-14+ 2017-10-10 2017-10-31 2017-11-24 2018-02-05 2018-05-18 2018-06-04 2018-06-18

We collected discrete samples for ONC carbon system sensor validation and correction at the ONC site through all three deployments (Table 3). During the 2015-2016 deployment sampling took place opportunistically with samples taken at the start of deployment, at the start and end of a separate field campaign in February – March, weekly through May and early June, and at recovery (Table 3). During the 2016-2017 deployment samples were taken roughly weekly from the end of January until the start of August (Table 3). The harsh conditions became particularly apparent during our 2016-2017 sensor deployment when winter discrete sampling was emphasized. 23 samples total were collected from January to the beginning of August in 2017.

Only 13 of those samples were deemed useable for sensor evaluation. Samples went unused based on sensor data availability, discrepancies in salinity measured *in situ* and in the lab, integrity of the bottle seal, and trends in dissolved inorganic carbon and total alkalinity resembling improper biologic fixing or gas exchange in the bottle. Previous studies have found that depending on operator experience, the collection and preservation of calibration and reference samples can vary in accuracy (McLaughlin et al., 2017). Experience also contributed to the loss of discrete samples useable for evaluation. The majority of sampling carried out during the most difficult collection interval (February – March 2017) was conducted by a newly trained local field technician. During the 2017-2018 deployment, samples were taken nearly monthly from September deployment to June recovery (Table 3).

Using discrete samples as the source of reference carbon data in sensor validation and correction does have complications. Identifying the source of the difference between the discrete sample references and the deployed sensor may be difficult. The difference can be attributed to a number of factors, acting independently or in combination. Factors influencing discrete sample differences include: small errors in the analysis of discrete bottle samples (Bresnahan et al., 2014; McLaughlin et al., 2017); uncertainty in the thermodynamic constants used to calculate pH^{disc}_{DIC-TA} or $pCO_2{}^{disc}_{DIC-TA}$ (Rérolle et al., 2016); environmental pH or pCO_2 gradients of varying magnitudes (Bresnahan et al., 2014); and other sources of sampling/handling error in the field or the lab (McLaughlin et al., 2017; Rerolle et al., 2016).

Sensor offset is inferred to be caused by improper sensor calibration preceding deployment, or inadequate sensor conditioning. Sensor drift can be due to either sensor calibration drift,

caused by changes in the internal sensor components and measurement devices, electronic wear, or for the SeaFET, the dilution between sensor calibrations of the pH reference (Bresnahan et al., 2014). Drift due to sensor exposure to the seawater environment, particularly due to bio-fouling is also common depending on the environment.

The majority of samples deemed unfit for sensor evaluation were discarded due to sampling/ handling error described above. Discrepancies between sensor and reference samples attributed to sensor performance includes: sensor instability at the start of deployment (sensor conditioning), sensor failure that manifested as drift, or sensor offset throughout deployment.

3.4.2. Oceanographic Context Sampling

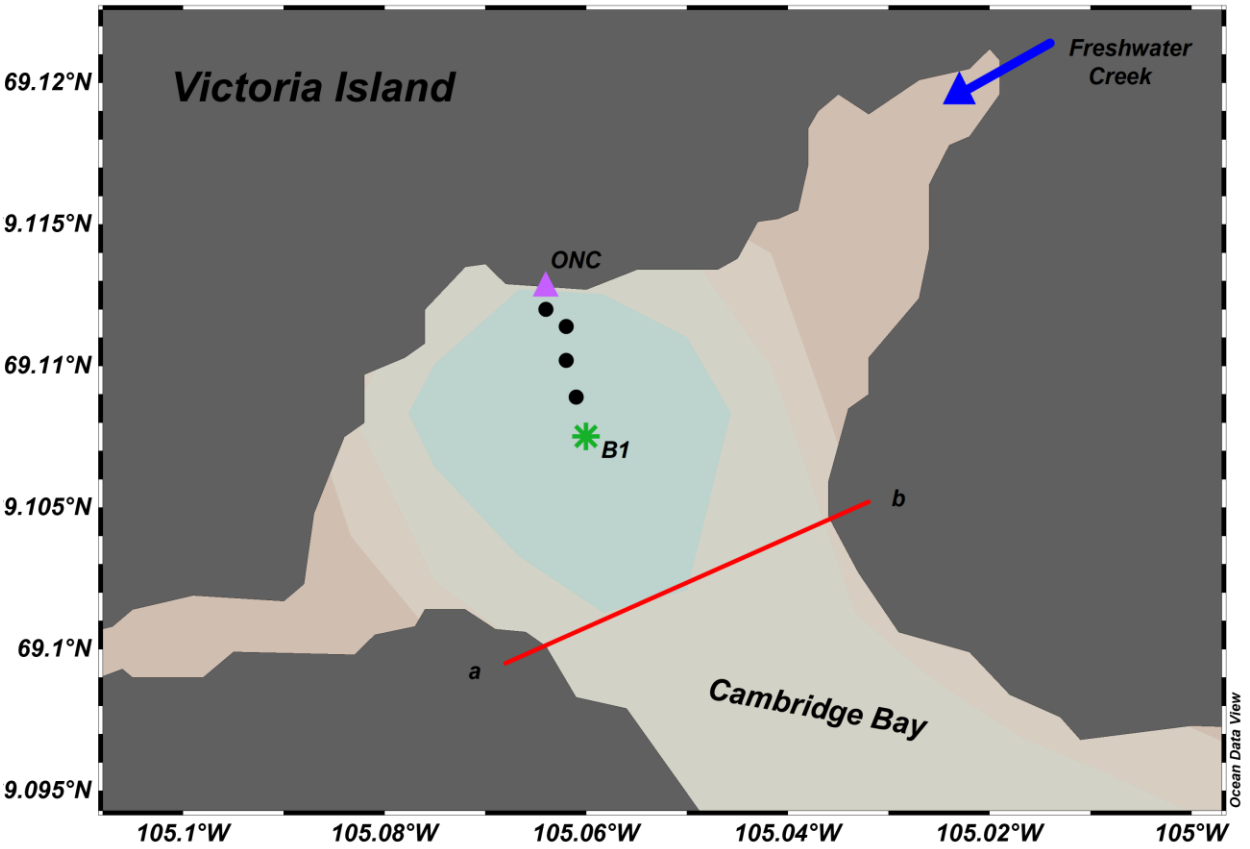

Figure 6 Cambridge Bay time-series spatial sampling site map. ONC is denoted by a pink triangle, B1 by a green asterisk, CTD only sampling sites by black dots between them. Where Freshwater Creek discharges into CB is marked by a blue arrow. The bay sill closest to our sites runs from a-b, approximately along the red line at a maximum depth of 20 m.

As the water column changes through the season, especially during sea ice melt, the ONC platform may no longer be representative of the surface layer. Using complete water column conductivity-temperature-depth (CTD) casts taken throughout the year along a transect reaching further into the bay, the spatial and temporal representation of the platform relative to the greater oceanography of CB was assessed. RBR Concerto CTD measurements were taken along a six station transect in conjunction with the ONC sensor evaluation time-series starting

during the 2016-2017 deployment (Table 3). The oceanographic transect encompassed the distance from the ONC platform, to station B1 (Figure 6). The CTD time series and additional discrete samples also provided a reference of conditions further off shore and near the seafloor. The B1 site was selected as it represents near maximum depth of CB, north of both bay sills (Figure 4) (Gade et al., 1974). The four intermediate sites were dispersed between the ONC site and B1 (Figure 6). Intermediate sites were collectively chosen to represent different depths, and cover spatial variability between the two water sampling sites in the bay (Figure 6; Table 4). The steep drop off of the shoreline into the deep curvature of the bay happens quickly in relation to horizontal distance. Thus, three CTD-only sites were grouped closer to the ONC site, with MB representing the geographic midpoint between the ONC and B1 site, and CTD-3 the geographic midpoint between MB and B1 (Figure 6; Table 4).

Table 4 Cambridge Bay time-series sample site details including: name, geographic location, and sampling activities conducted.

Site (depth [m])	**Latitude [degrees north]**	**Longitude [degrees west]**	**DIC/TA Discrete sampling depths [m]**
ONC Site (7)	69.113117	105.064083	surface,7
CTD-1 (21)	69.112000	105.063611	CTD Cast Only
CTD-2 (34)	69.111500	105.062733	CTD Cast Only
MB (52)	69.110278	105.061889	CTD Cast Only
CTD-3 (65)	69.108913	105.060778	CTD Cast Only
B1 (72)	69.107556	105.059667	surface,7,30,71

Discrete sampling to understand the broader chemical oceanographic context of the ONC site included depths of 2, 7, 30, and 70 m at station B1 further into the bay (0.65 km), as well as 2 m depth at the ONC platform location (Table 4). 2 m was chosen as an indication of the ocean ice-sea interface. We changed this depth to 0.5 m following ice breakup to capture the air-sea

interface annually; 7 m was sampled for comparability to the ONC platform sensor depth; 30 and 70 m depths were sampled to contrast measurements located below the pycnocline, and near the seafloor of the deeper site respectively (Lewis & Walker, 1970). The sampling timetable for ancillary CTD measurement and discrete sample collection roughly corresponded to the ONC sensor validation sampling during the 2016-2017, and 2017-2018 deployments (Table 3).

All discrete samples measured DIC and TA. All water samples were collected and analyzed according to best practices (Dickson et al., 2007). Water was collected through the use of oversized Niskin bottles (1.25 L), followed by bottom-filling and overflowing triple rinsed 125 mL borosilicate bottles to prevent samples from equilibrating with the atmosphere. Samples were then fixed to 0.04% v/v of mercuric chloride ($HgCl_2$) solution to prevent biological activity. Depending on the time of year samples were collected (Table 3), the sample fixation period varied between immediately during the spring and summer, to upwards of one hour during the winter months. Following the fixing procedure, samples were capped using chlorobutyl-isoprene rubber stoppers and aluminum caps, and moved to be preserved in 4°C for future analysis (Jiang et al., 2008). All samples collected in 2015-2016, and some samples in 2017-2018 which were included in the ONC sensor evaluation were collected in the same manner described above except using a 6 L Niskin bottle and 250 mL glass bottles with ground glass stoppers, for analysis by Department of Fisheries and Oceans, Institute of Ocean Sciences in Sidney, BC, Canada.

3.4.3. Analytical Methods

All 125 mL samples were analyzed at the University of Calgary, where DIC was determined through acid extraction by quantifying the released CO_2 using an infrared gas analyzer (AIRICA and LiCOR-7000); TA was measured by Gran Titration (Gran, 1950, 1952) using a semi-automated open-cell titration system (AS-ALK2 Apollo SciTech) (Cai et al., 2010). All 250 mL bottles analyzed at Institute of Ocean Sciences, determined DIC coulometrically (Andrew G Dickson & Goyet, 1997) using a SOMMA extraction system (Johnson et al., 1993) and a UIC, Inc. model no. 5011 coulometer; TA was measured by Gran Titration (Gran, 1950, 1952) using a semi-automated open-cell titration system (Haraldsson et al., 1997).

All measurements were calibrated against certified reference materials (provided by A.G. Dickson from Scripps Institute of Oceanography) with a standard bottle precision of ±2.2 µmol/kg. The independent reference pH and pCO_2 values used for sensor assessment were calculated from the measured DIC and TA at *in situ* temperature, salinity, and pressure using the inorganic carbon dissociation constants from Lueker et al. (2000), bisulfate ion acidity constant of Dickson (1990) and the boron-to-chlorinity ratio of Lee et al. (2010), in the Microsoft Excel macro CO2SYS (Pierrot et al., 2006). These same constants were used for all other CO2SYS calculations performed. The inorganic carbon dissociation constants from Lueker et al. (2000) were found most suited to calculations within the temperature range of $-1.5 \leq T \leq 10.5$ °C and salinity range of $25.8 \leq S \leq 33.1$ (Chen et al., 2015).

3.5. Sensor Calibration

3.5.1. SeaFET Calibration

SeaFET sensor evaluation was based on discrepancies between factory calibration reported values ($pH_{raw}^{INT}, pH_{raw}^{EXT}$) and *in situ* discrete sample values (pH_{DIC-TA}^{disc}). For pH, we derived sensor values from sensor voltage readings, and appropriate calibration coefficients from pre-deployment factory single-point calibrations.

Eq. 1B $$pH^{INT} = \frac{(E_{INT} - E_{INT}^{*})}{S}$$

Eq. 2B $$pH^{EXT} = \frac{(E_{EXT} - E_{EXT}^{*}) + S(log_{10}\gamma_H\gamma_{Cl}m_{Cl})}{S}$$

Eq. 3B $$S = \frac{RT}{F}(\ln(10))$$

The above equations (Eq. 1B – 3B) are used to calculate pH, where E_{INT} and E_{EXT} are the measured sensor voltages, E_{INT}^{*} and E_{EXT}^{*} are the calibration constants, γ is the ion activity coefficient for either H^+ or Cl^- (γ_H and γ_{Cl} respectively), m_{Cl} is the molar concentration of Cl^-, and S is the Nernst slope. The Nernst slope is dependent on: R the gas constant (8.3145 J mol^{-1} K^{-1}), F the faraday constant (96485 C mol^{-1}) and temperature in Kelvin (T). For greater detail on ISFET sensor pH calculation from electrode voltages see Martz et al. (2010).

Given that a conditioning period is required for SeaFET sensors (Bresnahan et al., 2014), the factory calibrated coefficients are likely inadequate once the sensor becomes conditioned to the deployed *in situ* environment (Table 2). The SeaFET corrections tested in this study followed established methods using *in situ* single-point calibration, and *in situ* multi-point calibration

derived coefficients in combination with *in situ* temperature and salinity (Bresnahan et al., 2014; Gonski et al., 2018). Following Bresnahan et al. (2014), using the measured SeaFET FET|INT and FET|EXT voltages, *in situ* temperature and salinity from the co-located Sea-Bird SeaCAT SBE19plus V2, and the discrete sample pH corrected to *in situ* temperature and salinity measured by our RBR Concerto CTD, new calibration coefficients specific to each reference electrode were calculated. We tested all viable individual discrete sampling points to derive calibration coefficients following adequate conditioning time (~1 week) for *in situ* single-point calibrations. The multi-point calibration method averaged all the calibration coefficients from the single-point calibrations, producing a single calibration coefficient for each reference electrode.

A comparison of the sensor pH_{final}^{INT}, pH_{final}^{EXT} and pH_{DIC-TA}^{disc} was evaluated based on its Model II least squares fit (Peltzer, 2007) which generates fit parameters including a sensor offset or intercept (c0) and a sensor gain or slope (c1). Under a perfect deployment situation these parameters would equal 0 and 1 respectively (Bresnahan et al., 2014). The root-mean squared error (RMSE) calculated from this fit becomes the degree to which the constraint of the difference between pH_{final}^{sensor} and reference pH_{DIC-TA}^{disc} can be characterized, or the accuracy of the sensor pH relative to discrete sample pH. Previous studies have shown that single-point calibration methods – factory pre-deployment and *in situ* – are best for relatively static environmental conditions, whereas multi-point *in situ* calibrations are best suited for more dynamic nearshore environments (Bresnahan et al., 2014; Gonski et al., 2018; Miller et al., 2018).

3.5.2. CO2-Pro Calibration

CO2-Pro sensor evaluation was also based on discrepancies between multipoint factory calibration reported values $\left(pCO_{2_{raw}}^{sensor}\right)$ and *in situ* discrete sample values ($pCO_{2_{DIC-TA}}^{disc}$). A comparison of $pCO_{2_{raw}}^{sensor}$ and $pCO_{2_{DIC-TA}}^{disc}$ was evaluated based on its Model II least squares fit (Peltzer, 2007). Sensor offset or intercept (c0) and a sensor gain or slope (c1) were used to validate sensor time series data. The root-mean squared error (RMSE) calculated from this fit becomes the degree to which the constraint of the difference between $pCO_{2_{raw}}^{sensor}$ and reference $pCO_{2_{DIC-TA}}^{disc}$ can be characterized, or the accuracy of the sensor pCO_2 relative to discrete sample pCO_2. Correction of CO2-Pro sensor data involved using the sensor measurement difference from discrete samples to adjust observed pCO_2 throughout a given deployment, only if c1 was statistically insignificantly from 1 (indicating no sensor drift). CO2-Pro correction was based on an *in situ* multi-point calibration approach where the average difference of the sensor $pCO_{2_{raw}}^{sensor}$ minus $pCO_{2_{DIC-TA}}^{disc}$ acted as the inferred sensor offset which was applied to $pCO_{2_{raw}}^{sensor}$ measurements to yield $pCO_{2_{final}}^{sensor}$.

3.6. Seasonal Inorganic Carbon Cycles

Following sensor correction and production of final carbon system time-series datasets, an investigation into the influencing factors on the carbon system seasonally was carried out. Due to data coverage for both sensor and ancillary field acquisition, the 2016-2017 ONC deployment interval was used as the primary case study investigating seasonally driven cycles in marine inorganic carbon at the platform.

3.6.1. Seasonal Definitions

Investigating seasonally driven carbon cycles requires defined seasonally specific time intervals. Sea ice draft from the ASL Shallow Water Ice Profiler, in conjunction with photosynthetically active radiation (PAR) from the Biospherical PAR Irradiance sensor both onboard the ONC platform served as proxy variables to differentiate seasonal endpoints (Table 1).

The fall period was defined as the interval from the start of deployment (2016-08-25) until land fast sea ice freeze-up (2016-10-23) (Table 5). Land fast sea ice freeze-up was defined as the first date of continuous ice coverage of at least 0.1 m ice thickness to ensure mobility had halted within the bay. 0.1 m was chosen as the upper limit of ice draft variability to ensure mobile ice is no longer present.

Early winter was defined as beginning on this freeze-up date, and ending when the sun rose under the ice (2017-02-28), differentiated by a distinctive signal in PAR (Table 5). The under-ice "sunrise" indicated the end of polar night at the ONC platform location, at a depth of 7 m under the ice. A value of PAR ≥ 2 µmol/m^2s was chosen as signifying the under-ice sunrise, as it is the reported lower limit of ice algal compensation light intensities (Gosselin et al., 1986; Horner & Schrader, 1982). Ice algae are commonly thought to be the first algal bloom taking place in Arctic ice-covered seas as light returns at the end of winter (Leu et al., 2015).

Late winter was from "sunrise" until sea ice reached a maximum thickness (2017-05-24), before the onset of melt (Table 5). The spring interval ranged from the date of maximum sea ice

thickness until the first occurrence of a zero sea ice draft measurement (2017-06-27) (Table 5). At the first zero ice draft measurement, it was assumed the ice pack in CB becomes mobile above the platform and the open water season began. Summer was defined as the start of open water until the end of deployment (2017-09-02) (Table 5). Unfortunately due to failure of the CO2-Pro SN 36-314-75 coincidentally on 2017-06-27, carbon system parameters were not available for summer interpretation.

Table 5 Defined seasonal time interval summary for 2016-2017 ONC platform deployment.

Fall **59 days**	**Early winter** **128 days**	**Late winter** **85 days**	**Spring** **34 days**	**Summer** **67 days**	
2016-08-25 Deployment	2016-10-23 Land fast sea ice (≥ 0.1 m thickness)	2017-02-28 Sunrise (PAR ≥ 2.0 µmol/m^2s)	2017-05-24 Maximum sea ice thickness	2017-06-27 Mobile sea ice (= 0 m thickness)	2017-09-02 recovery

3.6.2. Determination of Processes Controlling Dissolved Inorganic Carbon

Determination of seasonal controls on DIC at the platform through the distinct seasonal intervals outlined above were derived through the use of an adapted diagnostic box model (Eq. 1C). A diagnostic box model approach is common practice in analysis of long duration time-series sites (Gruber et al. (1998); Brix et al. (2004); Keeling et al. (2004)). A diagnostic box model approach is useful in describing and analyzing relationships among a multivariate time-series dataset, making use of the high frequency data and temporal coverage granted by the platform. Specifically, the model simplified the complexities of influencing processes on the marine carbon system, allowing us to quantify seasonal processes observed at the platform. Following past examples, we designed a model to include various physical, chemical, and biological

processes contributing to the observed changes in computed DIC at the platform using the final carbon system sensor datasets (pH and pCO_2) and CO2SYS (Van Heuven et al., 2011) (Eq. 1C; Figure 7).

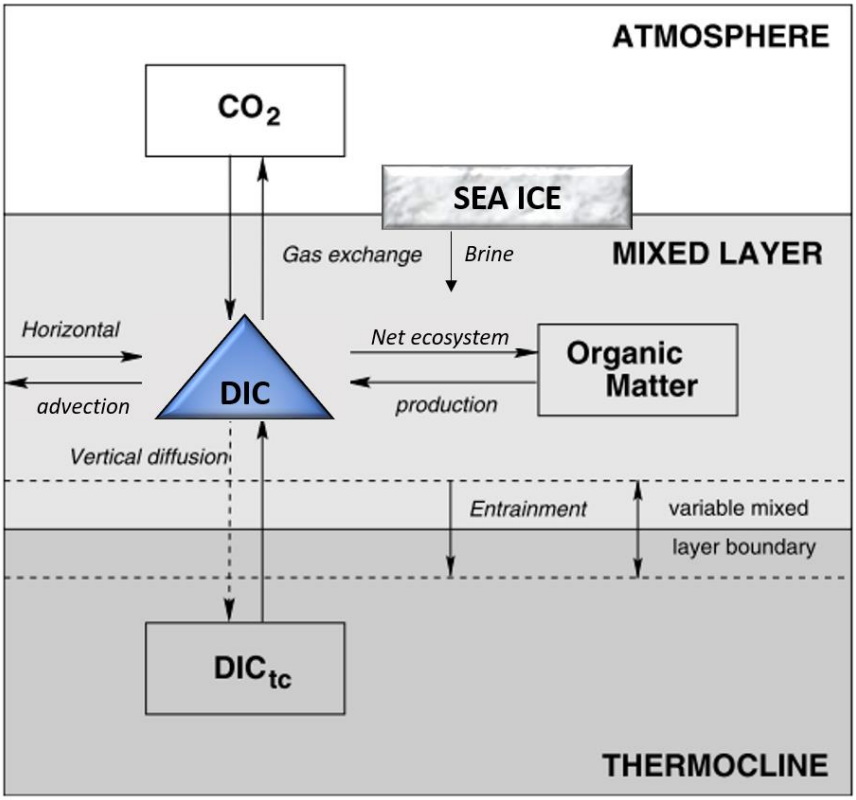

Figure 7 Schematic representation of the diagnostic box model used to compute changes in DIC due to air–sea exchange (C_{ex}), vertical diffusion (C_{diff}), horizontal advection (C_{adv}), entrainment (C_{ent}), salinity changes from sea ice growth/ melt and Freshwater Creek river input (C_{sal}), and biological controls (C_{bio}). The blue triangle represents the ONC CB platform. Adapted from Gruber et al. (1998) with permission from Elsevier.

Eq. 1C $$\frac{dDIC}{dt} = C_{ex} + C_{diff} + C_{adv} + C_{ent} + C_{sal} + C_{bio}$$

The model we used took into account methodologies spanning multiple studies (Else et al., 2012; Gruber et al., 1998; Shadwick et al., 2011) based on: air–sea exchange (C_{ex}), vertical diffusion (C_{diff}), horizontal advection (C_{adv}), entrainment (C_{ent}), salinity changes from sea ice

growth/ melt and river input (C_{sal}), and biological controls including photosynthesis/ respiration and calcium carbonate precipitation/ dissolution (C_{bio}). Assumptions were made similar to Else et al. (2012), Shadwick et al. (2011), and Gruber et al. (1998) for all source terms contributing to the total variation in DIC over the 2016-2017 ONC deployment interval, and are described below.

For C_{ex} we assumed that the summer mixed layer depth is sufficiently deep enough to encompass the ONC platform depth through the fall (Section 5.2.). The platform is therefore representative of the active air-sea gas exchange surface during the fall. C_{ex} was obtained using the bulk flux parameterization for air-sea gas exchange (Eq. 4A), scaled to incorporate sea ice concentration (Butterworth & Miller, 2016). Once sea ice reached a thickness of 0.1 m, air-sea gas exchange was assumed to be cut off (Loose et al., 2011) (Table 5). Gas transfer velocity was obtained using the Wanninkhof (2014) parameterization, with measured hourly wind speed from the nearby ONC metrological shore station. CO_2 solubility was calculated from temperature and salinity measured by the Sea-Bird SeaCAT SBE19plus V2 onboard the ONC platform, according to Weiss (1974). A constant value of 407 µatm was used for $pCO_{2(air)}$ (Eq. 5A), averaged from observed values reported by Butterworth & Else (2018) at a nearby eddy covariance tower in Dease Strait.

Important for C_{ent} and C_{diff} we needed to estimate the mixed layer depth the platform encompassed, as well as DIC concentration below the mixed layer. We used a cosine function estimate for the mixed layer depth [$h = 5\cos(\frac{5t}{365} - 9) + 23$] with an r^2 value of 0.98, compared to multiyear CTD measurements taken at station B1 (n = 17). The mixed layer depth

was defined using a density increase of 0.1 kg/m^3 as identified in CTD profiles (Peralta-Ferriz & Woodgate, 2015). The mixed layer depth estimate included a shoaling interval in the fall before deepening through the winter, followed by shoaling once sea ice reached near maximum thickness. Station B1 30 m bottle samples were used to estimate DIC concentration below the mixed layer [$DIC_{pyc} = 25\cos(\frac{5t}{365} - 8) + 2050$]. A cosine estimate was also used and did a good job of capturing seasonal variability while making use of poorly constrained bottle sample error, due to uncertainty during collection. DIC below the mixed layer estimate ranged from 2075 – 2096 µmol/kg, with the minimum occurring early in September and the maximum occurring in late February. The below mixed layer DIC estimate compared to the B1 30 m bottle samples returned an r^2 value of 0.39 (n = 13). Salinity below the mixed layer was based on B1 CTD casts (n = 22), and was assumed constant throughout the year (29.35±0.04 PSU) (Section 5.2.).

Eq. 2C $$C_{diff} = \frac{1}{h} K_v \frac{dDIC}{dz} \rho$$

Vertical diffusion is determined following methods outlined in previous studies (Gruber et al., 1998). In Eq. 2C, C_{diff} (µmol/kg day) is the diffusive flux, *h* is the mixed layer depth estimate, K_v (m^2/s) is the eddy diffusive coefficient, $dDIC/dz$ (µmol/kg m) is the vertical gradient of DIC between the surface mixed layer and within the pycnocline below the mixed layer (23 m from ONC platform depth to B1 30 m depth), and ρ (kg/m^3) is water density. Reported K_v values in the region were scarce in the literature so similar to Shadwick et al. (2011), we used the eddy diffusive coefficient from Rudels et al. (1996) (K_v = 1.1x10^{-6} m^2/s). For comparability this

diffusivity coefficient is of the same order of magnitude compared to heat and salt flux diffusive coefficients observed from below the mixed layer in Parry Channel (Melling et al., 1984).

Horizontal advection was assumed to be negligible throughout the entire deployment and is ignored in the box model. No strong horizontal DIC gradients were observed in CB at our ancillary data collection sites and currents are notoriously still through the winter. Lewis & Walker (1970) selectively choose CB in their study in an attempt to deal with circulation exclusively related to ice growth, as other processes influencing circulation through the winter are negligible. We therefore ignored horizontal advection as a potentially important influence on DIC.

Eq. 3C $$C_{ent} = \frac{1}{h}\left(\frac{dh}{dt}\right)\left(DIC_{pyc} - DIC_{onc}\right)$$

Vertical entrainment was estimated using simple vertical mixing caused by mixed layer deepening. In CB there exists a vertical gradient of DIC through much of the year. Entrainment of DIC from waters below the mixed layer are affected by variability in the mixed layer depth and can be described by Eq. 3C following Gruber et al. (1998). C_{ent} (µmol/kg day) is the entrainment flux, and *h* is the mixed layer depth estimate. DIC_{pyc} estimates DIC below the mixed layer, DIC_{onc} describes the DIC values at the platform computed from pH and pCO_{2sw} (Van Heuven et al., 2011). We did not calculate any change in DIC in the mixed layer due to entrainment for time periods where the mixed layer shoaled (approximately fall, spring and summer periods).

Eq. 4C $$C_{sal} = \left(\frac{dSal}{dt} - Sal_{ent}\right)\frac{\Delta DIC_{brine}}{\Delta Sal_{brine}}$$

Eq. 5C $$DIC_{\text{brine}} = 63.3(\text{Sal}_{brine}) + 24.7$$

C_{sal}, describes the influence of sea ice carbon rejection as computed based on salinity changes during the winter period. High density brine migrates down through the water column, changing salinity in the mixed layer containing the platform. Subtracting the salinity change due to entrainment from the total change in salinity during the winter, yields the change in salinity due to brine rejection (Eq. 4C). A brine salinity (Sal_{brine}) of 126 PSU was used from Miller et al. (2011). This value was chosen as there are limited reported literature values in similar conditions to CB (e.g. seawater salinity, freeze up timing and maximum ice thickness). Brine DIC was estimated from the relationship reported by Geilfus et al. (2012) based on salinity of brine and seawater samples (Eq. 5C). DIC for bulk sea ice and seawater samples are of the same order of magnitude as those reported by Miller et al. (2011) and Rysgaard et al. (2007) who both presented DIC and TA measurements from landfast sea ice in Franklin Bay, Canada. The relationship describing DIC in brine (Eq. 5C), yields a brine DIC concentration at a salinity of 126, as ~8000 µmol/kg.

Eq.6C $$C_{bio} = \frac{dDIC}{dt} - (C_{ex} + C_{diff} + C_{ent} + C_{sal})$$

The Shadwick et al. (2011) diagnostic box model assumed that any residual change in DIC not accounted for in gas exchange, vertical diffusion, and salinity source terms was caused by biological activity. The C_{bio} term in our study also takes this approach. Net ecosystem production (C_{bio}), as defined in this study, is the net effect of biological processes estimated from the difference between the total observed change in DIC ($\frac{dDIC}{dt}$) and the change accounted

for in C_{ex}, C_{diff}, C_{ent}, and C_{sal}. C_{bio} represents a generalized biology term inherently comprised of photosynthesis, respiration/ remineralization, $CaCO_3$ precipitation and dissolution, as well as exchanges of carbon with sediments, but also any error in both accounted for and unaccounted for processes.

4.0. Results: Sensor Assessment

In order to assess influencing seasonal processes on the marine carbon system at the platform, onboard carbon system sensor measurements needed to be validated and if necessary corrected. First we present results of additional inspection in assessing the SeaFET sensor performance. This initial section is meant to test built in onboard checks for the SeaFET to warrant reference measurement calibration.

4.0.1. SeaFET Thermistor Response

Before any carbon reference discrete sample comparisons, the SeaFET's internal thermistor was evaluated. Overall the internal thermistor displayed excellent alignment when compared to the co-located Sea-Bird SeaCAT SBE19plus V2 over both deployments (r^2 = 0.99). There was a mean temperature difference of 0.19°C, and 0.17°C, with a maximum difference of 9.73°C, and 0.29°C, resulting in a mean uncertainty of 0.0144 and 0.0015 pH over the 2016-2017, 2017-2018 deployments respectively. The maximum difference of 9.73°C in early 2016 was consistent with delayed thermistor response following a power outage. Although the correlation coefficient is high, the uncertainty values warrant some correction based on temperature.

4.0.2. Evolution of pH INT-EXT Anomalies

The dual-reference electrode configuration of the SeaFET provides a simple and powerful tool for detecting the effects of fouling or sensor failure when directly comparing pH_{raw}^{INT} and pH_{raw}^{EXT} through the deployment (Bresnahan et al., 2014; Rivest et al., 2016). Ideally

during a perfect sensor deployment there should be no difference between pH_{raw}^{INT} and pH_{raw}^{EXT}. In our study there is a noticeable difference between pH_{raw}^{INT} and pH_{raw}^{EXT} through both deployments. There is a mean difference of 0.0595, and 0.0323 $pH_{raw}^{INT-EXT}$ in 2016-2017 and 2017-2018 respectively. A large discrepancy exists during early deployment in fall of 2016 (Figure 8). There is a maximum difference of -0.1386 in the Δ $pH_{raw}^{INT-EXT}$ anomaly (pH_{raw}^{INT} < pH_{raw}^{EXT}) during this period. Gonski et al. (2018) observed larger magnitude changes in salinity (Δ 20 PSU), much more rapidly (< 12 hours) and reported Δ $pH^{INT-EXT}$ of > 0.15 pH units. Bresnahan et al. (2014) also reported Δ $pH^{INT-EXT}$ anomalies (< 0.005 pH units) following rapid salinity changes in a test tank. Bresnahan et al. (2014) suggested that a salinity lag may account for anomalies due to inadequate flushing of the instrument flow path and housing. The reduced rate of flushing in the SeaFET results in differences in the water sampled by the electrodes resulting in discrepancies between pH^{INT} and pH^{EXT}.

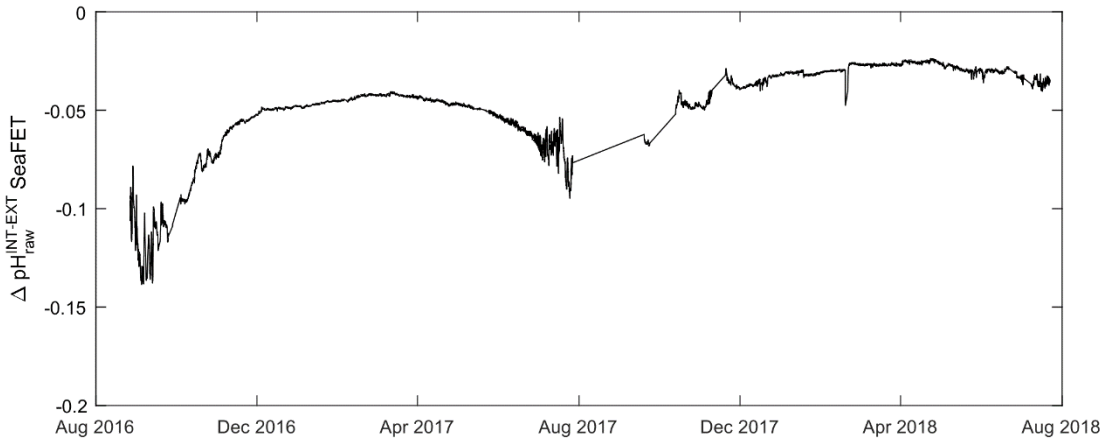

Figure 8 Δ $pH^{INT-EXT}$ during ONC 2016-2017, and 2017-2018 deployments.

Unlike the Δ $pH^{INT-EXT}$ anomalies reported by others, during the fall period in this study significant anomalies persist consistently for four weeks compared to only a few hours. In that time, salinity increased only 2.3 PSU while temperature decreased 5.5°C. The temperature swing even as gradual as was observed strongly correlated with the variability in Δ $pH^{INT-EXT}$ (r^2 = 0.83). Given that the anomaly is persistent through the interval of highest environmental variability coinciding with the deployment conditioning period (Table 2), it is difficult to discern the cause. Looking at the same period during the 2017-2018 deployment, temperature and salinity remain relatively constant and the anomaly remains relatively small ~0.05 pH. Any variability in Δ $pH^{INT-EXT}$ apart from zero is reason for concern, and makes a strong case for sensor data correction post-deployment based on new calibration coefficients.

4.1. Discrete Sample Comparison

Here we present results of discrete sample reference comparisons to the deployed SeaFET and CO2-Pro sensor measurements on the platform through each deployment. This section is meant to determine sensor accuracy based on factory calibrations relative to reference pH and pCO_2.

4.1.1. SeaFET Evaluation

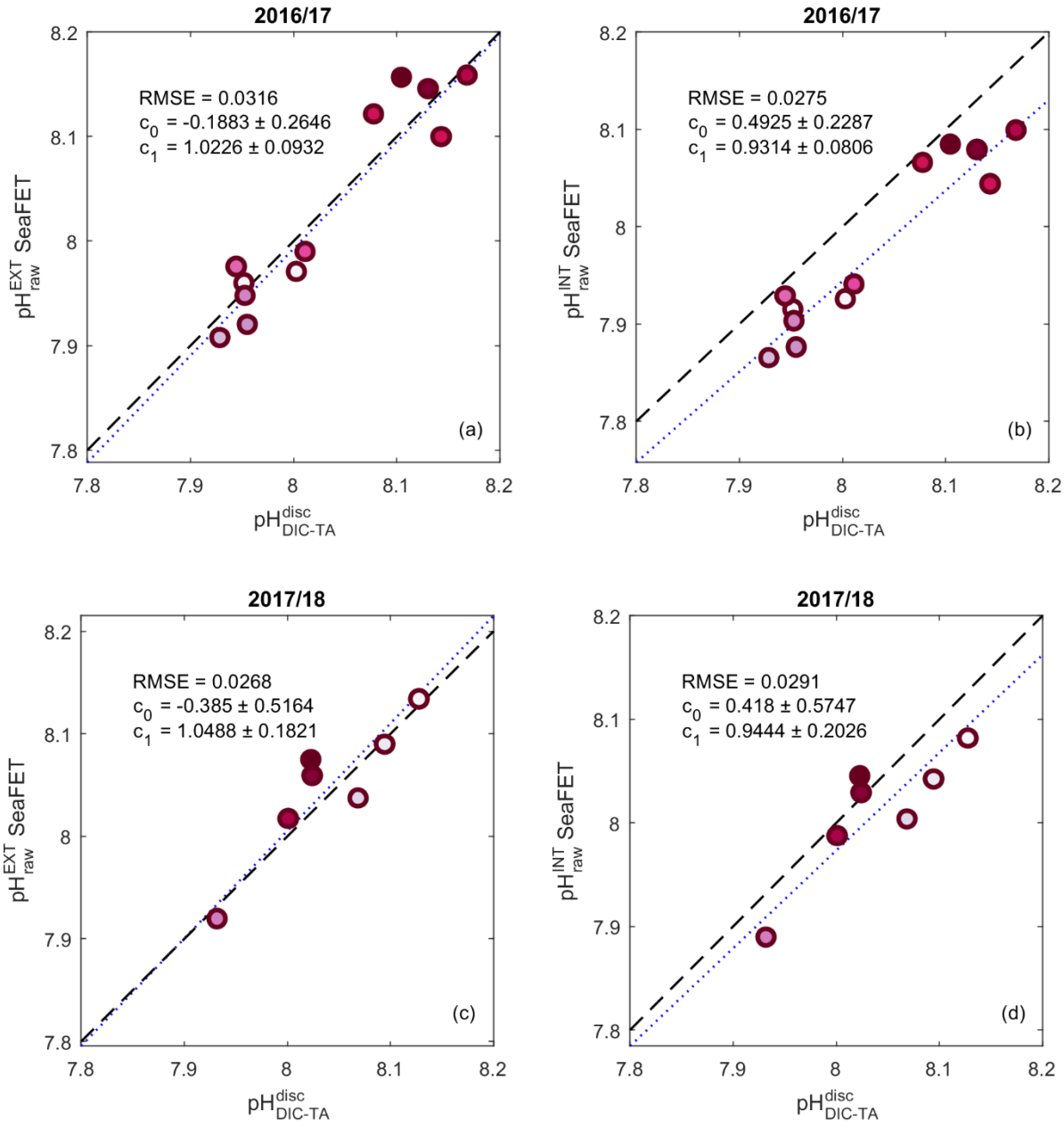

Figure 9 Property to property plots of raw SeaFET sensor pH and discrete sample pH from CO2SYS. Type II linear regression was used to calculate slope (c1), intercept (c0), and root mean square error (RMSE). The relationship is visualized by the dotted blue line. The dashed red line represents a perfect fit of c1 = 1 and c0 = 0. The color coding is used to compare samples relative to deployment time, as the light color is early in deployment getting darker as deployment continues.

The Satlantic SeaFET Ocean pH Sensor SN 246 preformance during the 2016-2017 deploment interval displayed a large difference between both pH_{raw}^{INT} and pH_{raw}^{EXT} in comparision to 13 viable pH_{DIC-TA}^{disc} reference values (Figure 9a-b). Sensor minima and maxima values corresponded to late winter and early summer time periods respectively, with a range of 7.90-8.13 pH. There is a mean difference of -0.0591±0.0292 pH units between pH_{raw}^{INT} and pH_{DIC-TA}^{disc} with the FET|INT consistently underestimating pH. This underestimation is reflected in the Model II least squares fit with the FET|INT showing the largest sensor offset (c0) being statistically different from 0, observed through all deployments (Figure 9b). The slope (c1) is close to 1 and demonstrates no drift. The mean difference between the pH_{raw}^{EXT} and pH_{DIC-TA}^{disc} is -0.0061±0.0313 with FET|EXT inconsistently both over and underestimating pH compared to the reference. The inconstancy in FET|EXT resulted in the largest standard deviation of difference across all deployments (±0.0313). The FET|EXT exhibits a much closer relationship to the ideal fit with c0 close to 0, and c1 close to 1 (Figure 9a). The RMSE reflects the accuracy of the sensor pH relative to discrete sample pH at 0.0275 and 0.0316 pH units for the single point factory calibrated FET|INT and FET|EXT respectively. Both independent electrodes showed no distinguishable drift with deployment duration as points are randomly distributed around the fit line (Figure 9a-b).

The Satlantic SeaFET Ocean pH Sensor SN 452 preformance during the 2017-2018 deploment interval produced a tighter relationship between both pH_{raw}^{INT} and pH_{raw}^{EXT} with the 7 viable pH_{DIC-TA}^{disc} reference values compared to SN 246 (Figure 9c-d). Again sensor minima and maxima pH values corresponded to late winter and early summer time periods respectively, ranging

from 7.85-8.12. There is a mean difference of -0.0288±0.0301pH units between pH_{raw}^{INT} and pH_{DIC-TA}^{disc} with the FET|INT underestimating pH during the start of deployment while overestimating compared to the last two reference samples. The Model II least squares fit for the FET|INT displays a offset close to 0 but a slope slightly further from 1 compared to other relationships (Figure 9d). The distribution of points about the fit line with time shows a pattern of increasing distance from the fit as deployment duration increased. This could be potential drift, however it is not statistically significant to a meaningful degree (*p*-value = 0.6) based on the number of reference points and uncertainly associated with the discrete samples. The mean difference between the pH_{raw}^{EXT} and pH_{DIC-TA}^{disc} is 0.0073±0.0264 with FET|EXT both over and underestimating pH compared to the reference through the deployment. The FET|EXT displayed a much closer relationship to the ideal fit with c0 closer to 0, and c1 closer to 1 compared to the FET|INT (Figure 9c). However, the distribution of points about the fit line with time shows the same pattern of drift as compared to FET|INT, but is again statistically insignificant (*p*-value = 0.6). The RMSE reflects the accuracy of the sensor pH relative to discrete sample pH at 0.0291 and 0.0268 pH units for the single point factory calibrated FET|INT and FET|EXT respectively.

4.1.2. CO2-Pro Evaluation

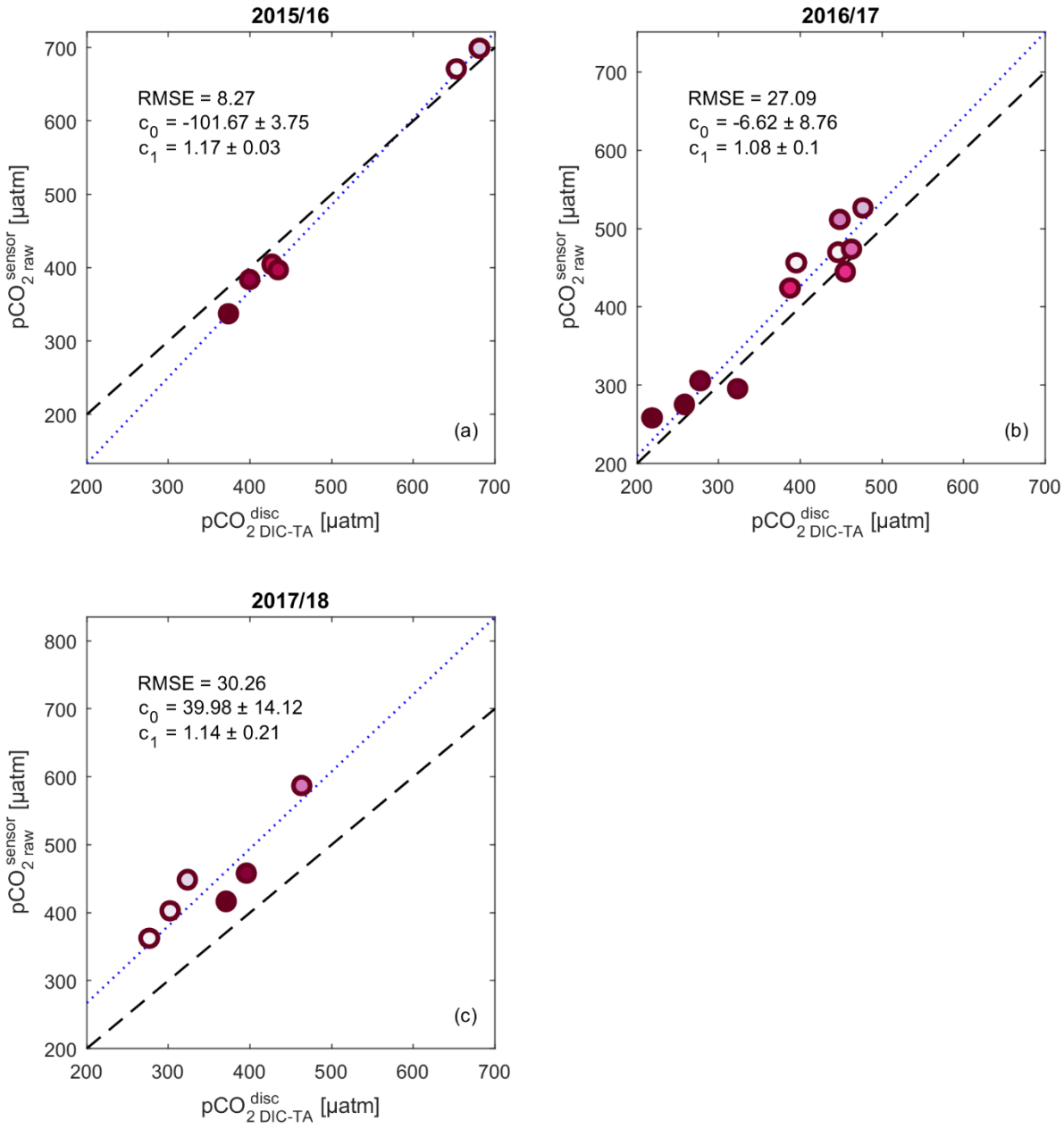

Figure 10 Property to property plots of raw CO2-Pro sensor pCO_2 and discrete sample pCO_2 from CO2SYS. Type II linear regression was used to calculate slope (c1), intercept (c0), and root mean square error (RMSE). The relationship is visualized by the dotted blue line. The dashed red line represents a perfect fit of c1 = 1 and c0 = 0. The color coding is used to compare samples relative to deployment time, as the light color is early in deployment getting darker as deployment continues.

During the 2015-2016 deplomentinterval the Pro-Oceanus CO2-Pro CV (SN 35-250-75) displayed the best fit compared to other deployments in comparision to 6 viable $pCO_2{}_{DIC-TA}^{disc}$ reference values (Figure 10a). Sensor minima and maxima values corresponded to early summer and late winter time periods respectively, ranging from 331-698 µatm. There exists a difference of -14.95±25.09 µatm between $pCO_2{}_{raw}^{sensor}$ and $pCO_2{}_{DIC-TA}^{disc}$ with the CO2-Pro mostly underestimating pCO_2. The sensor offset (c0) and slope (c1) from our fit yields values significantly skewed by the distribution of data points, particularly from winter collection corresponding to the captured pCO_2 maxima (Figure 10a). The RMSE reflects the accuracy of the sensor pCO_2 relative to discrete sample pCO_2 at 8.27 µatm.

The performance of the Pro-Oceanus CO2-Pro CV (SN 36-314-75) during the 2016-2017 deployment compared to 11 viable $pCO_2{}_{DIC-TA}^{disc}$ reference values is shown in Figure 10b. Sensor minima and maxima values corresponded to early summer and late winter time periods respectively, ranging from 257-530 µatm. There exists a difference of 24.56±28.33 µatm between $pCO_2{}_{raw}^{sensor}$ and $pCO_2{}_{DIC-TA}^{disc}$ with the CO2-Pro dominantly overestimating pCO_2. The sensor offset (c0) and slope (c1) from our fit yields values closest to ideal sensor deployment compared to other deployments (Figure 10b). The RMSE reflects the accuracy of the sensor pCO_2 relative to discrete sample pCO_2 at 27.15 µatm. The points are randomly distributed about the fit line showing an indistinguishing trend with distance from fit over time, with close groupings at the beginning and end of deployment (Figure 10b).

Pro-Oceanus CO2-Pro CV (SN 35-250-75) displayed the largest observed offset during the 2017-2018 deplomentinterval in comparision to 6 viable $pCO_{2}^{disc}_{DIC-TA}$ reference samples (Figure 10c). Sensor minima and maxima values corresponded to early summer and late winter time periods respectively, ranging from 361-585 µatm. There exists a difference of 88.25±32.21 µatm between $pCO_{2}^{sensor}_{raw}$ and $pCO_{2}^{disc}_{DIC-TA}$ with the CO2-Pro quite significantly overestimating pCO_2 through the entire deployment. The sensor offset (c0) and slope (c1) from our fit yields a fairly good sensor slope (c1) being close to 1 (1.14±0.21), but a large sensor offset (c0) that is statistically significantly different from zero (*p*-value < 0.1) (Figure 10c). The large offset remained consistent throughout the deployment with the largest difference in $pCO_{2}^{sensor}_{raw}$ and $pCO_{2}^{disc}_{DIC-TA}$ occurring in November and February at 122.80 µatm, and 121.09 µatm respectively. The RMSE reflects the accuracy of the sensor pCO_2 relative to discrete sample pCO_2 at 30.26 µatm.

4.2. Sensor Correction

Sensor correction for both instruments during all deployments was deemed necessary to produce final pH and pCO_2 values for biogeochemical process interpretation and distinguishing seasonal trends. Tested methods of correction from raw factory single point calibration for the SeaFET (Section 3.3.1.) and factory multipoint for the CO2-Pro (Section 3.3.2.) included: factory end point calibration, single point *in situ* calibration, and multi-point *in situ* calibration. Method of correction varied instrument to instrument and needed to consider: neglected steps in sensor pre-deployment procedures, mechanical issues resulting in sensor

offset or drift through deployment, and sensor failure resulting in the abrupt end of data collection.

Table 6 Sensor calibration method summary. Shown are single point factory calibration (SPF), multi-point factory calibration (MPF), multi-point in situ calibration (MPis). Not shown are individual single point in situ calibrations and factory end point calibrations.

Sensor ID	Deployment	Electrode	Calibration Method	RMSE	c0 (Intercept)	c1 (Slope)
Satlantic SeaFET Ocean pH Sensor						
SN 246	2016-2017	FET|INT	SPF	0.0275	0.4925±0.2287	0.9314±0.0806
SN 246	2016-2017	FET|EXT	SPF	0.0316	-0.1883±0.2646	1.0226±0.0932
SN 246	2016-2017	FET|INT	MP*is*	0.0273	0.5705±0.2272	0.9291±0.0800
SN 246	2016-2017	FET|EXT	MP*is*	0.0304	0.0418±0.2543	0.9948±0.0896
SN 452	2017-2018	FET|INT	SPF	0.0291	0.4180±0.5747	0.9444±0.2026
SN 452	2017-2018	FET|EXT	SPF	0.0268	-0.3850±0.5164	1.0488±0.1821
SN 452	2017-2018	FET|INT	MP*is*	0.0291	0.4454±0.5757	0.9446±0.2030
SN 452	2017-2018	FET|EXT	MP*is*	0.0377	0.4902±0.8082	0.9390±0.2850
Pro-Oceanus CO2-Pro CV						
SN 35-250-75	2015-2016		MPF	8.27	-101.67±3.75	1.17±0.03
SN 36-314-75	2016-2017		MPF	27.15	-6.63±8.78	1.08±0.10
SN 35-250-75	2017-2018		MPF	30.26	39.98±14.12	1.14±0.21

4.2.1. SeaFET Correction

SeaFET sensor correction was necessary as there were noted discrepancies in pH_{raw}^{INT} and pH_{raw}^{EXT} through both deployments (Figure 8), as well as the temperature discrepancies in the SeaFET thermistor response (Section 4.0.1). Correction methods were evaluated to yield lowest RMSE while remaining consistent in correction method across deployments. Both SeaFET SN 246 and SN 452 had roughly similar evaluations in FET|INT and FET|EXT performance over their respective deployment intervals (Figure 9). Neither had evidence of statistically significant drift (c1) and both displayed offsets (c0) near 0.

Single point *in situ* calibrations for all 13 and 7 discrete samples respectively were used to generate new calibration coefficients (Eq. 1B – 3B) to correct SN 246 and SN 452. SN 246 (2016-2017 deployment) displayed no distinguishable trend between *in situ* single point calibrations improving sensor performance taken at any particular time during deployment (data not shown). Differences in RMSE were comparable across all *in situ* single point calibrations in SN 246 when compared to factory single point calibrated data. *In situ* single point calibration improvement of RMSE ranged from 0.001-0.003 pH units in FET|INT, and 0.011-0.013 pH units in FET|EXT. A multi-point *in situ* calibration was determined to be the most robust and applicable given the long deployment interval (~12 months), yielding an improvement of 0.002 and 0.012 in FET|INT and FET|EXT pH respectively (Table 6). In SN 246 the consistent underestimation of pH in FET|INT (Figure 9b), and high standard deviation in pH difference between the FET|EXT and the reference were corrected.

In SN 452 (2017-2018), there was again no distinguishable trend between *in situ* single point calibrations improving sensor performance at any particular time during deployment (data not shown). *In situ* single point calibration at any point during deployment did not change RMSE from the factory single point calibration for FET|INT. A multi-point *in situ* calibration also did not change RMSE and had little effect on improving sensor drift or offset, keeping all measures of performance relatively the same (Table 6). FET|EXT had a profoundly different result when the raw voltage dataset incorporated new calibration values (Eq. 2B). RMSE of fit compared to discrete samples increased between 0.0108-0.0109 pH units with *in situ* single point calibrations, reducing the accuracy of the sensor pH relative to discrete sample pH. Multipoint

in situ calibration yielded similar results with a reduction of sensor accuracy relative to references from 0.0268 to 0.0377 pH units (Table 6).

Given that both deployment pH datasets required correction based on $\Delta\, pH^{INT-EXT}$ anomalies and temperature discrepancies, the *in situ* multipoint calibration method was determined to be the most applicable for both electrodes to maintain consistency. The final corrected sensor pH time-series of ONC over both deployments is shown below (Figure 11). Given the RMSE values of the final dataset (Table 6), the uncertainty in SeaFET sensor accuracy over both deployments lies outside of the "climate level" quality data product designation with an uncertainty greater than 0.003 in pH (Newton et al., 2015). However, all deployments preformed within the order of magnitude needed to reach "weather level" data, lying just outside the uncertainty cutoff of 0.02 pH units.

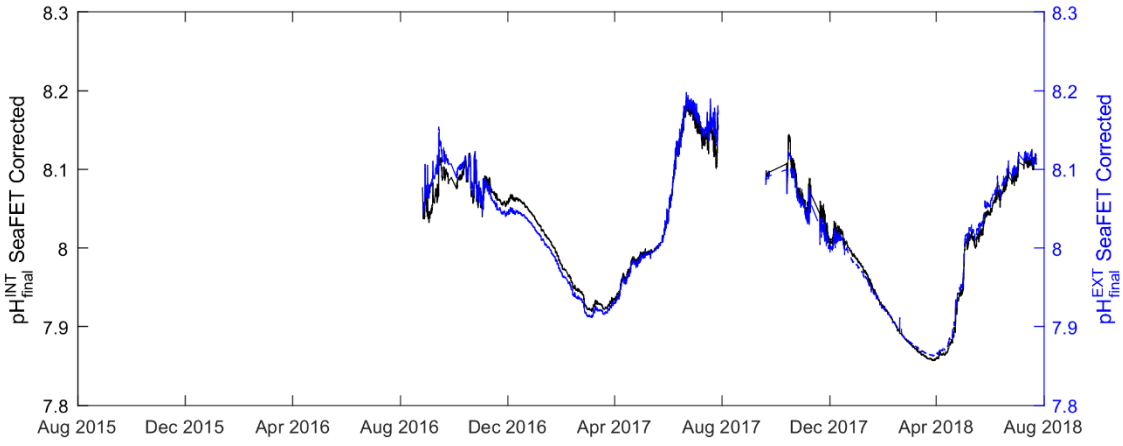

Figure 11 Final corrected SeaFET sensor pH for SN 246 and SN 452 over the 2016-2017 and 2017-2018 deployments respectively.

4.2.2. CO2-Pro Correction

The two Pro-Oceanus CO2-Pro CV sensors had varied results through three deployments capered to discrete samples. During the 2015-2016 deployment, SN 35-250-75 had issues with power outages and zero point calibration equilibration rebounding (Section 4.0). However, SN 35-250-75 still performed quite well relative to discrete sample pCO_2 (RMSE = 8.27 µatm). Based on the fit of sensor data compared to reference data (Figure 10), correction of CO2-Pro data based on the produced offset coefficient (c0) was determined to be inadequate (Table 6). Instead of c0, the average difference of $pCO_{2_{raw}}^{sensor}$ and $pCO_{2_{DIC-TA}}^{disc}$ acted as the multipoint *in situ* sensor offset correction. The trend in differences reflected the result shown earlier (Figure 9a), of SN 35-250-75 dominantly underestimated pCO_2. An average sensor difference of -14.95 µatm acted as the correction factor, increasing sensor pCO_2 by a constant throughout the deployment (Figure 12). The constant seems appropriate as Pro-Oceanus followed up with a post deployment multipoint factory calibration using National Institute of Standards and Technology traceable CO_2 calibration gases, returning a mean difference of -24.15±5.46 µatm with four gas standards having a greater than zero CO_2 concentration. This is within the standard deviation (±22.90) of our discrete sample comparison inferred offset used for correction.

CO2-Pro SN 36-314-75 during the 2016-2017 deployment showed no indication of significant drift or offset (Figure 10b; Table 6). However the RMSE of the sensor compared to reference samples was 27.15 µatm. This RMSE is more an indication of uncertainty in the reference DIC-TA discrete samples used for comparison. Of the total 23 samples that were collected from

January to the beginning of August in 2017, 10 were deemed unfit for sensor evaluation (Section 3.4.). This reflects somewhat poorly on the remaining 13 samples used in sensor correction as similar methods were used to collect, store and analyze. However, obvious indicators to discard the remaining samples were not present (Section 3.4.1.). The correction method used was the same as SN 35-250-75 during the 2015-2016 deployment, utilizing the inferred sensor offset from the mean sensor difference compared to reference values (Figure 12). There exists a difference of 24.41±26.95 µatm, where the standard deviation is larger than the mean value as the sensor fluctuated randomly in both over and underestimation throughout the deployment. Unfortunately there was no post deployment multipoint factory calibration as the infrared lamp failed on 2017-06-27, before platform recovery on 2017-09-02.

SN 35-250-75 was recalibrated and redeployed for the 2017-2018 interval. The fit yielded a fairly good sensor slope (c1), but a large sensor offset (c0) that is statistically significantly different from zero (Table 6). During 2015-2016, SN 35-250-75 intercept (c0) was skewed by the natural pCO_2 sampling range; which is not the case in 2017-2018. SN 35-250-75 quite significantly overestimated pCO_2 through the entirety of the deployment with a difference relative to reference values of 88.25±29.41 µatm. The large inferred sensor offset was corrected by decreasing sensor pCO_2 by a constant, being the mean difference to reference values (88.25 µatm), throughout the deployment (Figure 12).

The final corrected sensor pCO_2 time-series of ONC over all three deployments is shown below (Figure 12). Over the 2015-2016 and 2017-2018 deployments only six discrete samples were used as reference carbon system data to evaluate then correct pCO_2 sensor performance. This

value is likely approaching the minimum number needed to confidently constrain sensor behavior post-deployment. Given the inability to correct and validate using the same reference samples compared to the CO2-Pro sensor, a new RMSE of the final dataset could not be produced (Table 6). Given this condition on the method of correction we cannot confidently categorize any CO2-Pro deployment as producing a “climate level” quality data product (Newton et al., 2015). However, all deployments are very close to “weather level” cutoffs (uncertainty of 2.5% in pCO_2), offering a promising dataset for investigating regional seasonal biogeochemical influences.

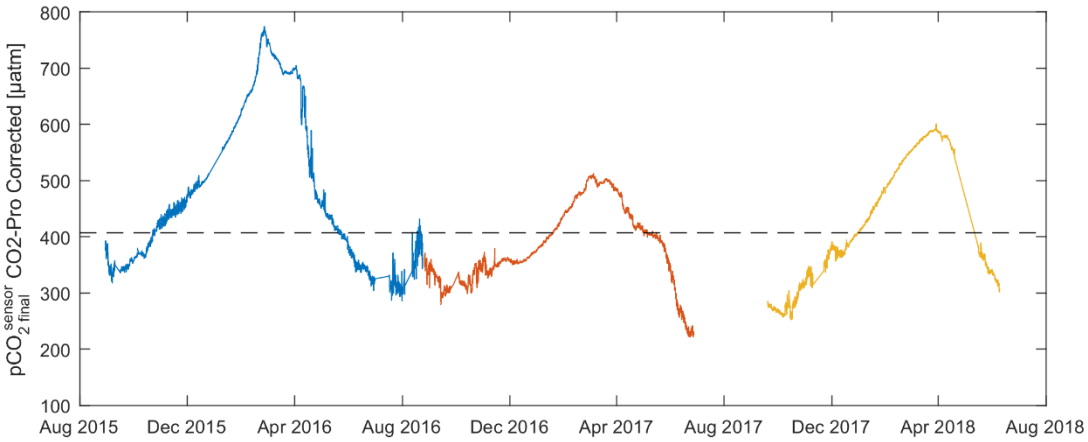

Figure 12 Final corrected CO2-Pro pCO_2 for SN 35-250-75, SN 36-314-75, and again SN 35-250-75 over the 2015-2016, 2016-2017 and 2017-2018 deployments respectively.

5.0. Results: Oceanographic Setting

In the previous section, the final corrected sensor pH and pCO_2 plots at the platform clearly indicate seasonal trends and inter-annual variability (Figure 11-12). Based on these plots there is significant potential to describe influencing biogeochemical controls on the carbon system over a complete cycle of sea ice growth and melt at the platform. However, in order to describe processes and build a carbon budget, we need to understand the oceanographic context of what the near-shore subtidal site where the platform resides in CB represents. In order to establish this context we looked at the broader oceanographic setting in CB. Extended spatial sampling was used to determine if/ when the platform could accurately estimate air-sea gas exchange of CO_2 at the site, and how the site represents carbon cycling further off shore. The sampling period providing the most extensive temporal coverage in space was from January until November 2017 (Figure 13).

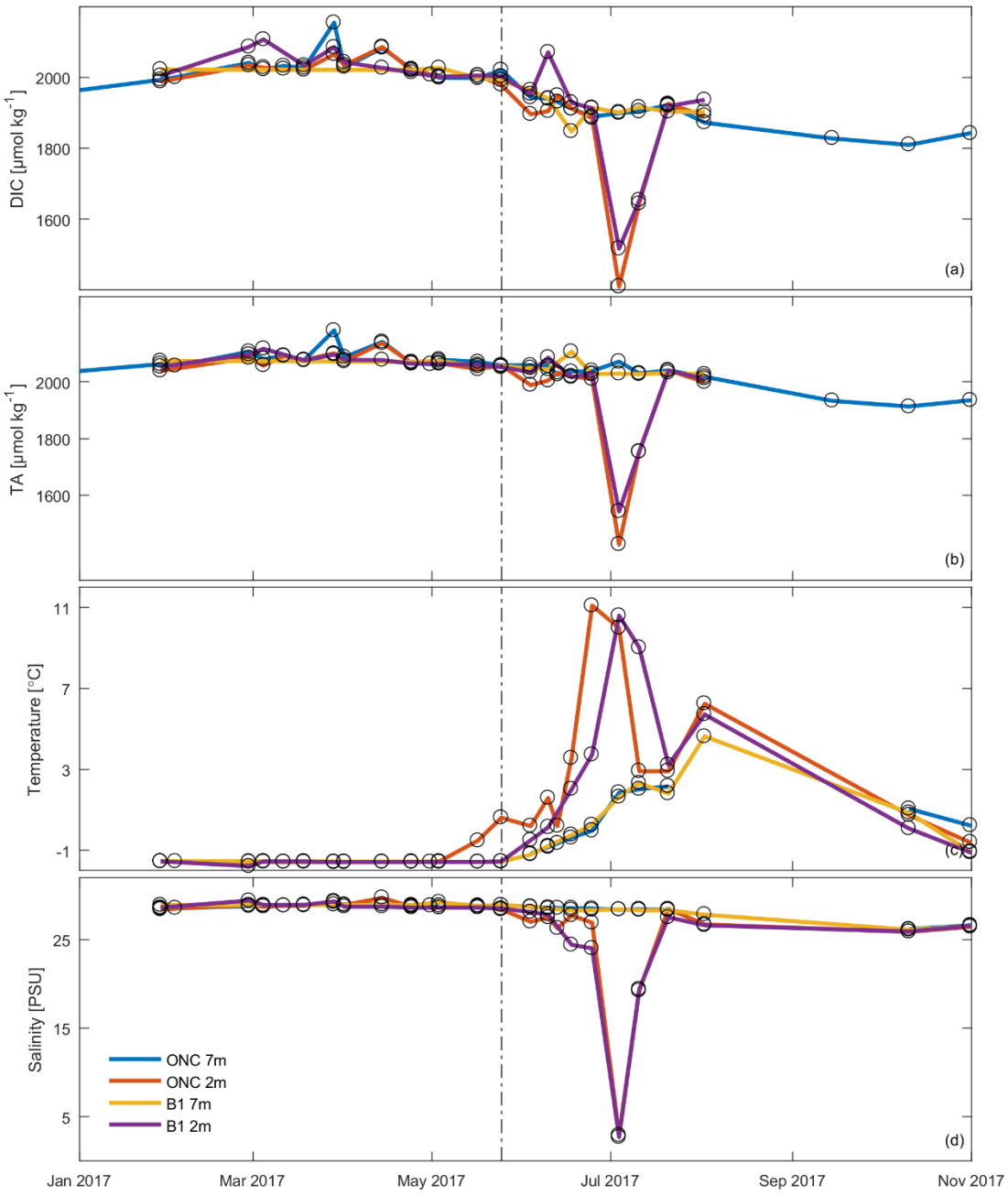

Figure 13 Discrete sample DIC, TA, temperature, and salinity at ONC 7 m, ONC 2m, B1 7 m, and B1 2 m from January through November 2017. Spring transition is denoted by the vertical dashed black line (2017-05-24, when sea ice reached a maximum thickness).

5.1. Discrete Sample Oceanographic Setting

During the extended spatial sampling regime, DIC and TA discrete samples were collected from January to August 2017 at the ONC platform depth (ONC 7 m), ONC surface, B1 7 m depth, and B1 surface (Figure 13a-b). Focusing on the platform depth, it appears the platform mirrors trends in DIC and TA at the ONC and B1 surface through the winter months and into the late spring (Figure 13a-b). As displayed in Figure 13a-b, DIC and TA significantly decrease around early July 2017 in the surface sites. The surface and 7 m depth at both ONC and B1 chemically diverge on July 3rd and July 10th 2017, as DIC and TA values at the surface plummet (~1400 µmol/kg). This is likely caused by some combination of river runoff from Freshwater Creek (Figure 6), and sea ice melt. Peak discharge from Freshwater Creek typically occurs during late June/ early July (Environment and Natural Resources Canada, 2019). The input of melt water chemically isolates the air-sea interface layer from detection by the platform during this time. Following the freshet period (July 20th 2017), DIC and TA values in the surface rebound to values characteristic of the developing summer surface mixed layer (Figure 13a-b).

Looking at the correlation coefficients for ONC 7m compared to all other locations (Table 7), it is immediately clear that the B1 7 m depth further off shore remains well represented by the platform year round (Table 7). There is substantially greater correlation between ONC 7 m DIC and TA with all other locations outside of the two week freshet period (Table 7). This is particularly true when comparing the platform depth with ONC 2 m and B1 2 m, where r^2 values increase once the chemically divergent dates are removed (July 3rd and July 10th 2017) (Table 7).

Table 7 Person's r comparisons of discrete sample DIC and TA at ONC 7 m compared to ancillary collection locations.

Person's *r* table	**ONC 2m**	**B1 2m**	**B1 7m**
All discrete sample values			
DIC [µmol/kg]	0.669	0.626	0.881
TA [µmol/kg]	0.284	0.269	0.334
Discrete samples excluding freshet dates (July 3rd, July 10th 2017)			
DIC [µmol/kg]	0.928	0.757	0.919
TA [µmol/kg]	0.810	0.698	0.865

Evaluating the discrete samples within the broader physical oceanographic setting in Figure 13c-d provides great clarity for processes influencing representation of the platform compared to the surface and further offshore. The winter sampling *in situ* conditions at the platform are very representative of the broader winter mixed layer within CB. Trends in salinity remain tight between the platform depth (ONC 7 m), ONC surface, B1 7 m and B1 surface through the winter and spring until June 3rd 2017 (Figure 13d). Melt pond drainage through open holes in the ice coupled and increased permeability of the ice act to separate the surface water salinity from the platform for nearly four weeks until June 24th 2017 (average difference of 1.5±0.5 PSU). Ice melt continues to decrease surface salinity until the Freshwater Creek freshet dominates the surface waters once ice is cleared from the bay. Through the next two weeks (July 3rd and 10th 2017) the surface (upper 0.5 m) and the platform are separated by even greater saline stratification of > 25 PSU (Figure 13d). Once the Freshwater Creek spring pulse recedes, the platform is again representative of the surface layer with respect to salinity on July 20th 2017 heading into the summer.

Temperature looks significantly different compared to salinity as the surface and underlying water are warmed at drastically different rates, with warming occurring nearly two weeks

earlier than the observed salinity changes (Figure 13c). The near shore surface water at ONC warms earlier on May 16th 2017 compared to the B1 surface site approximately two weeks later on June 3rd 2017 (Figure 13c). The delay in warming at B1 could be attributed to ONC being closer to shore experiencing an effect caused by the high specific heat capacity of the nearby coast. As temperatures increase at the surface as early as May 16th 2017, the platform becomes increasingly isolated from the active air-sea gas exchange layer (maximum difference of 10.9°C), but continued to represent the 7 m depth further into the bay at B1 (Figure 13c). On July 10th 2017, nearly eight weeks later the platform depth was again thermally representative of the surface as the summer surface mixed layer increased with turbulence, and received solar radiation decreased going into the Arctic summer.

5.2. Seasonal Water Column Oceanographic Setting

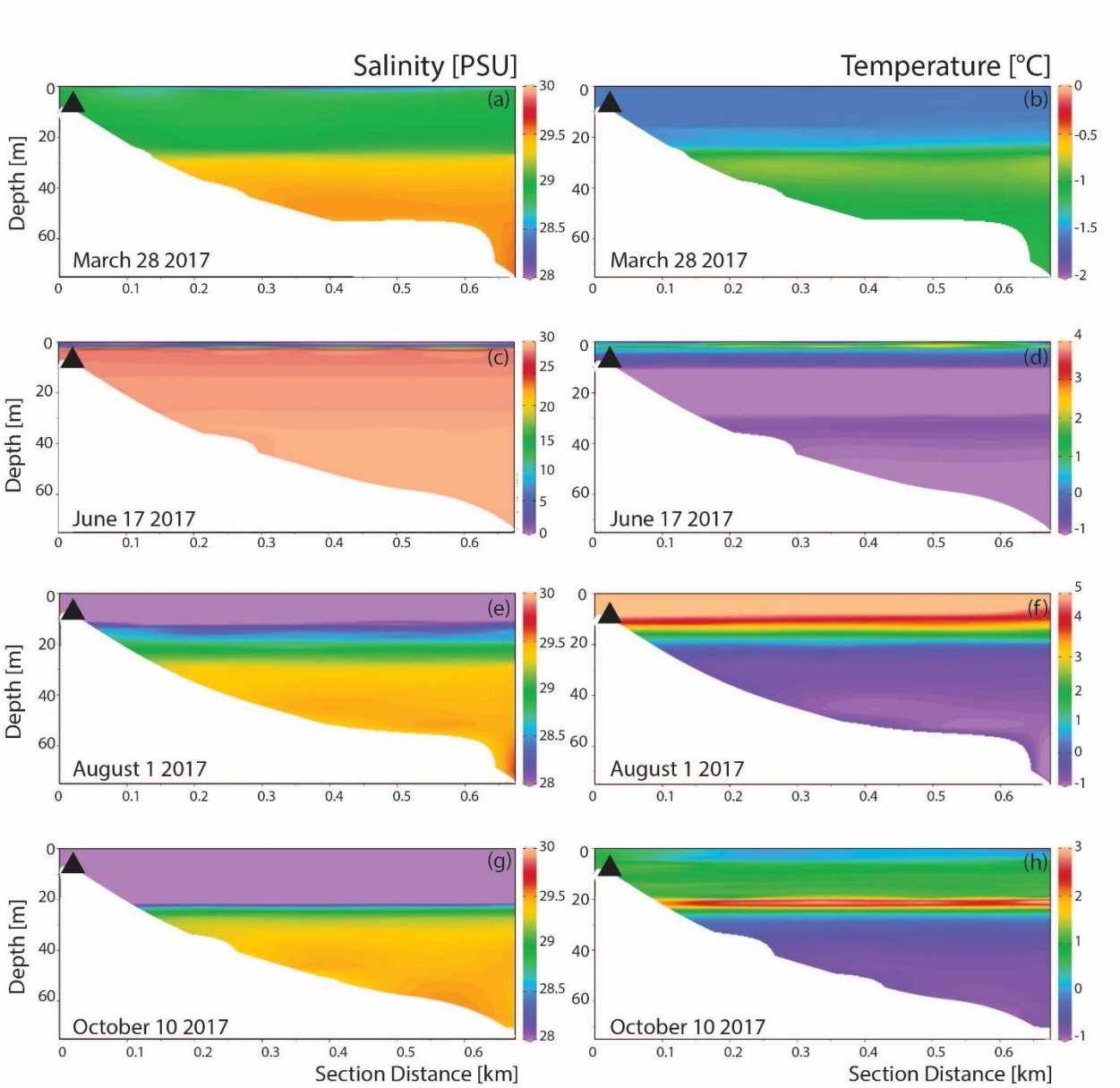

Figure 14 Salinity (left column) and temperature (right column) transects interpolated from RBR Concerto CTD measurements taken across CB, from ONC to B1 over March 28th (max ice thickness), June 17th (sea ice melt), August 1st (open water), and October 10th 2017 (sea ice formation). Note the different salinity color scale in c, and temperature color scale in b, d, f, and h. The ONC platform location is denoted by a black triangle.

CTD casts were used to interpret the physical oceanographic representation of the platform within CB throughout the year. Representative sample dates were selected as to best show environmental variability in the bay though the cycle of sea ice melt and formation (Figure 14). Dates include coverage of near sea ice maximum thickness in late winter (March 28th 2017), spring sea ice melt (June 17th 2017), summer open water (August 1st 2017), and early sea ice formation in the fall (October 10th 2017).

March 28th 2017 depicts the conditions typical of an under-ice winter water column. Sea ice was near maximum thickness at 1.28 m thickness. The thermocline, halocline, and pycnocline simultaneously co-exist at a depth of ~25 m. The deep surface mixed layer was a result of sea ice growth through the winter. There exists a temperature inversion as the coldest waters are located at the ice-water interface (~-1.6°C), with warming through the thermocline reaching a maximum temperature of ~-0.8°C at ~25 m (Figure 14b). Water temperatures below the thermocline continuously decrease through the annual bottom water.

During sea ice melt on June 17th 2017, the ice was nearly bare of snow cover, following the draining of surface melt. Salinity in the upper 2 m of the water column ranged from 2-4 PSU, and within 0.5 m depth, salinity increased to 27 PSU (Figure 14c). There exists a three-step halocline, at depths of 2.5, 11, and 28 m. The fresh water lens above 2.5 m was dominated by sea ice melt and surface drainage, and is very warm (~2°C). Waters between 2.5- 11 m are within a distinct steep thermocline with temperature dropping nearly 3°C from the surface (Figure 14d). Located between 11-28 m are the coldest waters with a consistent temperature ~-

1.4°C and salinities resembling those of the winter surface mixed layer (Figure 14a). Below 28 m were annual bottom waters.

During the summer into the open water season on August 1st 2017, the multi-step halocline has degraded through mixing enhanced by mobile sea ice during breakup, and wind driven mixing following complete open water sea surface coverage. The upper 5 m were thermally isolated as high Arctic radiative forcing had driven warming in the surface to ~6°C (Figure 14f). Below the surface co-existed a shallow sloped thermocline, halocline, and pycnocline down to ~25 m depth.

As sea ice started to form again on October 10th 2017, the summer surface mixed layer at the end of the season was clearly defined as wind mixing and tidal influences stirred up the bay through August and September to create a more definitive thermocline and halocline at 20 m (Figure 14g-h). Salinity was the dominant driver of density differences at this time of the year. As salts in sea ice brine are rejected into the underlying water, a source of potential energy is created for driving vertical convection currents, deepening the surface mixed layer under the ice. The thermocline is inverted due to surface cooling during sea ice formation (Figure 14h). Temperatures are just below 0°C at the surface as mobile pancake ice covered the majority of the sea surface. In the upper 5 m existed a shallow sloped thermocline. From 5-20 m depth in the water column temperatures remains relatively constant around 1°C. There exists an extremely steep thermocline to the temperature maximum of nearly 3°C at a depth of 20 m. Below 20 m temperature continuously decreases in the underlying water showing similar structure to that of the late winter profile (Figure 14b).

5.3. Oceanographic Summary

In an effort to understand the oceanographic context of the near-shore, subtidal location of the platform, an expanded spatial sampling regime was implemented. Overall, chemical (DIC and TA) and physical (temperature and salinity) *in situ* conditions at the platform depth and location are very representative of the greater oceanographic setting within CB (Figure 13-14). The platform is most representative of the greater sea surface mixed layer in CB following sea ice formation, and the development of a deep winter mixed layer. The site continues to be representative of the under-ice surface layer through the winter into the spring. Through the spring and summer the platform depth is thermally isolated from the surface layer for eight weeks due to radiative forcing. When solving for air-sea gas exchange thermal decoupling is critical, as even if DIC and TA values are similar, pCO_2 values used to solve for ΔpCO_2 (Eq. 4A & 5A) will be drastically different based on solubility in the temperature gradient to the surface. The platform is also stratigraphically isolated by salinity during sea ice melt, and Freshwater Creek discharge, which both bring chemically distinct waters to the surface layer of CB. The saline isolation of the platform from the surface occurs over approximately six weeks, but is offset, occurring two weeks later compared to surface warming. The physical and chemical forcing in the late spring isolate the platform from the air-sea interface, rendering the ONC platform inoperative in estimating air-sea CO_2 flux during this time period. It appears that into the summer the platform is again representative of the surface as the summer mixed layer becomes more developed into August. Given our observations, the platform was only limited during eight weeks (May 16th 2017 - On July 20th 2017) in estimating air-sea gas exchange of

CO_2 as it is isolated from the surface layer. The platform becomes useful again in this regard into the late summer and fall, before freeze up. The site is however very representative of carbon cycling further off shore year round, as evidenced by the strong correlation throughout the year at the B1 7 m sampling depth (Table 7).

6.0. Results: Seasonal Cycles

After describing the oceanographic context the platform represents within CB, we turn next to the seasonal cycles observed over the 2016-2017 ONC deployment. The objective of this section is to describe the influencing factors on the carbon system seasonally through a complete cycle of sea ice growth and melt. We will focus quantitatively on the relative roles of processes determining variability in the carbon system within the seasonal intervals described previously (Figure 7; Table 5).

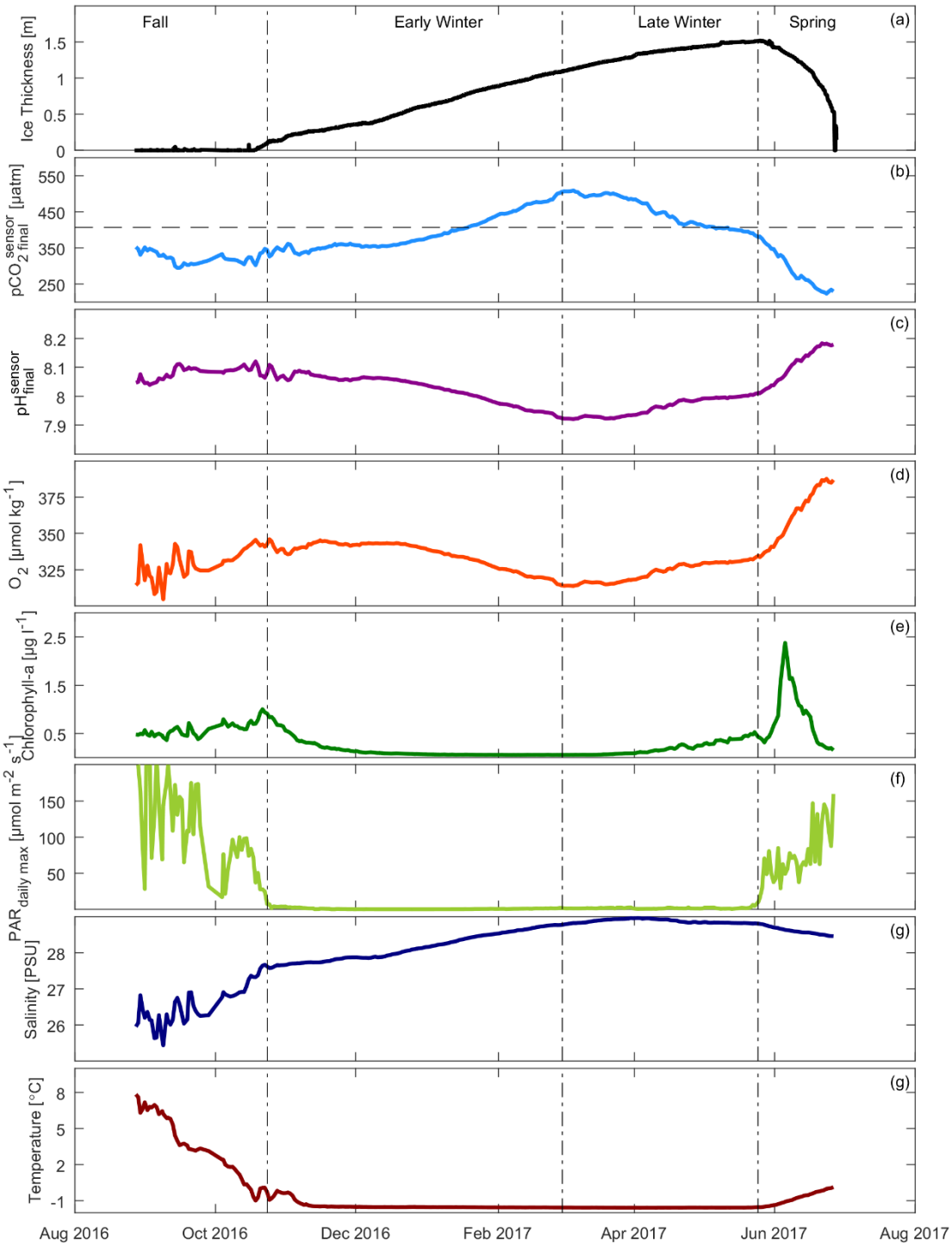

Figure 15 Observed ONC platform data during the 2016-2017 deployment. pCO_2 (b) and pH (c) observations are corrected final sensor values (Section 4.2.). Atmospheric pCO_2 is represented by the horizontal black dashed line on (b). PAR values represent the daily maximum observed in (f). The vertical dashed black lines denote seasonal endpoints as described: Fall from 2016-08-25 to 2016-10-23, Early

winter from 2016-10-23 to 2017-02-28, Late winter from 2017-02-28 to 2017-05-24, and Spring from 2017-05-24 to 2017-06-27.

6.1. Seasonal Observations

The observed time-series of pCO_2, pH, O_2, Chlorophyll *a*, PAR, salinity and temperature varied over different sea ice conditions throughout the deployment interval (Figure 14). CB is highly influenced by seasonality in sea ice conditions (i.e. sea ice growth and melt), sea surface warming and cooling, freshening of surface waters from Freshwater Creek runoff, and the seasonal availability of light and nutrients (Campbell et al., 2016). The seasonal cycle of pCO_2 at the platform shows some recognizable trends compared to Else et al. (2012) (Figure 3; Figure 15b). Through the fall pCO_2 was undersaturated with respect to the atmosphere but steadily increased as sea ice began to form (Figure 15b). On January 19th 2017, isolated from air-sea gas exchange by sea ice coverage, the waters at the platform became supersaturated with respect to the atmosphere (Figure 15b). pCO_2 continued to increase through the early winter until reaching a maximum March 5th 2017 of ~509 µatm. During late winter, shortly after the uder ice sunrise on February 28th 2017 there was a brief drawdown of pCO_2, followed by a slight increase in pCO_2 leading to a second peak around twenty days later (Figure 15b). Following the second peak, there was a steady drawdown of pCO_2 until sea ice reached a maximum thickness marking the start of spring on May 24th 2017. Before the beginning of spring, pCO_2 was already undersaturated with respect to the atmosphere as of May 5th 2017 (Figure 15b). The start of spring was also the start of a sharp drawdown in carbon as light penetration increased due to snow melt on the surface and increasing ice transparency (Figure 15f). pCO_2 reached a

minimum of ~223 µatm on June 23rd 2017, and the site entered the open water season significantly undersaturated with respect to the atmosphere (ΔpCO_2 = -177).

pH and O_2 show a distinct seasonal cycle approximately anti-phased to that of pCO_2 (Figure 15c-d). pCO_2 and O_2, as well as pH and O_2 are correlated over the full deployment with an r^2 value of 0.63, and 0.66 respectively. However, following freeze up through the early winter, late winter and spring periods the r^2 value of pCO_2 and O_2 as well as pH and O_2 are 0.97 and 0.96 respectively. The increased r^2 value over the interval of sea ice coverage signifies a more strongly correlated signal between the pCO_2 and pH with O_2. The strong correlation of the carbon system and O_2 outside of the influence of air-sea gas exchange suggests the conditions under the ice at the platform are biologically dominated. Through the fall pH remainsed relatively constant around 8.0806±0.0214 until freeze up and then steadily declined until around sunrise, reaching a minimum of 7.9203. pH increased through the late winter until the start of spring. Melt onset was followed by a sharp increase in pH reaching a maximum of 8.1825 on June 21st 2017. O_2 tracked the same seasonal pattern as pH but reached a minimum of 304.4 µmol/kg in the fall, and a maximum of 387.7 µmol/kg in spring.

Seawater temperature steadily decreased through the fall from a maximum right at deployment of 7.8°C (Figure 15h). Seawater temperature remained relatively constant around -1.5°C from approximately twenty days after freeze up until sea ice reached a maximum thickness in the late winter. With the onset of melt there was a steady linear increase in temperature through the spring at a rate of 0.049±0.026 °C per day.

In the salinity time-series, the effect of sea-ice formation can clearly be seen having an effect on the underlying water column (Figure 15g). Following freeze up, as the ice grew there was a steady increase in salinity due to sea ice brine rejection to a maximum of 28.96 PSU. The salinity decrease in the spring was also rather linear at a rate of 0.01± 0.005 PSU per day, potentially due to diffusion of melt water as vertical mixing rates remain very low. It is important to reiterate that due to stratification at the surface and the interval of sensor availability (Section 5.2) the impact of sea ice melt and terrestrial fluvial input are not discussed.

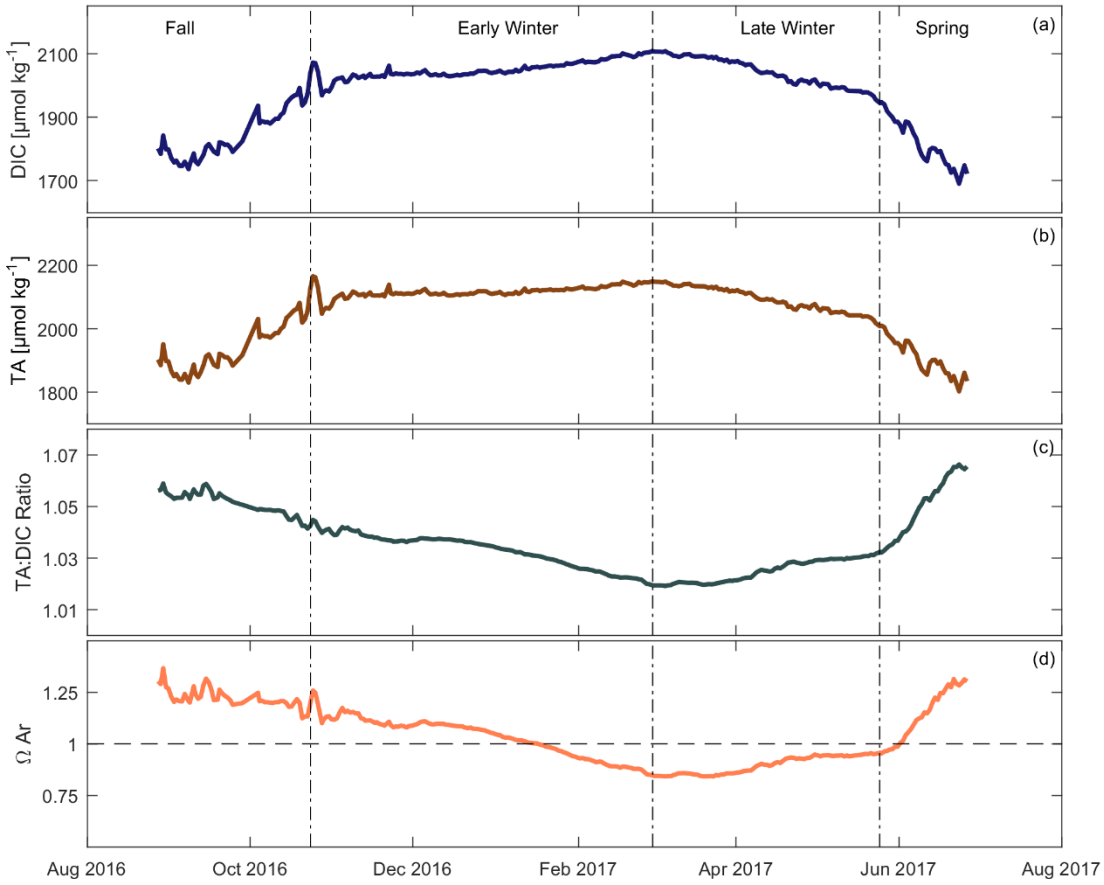

Figure 16 Calculated ONC platform data during the 2016-2017 deployment. Saturation of ΩAr is given by the horizontal dashed black line on (d). The vertical dashed black lines denote seasonal endpoints as described: Fall from 2016-08-25 to 2016-10-23, Early winter from 2016-10-23 to 2017-02-28, Late winter from 2017-02-28 to 2017-05-24, and Spring from 2017-05-24 to 2017-06-27.

The seasonal patterns of the CO2SYS calculated (Van Heuven et al., 2011) carbonate parameters very much reflect that of pCO_2 and pH (Figure 15b; Figure 16). In DIC and TA, which generally track the same seasonal pattern, we see a near consistent difference of TA being 94.3±5.6 µmol/kg greater than DIC. However, there was some seasonal change in the ratio of TA:DIC (Figure 16c). DIC and TA both increased through the fall with a noticeable spike in both parameters during sea ice formation (Figure 16a-b). Both DIC and TA steadily increased through the early winter until sunrise, while the TA:DIC ratio decreased, suggesting DIC increased at a greater rate compared to TA during this period. Immediately after the sun rose under the ice DIC and TA steadily decreased, before rapid decline following sea ice maximum thickness and the onset of melt in the spring. The ratio of TA:DIC also increased following sunrise before rapidly increasing through the spring (Figure 16c).

Conditions of aragonite undersaturation ($\Omega Ar < 1$) were observed for 134 days through the winter into spring from January 17th 2017 through May 31st 2017 (Figure 16c). The calcite saturation state remained supersaturated ($\Omega Ca > 1$) ranging from 2.21 - 1.36, tracking a very similar pattern to ΩAr (Section 3.4.2.; data not shown). Water below the mixed layer based on discrete samples at B1 30 m, remained undersaturated year round in aragonite (ΩAr = 0.72±0.11).

6.2. Diagnostic Box Model Overview

6.2.1. Seasonal Fluxes

The observations above show several competing processes influencing the marine carbon system at the platform through the cycle of sea ice growth and melt. To understand the relative contribution of those processes a diagnostic box model approach was taken. The model incorporated: air–sea exchange (C_{ex}), vertical diffusion (C_{diff}), entrainment (C_{ent}), brine rejection from sea ice growth (C_{sal}), and net ecosystem production (C_{bio}) (Figure 7; Eq. 1C). The seasonal variation of these five source terms, representing process rates affecting the total variation in DIC over the 2016-2017 ONC deployment are shown below (Figure 16).

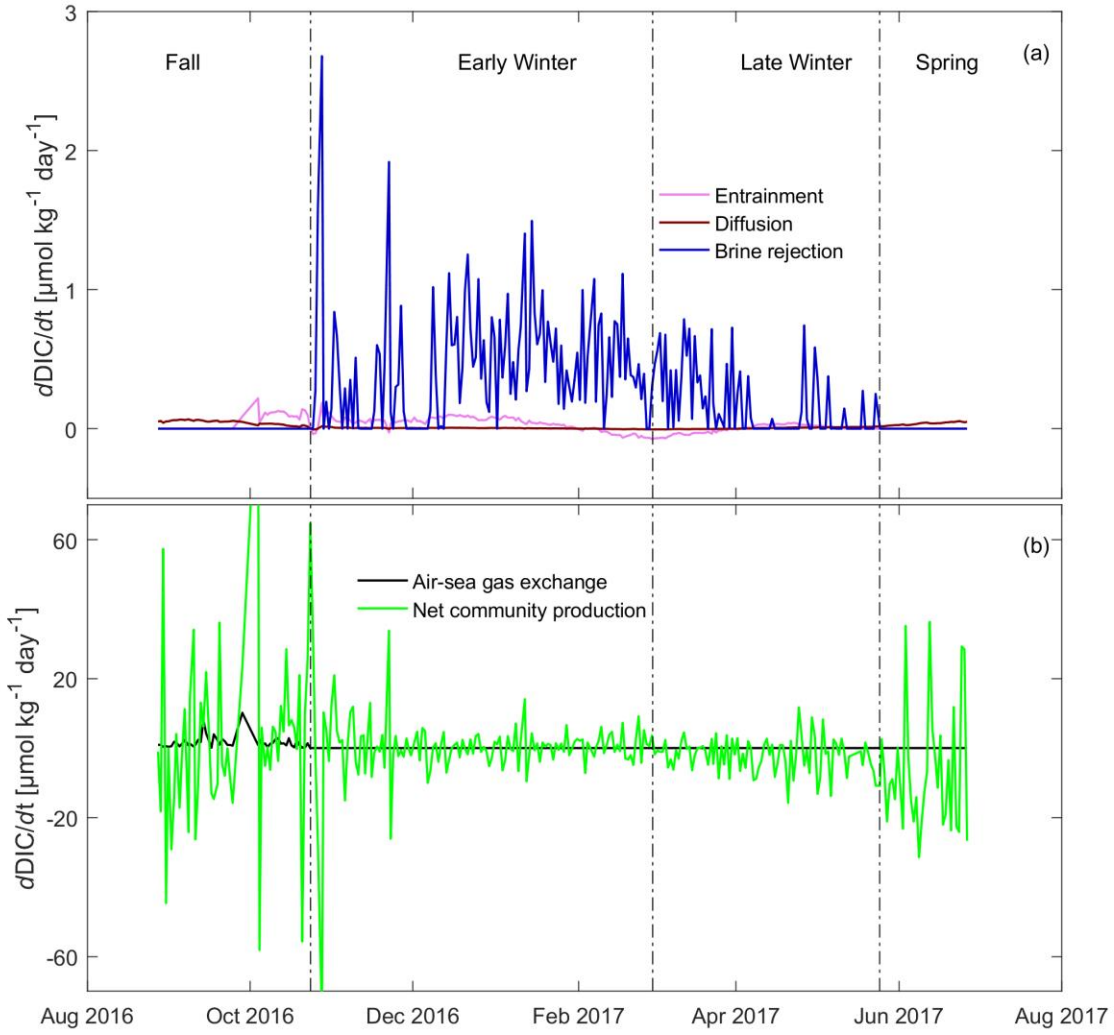

Figure 17 Diagnostic box model calculated source terms representing rates of processes affecting $\frac{dDIC}{dt}$ *over the 2016-2017 ONC deployment. The vertical dashed black lines denote seasonal endpoints as described: Fall from 2016-08-25 to 2016-10-23, Early winter from 2016-10-23 to 2017-02-28, Late winter from 2017-02-28 to 2017-05-24, and Spring from 2017-05-24 to 2017-06-27.*

Air-sea gas exchange, C_{ex} (Figure 16b) provided a prominent source of DIC to the mixed layer in the fall. C_{ex} was calculated operating under the assumptions that: the summer mixed layer depth was maintained through the fall, and the mixed layer was sufficiently deep enough to encompass the platform. These assumptions are based on the prolonged period of open water following spring surface conditioning, and multiyear CTD measurements taken at station B1 in

the fall (Figure 13). Through the fall, pCO_2 was always undersaturated with a mean fall value of 322.0±16.2 µatm, against a constant atmospheric value of 407 µatm (Butterworth & Else, 2018). Some variability in C_{ex} could be due to solubility as seawater cools, and becomes more saline through the fall. However, with the pCO_2 gradient between seawater and the atmosphere remaining relatively constant, almost all the variation in C_{ex} was caused by variation in gas transfer velocity driven by wind events. C_{ex} varies from 0.12 to 10.14 µmol/kg day. The largest rates coincided with high wind speeds of over 11m/s recorded at the nearby on-shore site.

The source term for vertical diffusion, C_{diff} (Figure 16a), varied little over the deployment, reaching a maximum of 0.067 µmol/kg day. The concentration gradient leads to the migration of DIC from depth into the mixed layer above the pycnocline through most of the year. However, for nearly two months from 2017-01-31 to 2017-04-01, DIC concentration at the platform was higher than the DIC below the pycnocline estimate, exporting carbon to depth at a maximum rate of 0.006 µmol/kg day (Figure 16a).

Vertical entrainment (C_{ent}) was only considered during times of mixed layer deepening from 2016-09-28 to 2017-05-11 (Figure 16a). Outside of this interval C_{ent} was equal to zero as the base of the mixed layer is assumed to be shoaling. In early October C_{ent} reached a maximum of 0.22 µmol/kg day. The max was a result of a large gradient that existed between the DIC at the platform and DIC below the pycnocline, in combination with deepening of the mixed layer. DIC entrainment into the mixed layer continued through the early winter until the gradient

narrowed and eventually flipped, where just as C_{diff}, between 2017-01-31 and 2017-04-01 there was a net export to depth at a maximum rate of 0.07 µmol/kg day (Figure 16a).

C_{sal}, described the influence of brine rejection computed based on salinity changes during the winter period (Figure 16a). Salinity below the mixed layer was assumed constant throughout the year, based on the multiyear CTD measurements taken at station B1 (Figure 13). Brine rejection was the only influence associated with a salinity change deemed necessary in the model (Section 3.6.2.). The contribution of brine rejection reached a maximum shortly after sea ice formation at a rate 2.68 µmol/kg day on 2016-10-27. Through the early winter the average contribution was 0.19±0.36 µmol/kg day. As sea ice in CB matured it becames denser and brine rejection rates slowed to 0.05±0.15 µmol/kg day in the late winter following sunrise, as fewer impurities remain within the ice; those that were are reported to be trapped in brine channels or pockets (Loose et al., 2011). Fifty days before sea ice reached a maximum thickness, salinity decreased before plateauing (Figure 15g). This could indicate a point of sea ice reaching maximum density and brine rejection coming to an end. The slight salinity decrease (difference of 0.17 PSU) could be due to lateral diffusion within the bay before reaching equilibrium and plateauing before spring. The horizontal salinity variability may be due to spatial and temporal heterogeneities within the sea ice (Miller et al., 2011).

Net ecosystem production was defined as the difference between gross primary production and total ecosystem respiration, representing the total amount of organic carbon in an ecosystem available for storage, export as organic carbon, or non-biological oxidation to carbon dioxide (Lovett, Cole, & Pace, 2006). Net ecosystem production rates appeared extremely variable

throughout the year (Figure 16b). This variability was tied to the method from which C_{bio} was derived. The net effect of biological processes were estimated from the difference between the total observed change in DIC ($\frac{dDIC}{dt}$) and the change accounted for in C_{ex}, C_{diff}, C_{adv}, C_{ent}, and C_{sal}. The method was inclusive of biological controls including photosynthesis/ respiration and calcium carbonate precipitation/ dissolution, but also of the error in all known terms, and in unaccounted for changes in DIC. However, given this uncertainty confidence in the average seasonal rates come from C_{bio} being of similar magnitude, and in the correct direction seasonally when compared to O_2 measurements. In the fall average C_{bio} rates are 2.90±27.68 µmol/kg day indicating the dominance of heterotrophic conditions. Following sea ice formation through the early winter C_{bio} average rate dropped to 0.06±10.15 µmol/kg day as temperature dropped and it became more ecologically expensive for respiration or remineralization of organic matter (Arrigo & Sullivan, 1992; Gasol & Kirchman, 2018). Immediately following sunrise and through the late winter autotrophic conditions took control and drew down DIC concentrations at average rate of 2.06±5.00 µmol/kg day. With the onset of melt and start of spring, the average rate of photosynthetic DIC drawdown increased to a relatively high rate of 6.90±17.70 µmol/kg day. These values are not outside of previously reported values in comparable regions (Subba Rao & Platt, 1984). Inclusive of the uncertainties, our diagnostic box model clearly demonstrates that net ecosystem production was the major driver for the seasonal variations in DIC in the mixed layer at the platform in CB over the described deployment.

6.2.2. Seasonal Carbon Budget

In order to establish a carbon budget for the mixed layer containing the ONC platform at different times of the year, we integrated the six source terms – which represent rates of change - over each of the four specified seasons ($J_i = \int C_i \, dt$). In doing so we yield an observed partitioning of carbon sources and sinks building a carbon budget over the described deployment (Table 8).

Table 8 Diagnostic box model temporally integrated source terms representing DIC [µmol kg^{-1}] contribution (+) or drawdown (-) of processes affecting $\frac{dDIC}{dt}$ over the 2016-2017 ONC deployment. Seasonal definitions include: Fall from 2016-08-25 to 2016-10-23, Early winter from 2016-10-23 to 2017-02-28, Late winter from 2017-02-28 to 2017-05-24, and Spring from 2017-05-24 to 2017-06-27.

	J_{ex}	J_{diff}	J_{ent}	J_{sal}	J_{bio}	$Total \frac{dDIC}{dt}$
Fall	83.82	2.22	2.28	0.00	148.15	236.47
Early winter	0.00	0.40	4.85	56.59	8.04	69.89
Late winter	0.00	0.29	-0.19	14.10	-166.97	-152.77
Spring	0.00	1.21	0.00	0.00	-234.74	-233.53

In the fall the dominant source of carbon to the site was due to biologic respiration/ remineralization (62.65%). There was also a significant contribution from air-sea gas exchange, as the site was undersaturated with respect to the atmosphere through this time (35.45%). Diffusion and entrainment contributed little to the site, with a combined net contribution of 4.50 µmol/kg.

Into the early winter following sea ice freeze up, air-sea gas exchange was halted and brine rejection became the largest source of DIC at the platform (80.97%). Contribution from mixed layer deepening was the largest at this time of year also (4.85 µmol/kg), as deepening was

driven by the salinity increase from sea ice growth. The contribution from diffusion slowed as the gradient between the mixed layer and below the pycnocline decreased. There was very little contribution from biology during this time (11.5%) as temperatures plummeted and light rapidly faded, making biologic activity ecologically expensive for organisms (Arrigo & Sullivan, 1992; Gasol & Kirchman, 2018).

In the late winter, the ecosystem at the platform experienced a profound change immediately following sunrise as photosynthesis very rapidly began dominating at the site through the late winter drawing down 166.97 µmol/kg of DIC. Surprisingly, this transition occured at very low light levels; with average daily maximum PAR values at this time on the order of 1.15±0.72 µmol/m^2s. Organisms could potentially begin building biomass and consuming DIC at the site as soon as PAR became available. The DIC concentration in the mixed layer at the site was now very close to that of the concentration below the pycnocline essentially halting entrainment and diffusion processes (combined 0.1 µmol/kg). As sea ice and snow cover thickened, the ice growth rate declined and the expulsion of brine slowed, thus the contribution of brine rejection in the late winter was significantly less than in the early winter (9.23%).

Into the spring following sea ice maximum thickness, the mixed layer shoaled and entrainment was no longer a factor. Due to the drawdown in the late winter from biology, the DIC gradient between the mixed layer and the water below the pycnocline increased and diffusion contributed an addition of 1.21 µmol/kg. The contribution of brine rejection was assumed to end in the spring as well. The platform, at a depth of 7m was isolated from the low salinity, low DIC stratification of sea ice melt and surface snow drainage, and so those factors are not

included in this analysis (Figure 13-14). The system warmed through the spring and received a substantial increase in available PAR until presumably, the snow cover melted and exponentially increasing light transmission (to an average of 65.28±28.77 µmol/m^2s through the spring). Biology effectively took over the system during this time drawing down a significant amount of DIC (234.74 µmol/kg) right before the open water season.

6.3. Detailed Discussion of Sub-Seasonal Processes

In this section we dive into a more targeted discussion on the sub-seasonal processes, which may be important in illustrating biogeochemical dynamics at the platform. Topics of interest include the discernable spike in DIC and TA during freeze up (Figure 16a-b), the steady increase in pCO_2 following freeze up to supersaturation with respect to the atmosphere (Figure 15b) and undersaturation in ΩAr (Figure 16d), the immediate change in the ecological system following sunrise under the ice (Figure 15; Figure 16), and the steep photosynthetic drawdown of carbon during the spring (Figure 16a).

6.3.1. Freeze-up Anomaly

The observed DIC and TA increase through the fall was dominantly driven by biology and air-sea gas exchange as discussed in pervious sections. However, there was a massive spike in DIC and TA coincident with sea ice freeze up around October 23rd 2016 (Figure 16a-b). Over the course of five hours DIC and TA increased 194.44 µmol/kg, and 208.64 µmol/kg respectively (Figure 18c; TA not shown). O_2 increased 5.73 µmol/kg over the same time frame, with temperature plummeting 1.03°C (Figure 18e-f). There was an observed decline in pCO_2 during

this time (7.85 µatm), which could result from of the change in TA being larger than the change in DIC, coupled with the thermochemical response to the drastic temperature fluctuation (Figure 18a). pH and ΩAr both also increased during this time by 0.0458, and 0.19 respectively (Figure 18b,d). The anomaly of increased DIC, TA, pH, ΩAr and O_2 with decreased temperature and pCO_2 persisted for approximately four days following freeze up. Following the anomaly, all variables return to steadier concentrations all lower than preceding conditions. DIC and TA are 63.71 µmol/kg and 70.25 µmol/kg lower than before the anomaly respectively, while O_2 and temperature were 2.37 µmol/kg and 0.27 °C lower respectively.

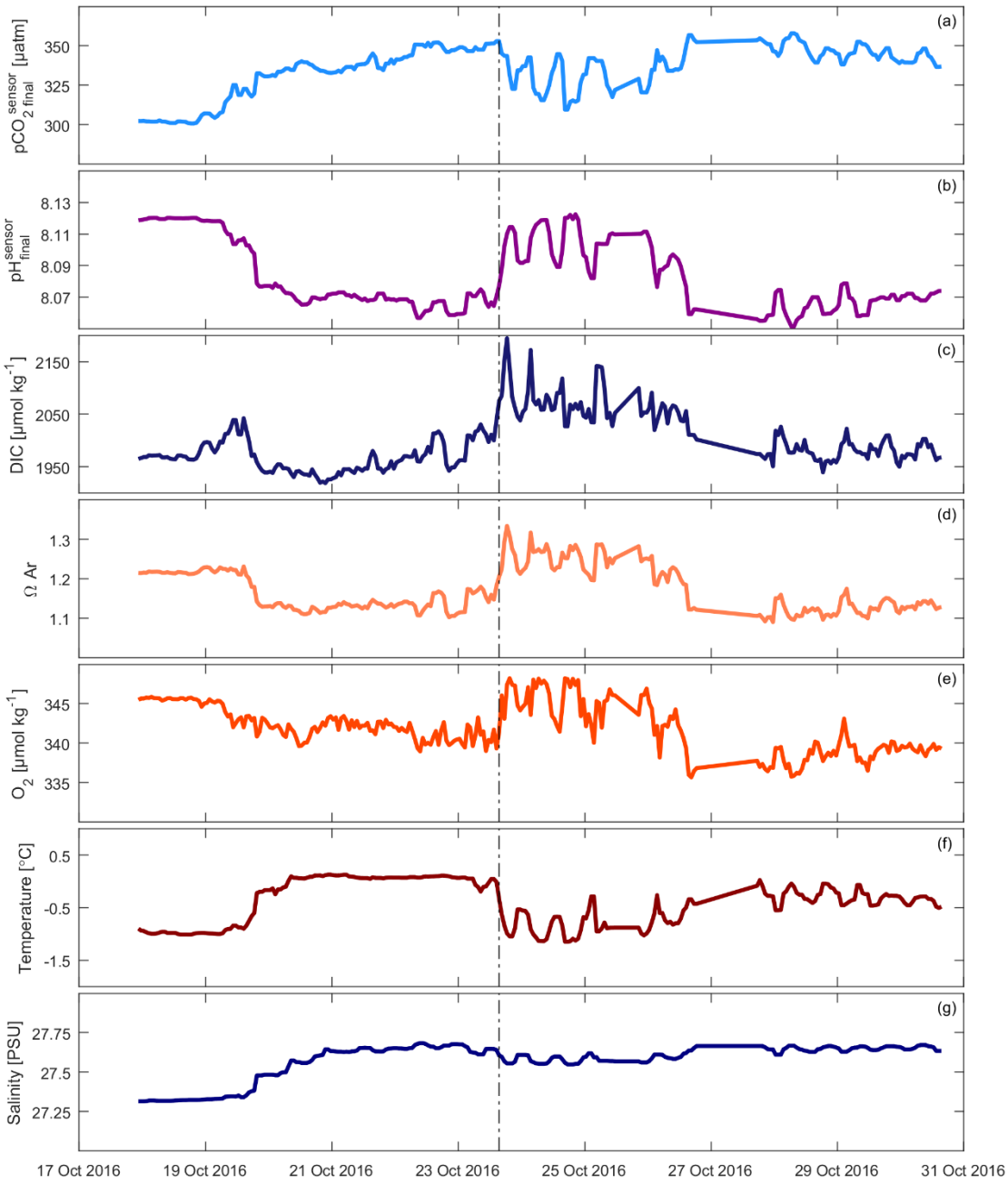

Figure 18 Hourly ONC platform data capturing the fall anomaly event occurring from October 23rd 2016 – October 27th 2016. The vertical black dashed line represents freeze up on October 23rd 2016 when sea ice becomes land fast in CB as defined by an ice thickness of > 0.1 m.

One possible explanation for the short lived massive input of DIC and TA into the system could be due to the movement of a unique water mass past the platform. Given the coincident timing of freeze up and the near shore location of the platform, a denser water plume possibly formed

closer to shore could be what was detected at the platform. The driver of such a process could be a shoreline cooling effect due to a much lower specific heat capacity, producing sea ice formation and cold water in the shallows. An indicator for a different water mass at the sensor during this time would need to be tied to both chemical and physical tracers. High water-side turbulence during sea ice freeze up has been linked to modifications of the physical and chemical properties of the surface seawater by cooling and brine rejection (Else et al., 2011). Water-side turbulence could be evidence justifying the hypothesized process, as the observed rise in O_2 could support the idea that this anomaly is from a water mass originating closer to the surface. Before the event, the on-shore station recorded nearly twenty four hours straight of wind speeds greater than 5 m/s, enhancing air-sea gas exchange of oxygen (occurring more rapidly compared to CO_2) along with increased solubility due to cooling. Evidence for the movement of a separate water mass comes from the distinguishable warm water mass preceding freeze up, which temporally aligns with a very different, and much lower oxygen concentration (Figure 18e-f). This warmer, low oxygen water mass was rapidly forced out of the platform location, by the colder, denser, high oxygen water mass.

The rise in DIC and TA could be tied to the denser water masses ability to encapsulate unconsolidated marine sediment pore water, rich in DIC and TA, due to the wind driven mixing close to shore along the seafloor. The enriched water mass could then have passed by the sensor before dropping into the deeper bay bathymetry. The anomaly being tied to a brine plume rich in DIC and TA originating near shore from brine rejection, seems unlikely as shown in the Figure 18g. Salinity during this time remained incredibly constant, with any change being a

slight decline (0.09 PSU). With temperature being the only driver of density differences between the water at the platform before the anomaly and the transiting near shore generated water mass, it seems that the elevated DIC and TA values are likely tied to mixing of seafloor pore waters, reported previously as having elevated DIC and TA concentrations compared to a local water column (Lichtschlag et al., 2015).

Following the event, the denser nearshore generated water mass would much more slowly be replaced by water similar to what the platform observed before the event, circulating from further out in the bay. The cyclic variably in all variables following the event (after October 28th 2016 in Figure 18) could be tied to diurnal patterns in sunlight driving biology and sea ice growth variability before polar night above the ice on November 25th 2016.

6.3.2. Sea Ice Growth

Following sea ice freeze up on October 23rd 2019, there was a steady increase in DIC through the early winter (Figure 16a). The total increase in DIC was 69.89 µmol/kg, while the change in pCO_2 was around 150 µatm. The increase over this period was enough to drive the partial pressure of CO_2 at the platform to seasonal supersaturation, and ΩAr to undersaturation. The observations made by the platform confirm one major aspect of the Yager et al. (1995) "*seasonal rectification hypothesis*" at our site; pCO_2 supersaturation through the winter months. From the end of the fall through the polar night, biological respiration does indeed exceed carbon fixation contributing to the gradual rise in pCO_2 leading to supersaturation. Else et al. (2012) and Shadwick et al. (2011) also observed a gradual increase in

pCO_2 to a maximum in the winter at their Amundson Gulf site. However, the maximum they recorded was still undersaturated with respect to the atmosphere (Figure 3).

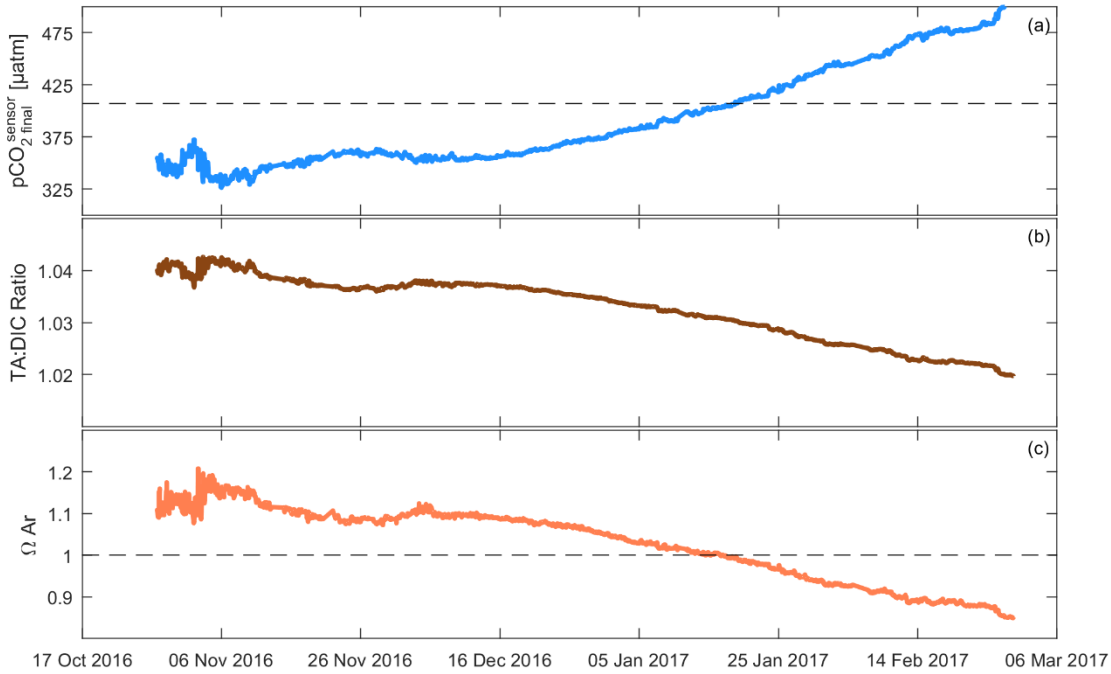

Figure 19 Early winter period during the 2016-2017 ONC deployment. Atmospheric pCO_2 is represented by the black dashed line on (a). Saturation of ΩAr is given by the dashed line on (c).

The high pCO_2 levels observed below the sea ice may be explained by potentially more efficient DIC rejection compared to TA during sea ice formation, elevating pCO_2 (Figure 19a). This was evidenced by the decreasing TA:DIC ratio over the early winter period (Figure 19b). The larger increase in pCO_2 compared to DIC is likely tied to an increase in the Revelle Factor as the TA:DIC ratio decreased. The Revelle Factor is a measure of the relative increase in pCO_2 with an increase in DIC as carbon speciation concentrations change (Eq. 1-3A). The Revelle Factor increased from ~17 at the end of fall to a maxima of ~19.5 at the end of early winter, values within the range reported by Shadwick et al. (2011). Rysgaard et al. (2007) hypothesized that

more efficient DIC rejection during sea ice formation compared to TA led to high pCO_2 levels in the water column below sea ice. Our observations contribute to validating this hypothesis as brine rejection at the platform accounted for 80.97% of the total change in DIC over the early winter period (Table 8). Rysgaard et al. (2007) suggested that calciulm carbonate precipitation out of the ice at low temperatures could enriched $CO_{2(aq)}$ in the underlying seawater as sea ice continues to grow (Eq. 13A). Our results build on Else et al. (2012) and Shadwick et al. (2011) findings in confirming the significance of brine rejection in the overall pCO_2 increase through the winter.

Only 11.5% of the change in DIC during the early winter period was attributed to respiration/ remineralization (Table 8). The low contribution from biologic processes was likely due to the strongly suppressed metabolic activity of bacterial populations and zooplankton (entering a state of diapause) as soon as sea ice formed (Grossmann & Dieckmann, 1994). All of the heterotrophic activity during the early winter interval was likely based on biogenic carbon produced during the previous light season (Berge et al., 2015). With CB still being influenced by biologic fluxes (Figure 17b), the amount of available carbon for remineralization during the fall and early winter was dependent on production during the spring and summer periods, before nutrients were exhausted.

The overall increase in DIC over the early winter also led to seasonal undersaturation of ΩAr (Figure 19c). Through the fall and winter, aragonite decreased until becoming strongly undersaturated on January 17th 2017. Brine rejection and remineralization increased the concentration of DIC while increasing pCO_2, lowering pH and ΩAr (Figure19c). The prolonged

undersaturated winter waters (Figure 16c) are potentially corrosive to calcifying benthic fauna (bivalves and echinoderms) found on the seafloor in CB. Previous studies reporting the annual cycle of ΩAr in seasonal ice covered Arctic waters did not report prolonged periods of undersaturation through the winter at the surface (Chierici et al., 2011; Shadwick et al., 2011). Impacts at the base of the food chain could lead to acidification effects being felt in larger benthic feeding mammals such as local ringed seals and possibly Arctic Char in the summer. The benthic ecosystem of CB is thus potentially vulnerable to future ocean acidification and suppression of $CaCO_3$ saturation states. It will be particularly interesting to monitor going forward how the duration of winter ΩAr undersaturation may change from the reported 134 days observed in this study. Influences to observe include sea ice thickness and duration of growth which will changing brine rejection DIC input, and spring and summer production which could change the pool of available organic carbon for remineralization through the fall and early winter.

6.3.3. Sunrise

Immediately following sunrise the observed carbon system in CB dramatically turned around near February 28th 2017 going into the late winter (Figure 15b-c; Figure 16 a-b). The system rapidly shifted from being net heterotrophic to net autotrophic (Table 8). Sunrise under the ice consequently brought a drawdown in DIC, reducing pCO_2, while increasing pH, O_2 and ΩAr (Figure 15-16). The end of polar night above the ice was on January 16th 2017 in Cambridge Bay, but "sunrise" under the ice at the platform was defined as the first occurrence of a PAR measurement ≥ 2 µmol/m^{2}s, which occurred on February 28th 2017.

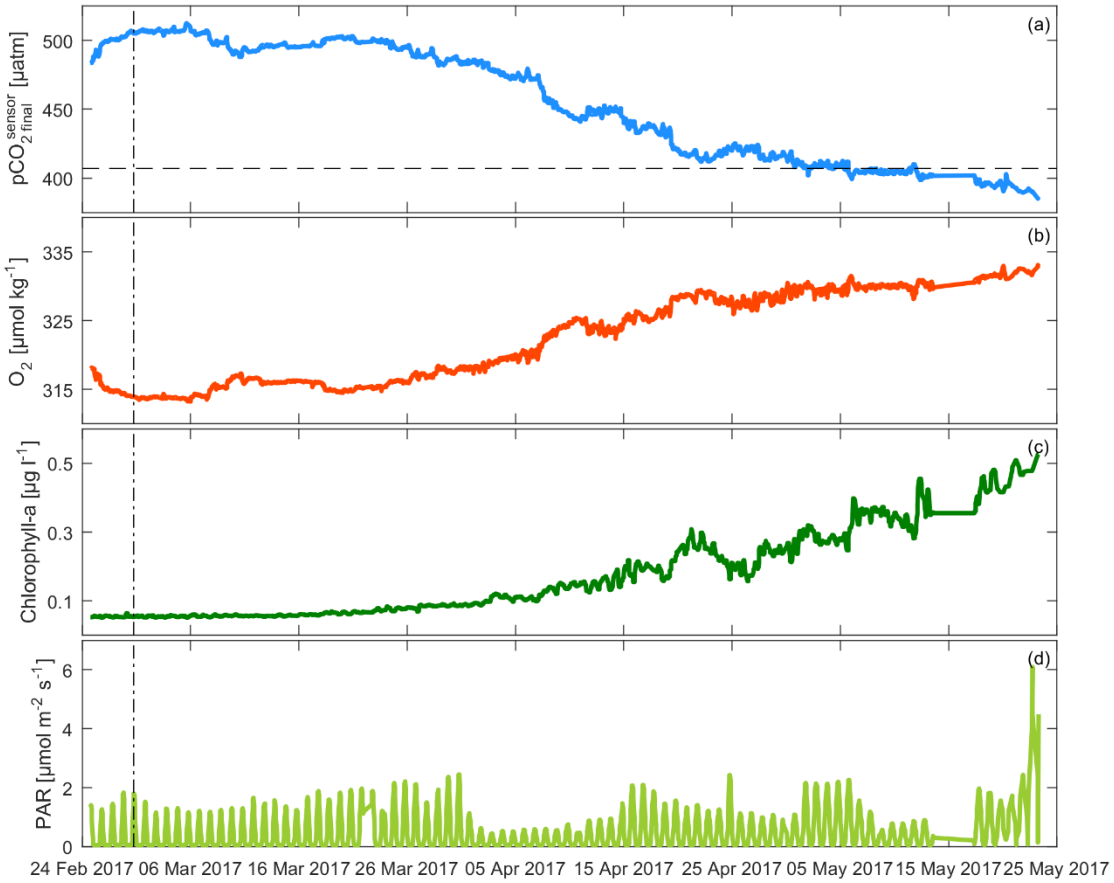

Figure 20 Late winter period during the 2016-2017 ONC deployment. Atmospheric pCO_2 is represented by the horizontal black dashed line on (a). Sunrise under the ice is denoted by the vertical dashed black line (2017-02-28, when PAR exceeds 2 µmol/m^{2}s).

The pCO_2 maximum occured near March 5th 2017, shortly after the sun rose on February 28th 2017 (Figure 20a). There was a brief drawdown of pCO_2 after the maximum (to a local minimum on March 10th 2017), followed by a brief pause causing a slight increase and second peak around fifteen days later (March 25th 2017). Following the second peak, a stronger biological response was likely triggered initiating a steeper steady drawdown of DIC (Figure 20a).

Through the late winter pCO_2 and O_2 patterns track anti-phase to one another while being strongly correlated (r^2 = 0.99), furthering evidence for the turnaround being biologically driven

(Figure 20a-b). Chlorophyll-*a* concentrations showed a steady increasing trend, but remained very low through this period, at least as observable in the water column by the platform (Figure 20c). The observed drawdown during this time period, before the onset of sea ice melt, is enough to force the undersaturation of pCO_2 with respect to the atmosphere (on May 5th 2017; Figure 20a). In the proposed model from Yager et al. (1995), it is suggested that biogeochemical processes occurring on the ice (i.e. ice algae) precondition pCO_2 of the seawater prior to ice break-up, and subsequent air-sea gas exchange. However, our data suggests that this preconditioning starts earlier than previously thought, occurring far before sea ice has even begun to melt (~65 days). Else et al. (2012) observed a similar pattern with an interesting early drawdown, followed by a slight increase in mid-March, and a second peak in late-April (Figure 3). The initial draw down was attributed to ice algae in Shadwick et al. (2011) and Else et al. (2012); which was later shown to be unlikely (Else et al., 2019).

Relatively high levels of benthic heterotrophic activity has been reported through the polar night, capable of creating relatively high levels of nutrient regeneration (Berge et al., 2015). At the platform, the deep winter mixed layer (~25 m) would encompass much of the shoreline sea floor, easily mixing nutrients to surface waters due to lack of water-column stratification (Figure 14a-b). With an apparent abundance of nutrients at the identified start of the late winter period (February 28th 2017), light availability was the dominant control on the ice covered ecosystem (Leu et al., 2015).

In this study we reported a drawdown of 166.97 µmol/kg of DIC due to biologic processes during the late winter period, from sunrise to the onset of melt (Table 8). Looking at previously

reported ice algae biomass values over the same period in the nearby Dease Strait from Campbell et al. (2017), particulate organic carbon in ice algae was equal to ~2000 mg/m^2 on May 25th 2014. Applying a simple calculation discussed in Else et al. (2019), the total calculated biologic uptake of DIC from ice algae would equate to only 5.8 µmol/kg over the CB surface mixed layer. Similarly, using observed chlorophyll-*a* concentrations to infer pelagic biomass, an uptake of only 2.1 µmol/kg of DIC was calculated. These community specific biomass calculations assume that particulate organic carbon is representative of total organic carbon based on data availability, and a carbon:chlorophyll-*a* ratio of 60:1 from Riedel et al. (2006) used in Else et al. (2019). The relative magnitudes of the calculated sympagic (i.e. ice-associated), and pelagic algae communities during this period are in proportion to previously reported values (Gradinger, 2009). Inclusive of the uncertainly, the production in these communities are not even of the same order of magnitude compared to drawdown we report. Comparing benthic microalgae production in a similar environment with respect to sea ice conditions, proximity to shore, and depth, production during this late winter period has been shown to be barely detectable (Horner & Schrader, 1982). In Horner & Schrader (1982) benthic microalgae production in the western Beaufort Sea only began after the formation of melt ponds and disappearance of ice algae. Ice algae shades both the water column and benthos as they are the first community to bloom, inhibiting production to some degree in those adjacent habitats (Horner & Schrader, 1982). The late winter drawdown observed in this study occurs in the absence of any previously reported significant photosynthetic communities, including under-ice or open-water phytoplankton blooms (Else et al., 2019).

Having ruled out ice algae, pelagic phytoplankton, and benthic microalgae as possible communities contributing to the sunrise drawdown, one possible explanation may be tied to the microbial community. Despite hash conditions through the polar night, virtually all taxonomic groups of Arctic microbes are sustained (Iversen & Seuthe, 2011; Niemi et al., 2011; Sherr & Sherr, 2003; Terrado et al., 2009; Weslawski et al., 1999) including chloroplast-bearing protists, such as diatoms and various flagellates. Without direct observations of microbial community activity over the deployment interval it cannot be concluded that the sunrise drawdown is attributed to microbes, however it does offer a new avenue for scientific inquiry.

We have identified a drawdown in pCO_2 to undersaturation with respect to the atmosphere soon after the sun rises that appears to be driven by an undiscovered process in the literature. Previous studies looking into annual DIC cycling were also unable to distinguish the specific community responsible (Bates et al., 2006; Else et al., 2012; Miller, et al., 2011; Papakyriakou et al., 2011), informing further need for primary and bacterial production to be measured throughout the polar night into the spring in order to examine what is driving production at the base of the food chain when the sun rises under the ice.

6.3.4. Spring Drawdown

As discussed in the previous section, immediately following sunrise there was biological fixation of carbon at relatively high rate (Figure 17; Figure 20a). With the onset of melt and start of spring, the rate of net ecosystem production increased to a rate greater than three times that of late winter (from 2.06±5.00 µmol/kg day to 6.90±17.70 µmol/kg day). Through the

spring over a period of only 34 days, biological drawdown constituted a removal of 234.74 µmol/kg of DIC at our site (Table 8).

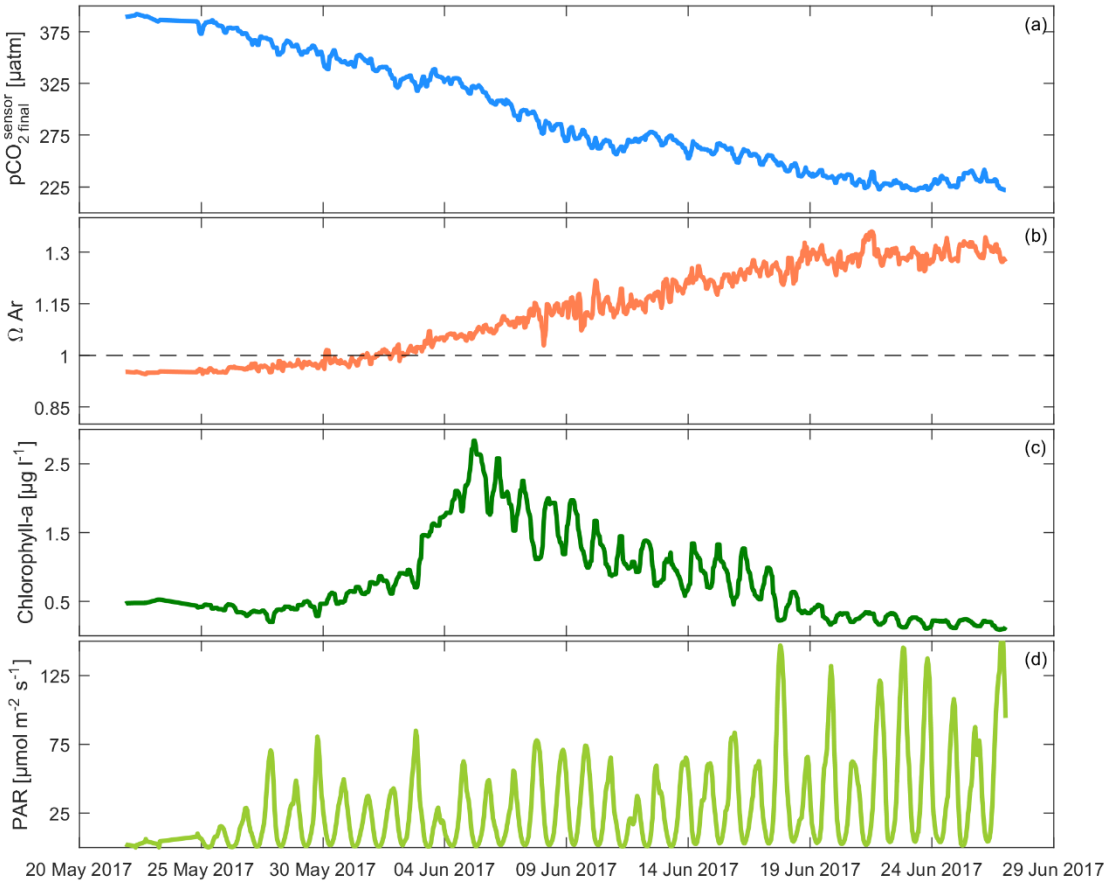

Figure 21 Spring period during the 2016-2017 ONC deployment, capturing the vernal bloom of under-ice phytoplankton. Saturation of ΩAr is given by the dashed line on (b).

Optical measurements under the ice have shown that beneath surface melt conditions there is a greater transmission of PAR to the underlying water column (Kevin R Arrigo et al., 2012). Looking at the two orders of magnitude change in PAR transitioning from late winter into spring, it is clear that the snow and ice cover's ability to attenuate incoming light had been drastically reduced with melt onset (Figure 20d-21d). Primary producers require both light and nutrients, but in the Arctic marine ecosystem there is typically a temporal mismatch in the

availability of these two resources. As discussed in the previous section, there is potential for nutrient regeneration through the winter months. Heading into spring, phytoplankton generally take advantage of the narrow time window when both resources are present. Opportunistically within this window, are characteristic intense Arctic marine spring blooms (Berge et al., 2015). The maximum observed chlorophyll-*a* concentration also occurs during this period (June 5th 2017; Figure 21c). It is likely that pelagic phytoplankton are productive before this maximum was recorded by the sensor but migrated through the water column as light availably increased and nutrients become depleted. It has been observed that under-ice phytoplankton blooms have an immediate and significant impact on DIC in the water column (Else et al., 2019). Comparable DIC drawdown magnitudes over a similar timeframe have also been reported (Else et al., 2019). The benthic community also likely plays a role in this drawdown. Following breakup of shorefast ice (occurring through the spring), benthic microalgae have been shown to become the most important source of primary production in similar nearshore seasonally ice covered ecosystems (Horner & Schrader, 1982).

It is difficult to discern the exact biologic uptake of DIC in the water column during the spring as there is apparent non-photochemical quenching of pelagic algae (Figure 21c-d). Non-photochemical quenching is a photoacclimation strategy algae use to protect themselves from the adverse effects of high light intensity, or excessive PAR (Macintyre et al., 2000). Non-photochemical quenching reduces photodamage of high irradiance by reducing photosynthetic pigment content such as chlorophyll-*a*, preventing overexcitement (Falkowski & LaRoche, 1991). Phytoplankton under-ice experience a very stable light environment with a narrow

spectral distribution (Neale & Priscu, 2013). This stability is due to optical attenuation and spectral filtering through the ice cover and the absence of vertical mixing (Neale & Priscu, 2013). Under-ice biological communities are well-adapted to these specific low light conditions (Mundy et al., 2009), with increases leading to quenching. Following the chlorophyll-*a* maximum (June 5th 2017), chlorophyll-*a* was visibly anti-phase compared to PAR suggesting non-photochemical quenching action (Figure 20c-d). The implications make it difficult to use chlorophyll-*a* as a proxy for production at this time of year, as the observed values are less indicative of the actual biomass present.

During the spring, the aragonite saturation state at our site returnd to supersaturation on May 31st 2017 (Figure 21b). Typically, high rates of phytoplankton primary production and net ecosystem production act to decrease both DIC and pCO_2, increasing $CaCO_3$ saturation states (Bates et al., 2009). Our site appears to follow similar trends reported in the Arctic of distinct seasonality of $CaCO_3$ saturation states, with summertime ΩAr and ΩCa values higher than wintertime conditions (Bates et al., 2009). However, our observations lend themselves to suggest that there is more than just a spatial component (between surface and subsurface waters) in Bates et al. (2009) described seasonal ‘‘*phytoplankton-carbonate saturation state*’’ interaction. Our calculated ΩAr and ΩCa time-series (Figure 16; not shown) were dominantly biologically induced over the entire deployment exclusive to the surface mixed layer. Increased fresh water contribution from either river runoff or sea ice melt water, has also be reported to result in decreased saturation states (Chierici & Fransson, 2009). We did not see the effect of sea ice meltwater on ΩAr at a depth of 7 m. Due to data availability and the determined

inadequacy of the platform during this period to represent the surface (Section 5.2.), the effects of freshet on $CaCO_3$ saturation states at our site are unknown. Further investigation would need to be conducted to determine the impact fresh water processes have on ocean acidification at our site.

6.4. Annual Inorganic Carbon Cycle Summary

The ONC platform in CB offers a rare and unique opportunity to describe the influencing factors on the marine carbon system seasonally through a complete cycle of sea ice growth and melt. The 2016-2017 deployment provided the temporal coverage to quantitatively partition the observed change in DIC throughout the year between five influencing processes including: air–sea exchange, vertical diffusion, entrainment, brine rejection from sea ice growth, and net ecosystem production.

Through the fall DIC increased 236.47 µmol/kg driven by air-sea gas exchange, as pCO_2 was undersaturated with respect to the atmosphere, and biologic respiration/ remineralization (Figure 15). An interesting anomaly was observed during sea ice formation in late October, where over the course of five hours DIC increased 194.44 µmol/kg (Figure 18). The anomaly persisted for approximately four days represented by increased DIC, TA, pH, ΩAr and O_2 with decreased temperature and pCO_2. Following the anomaly, all variables returned to steadier concentrations all lower than preceding conditions. Possibly a colder, denser water mass formed closer to shore enriched in O_2 from gas exchange and DIC/ TA through mixing of seafloor pore waters, could explain the short lived input of DIC observed at the platform.

DIC steadily increased through the early winter following sea ice freeze up, as air-sea gas exchange was halted and brine rejection became the largest input of DIC at the platform, accounting for 80.97% of the total increase in DIC (69.89 µmol/kg) (Figure 19). Our findings validate that a more efficient DIC rejection during sea ice formation compared to TA did indeed lead to high pCO_2 levels in the underlying water column (decrease in TA:DIC ratio of 0.02). The DIC increase was enough to drive pCO_2 at the platform to seasonal supersaturation with respect to the atmosphere, and the aragonite saturation state to become undersaturated.

Shortly after the sun rose under the ice in the late winter relative to biologic availability, the ecosystem at the platform rapidly shifted from being net heterotrophic to becoming net autotrophic (Figure 20). Surprisingly, this transition occurred at very low light levels with PAR values on the order of 1.15±0.72 µmol/m^2s. The steady drawdown in DIC of 152.77 µmol/kg returned pCO_2 to undersaturation before sea ice had reached a maximum thickness. These findings suggest that under-ice preconditioning of pCO_2 in the surface mixed layer prior to ice break-up, and subsequent air-sea gas exchange occur much earlier than previously thought. However, the biological community responsible for the significant carbon uptake during this late winter period remains unidentified. Having ruled out ice algae, phytoplankton, and benthic microalgae as possible communities, further work is required to determine what is driving net ecosystem production during this time of the year.

The system warmed through the spring and as sea ice melted the underlying water column received a substantial increase in available PAR to an average of 65.28±28.77 µmol/m^2s (Figure 21). Increased light availability coupled with the presumed abundance of nutrients regenerated

over the winter months, allowed biology to effectively drawdown a significant amount of DIC before the open water season (233.53 µmol/kg). It is difficult to discern the exact biologic fixation of DIC to biomass in the water column as there was observed non-photochemical quenching of pelagic algae during this time. The biologic uptake through the spring was also large enough to force the aragonite saturation state to return to supersaturation. The site entered the open water season significantly undersaturated in pCO_2 with respect to the atmosphere (ΔpCO_2 = -177.18 µatm).

6.5. Carbon Sequestration

The ONC site in CB is likely a net annual sink for atmospheric CO_2 based on our presented final time-series dataset for the 2016-2017 platform deployment (Figure 15) and subsequent discussion (Section 6.0.-6.4.). There was never an observed interval of outgassing to the atmosphere, although the platform was isolated from the surface for eight weeks (May 16th 2017 - On July 20th 2017) in which air-sea gas exchange could not be calculated. During this interval there were five weeks where sea ice would have been permeable and likely was exchanging with the atmosphere (Butterworth & Else, 2018), followed by three weeks of open water. However, before this eight week interval, pCO_2 in the surface mixed layer was undersaturated with respect to the atmosphere. The observed biologically driven spring draw down (Figure 21) was likely to continue until the depletion of available nutrients (Campbell et al., 2016). Following nutrient depletion, there likely exists some duration of net heterotopic conditions before the fall, during the late summer that might increase pCO_2. The strength of the ONC site as a potential sink for air-sea gas exchange during the open water period depends on

the gradient of ΔpCO_2, which may change as surface waters warm and CO_2 becomes increasingly less soluble, and the gas transfer velocity driven by wind speeds. Without being able to close the annual DIC budget during the 2016-2017 deployment due to sensor failure (Section 3.3.3.), the platform entered the open water season with an unbalanced DIC budget and difference of -77.94 µmol/kg. Net annual unaccounted for DIC is likely exchanged with the organic carbon pool and potentially exported below the pycnocline to the seafloor in CB as falling particulate matter.

Our study indirectly looked to evaluate the conceptual model first proposed by Yager et al. (1995) to describe annual Arctic marine carbon cycling, and predict air-sea gas exchange of CO_2 in seasonally ice covered seas. Yager's conceptual model described seasonally ice free regions in the Arctic as strong annual sinks for atmospheric CO_2, because the seasonal cycle of $pCO_{2(sw)}$ was in-phase with the seasonal cycle of sea ice formation/ melt. We presented a high resolution marine carbon dataset within the surface mixed layer through the complete cycle of sea ice growth and melt that largely validates the Yager et al. (1995) conceptual model. pCO_2 was in-phase with the seasonal sea ice cycle at our site, reaching supersaturation in the winter, and due to under-ice biological preconditioning, was undersaturated entering the open water season. For the most part Yager's "*seasonal rectification hypothesis*" holds true. However, the importance of brine rejection in the DIC budget was not prevalent in the Yager model, and the timing and biologic community responsible for the late winter draw down was not quite correct either. Brine rejection played a major role in the early winter increasing DIC (Figure 19), and the

“sunrise” biologic drawdown occurred earlier than previous thought, at extremely low light levels by an as of yet unverified biologic community.

The impact of atmospheric anthropogenic carbon sequestration was also estimated. The observed period of 134 days of ΩAr undersaturation during the 2016-2017 deployment is to the best of our knowledge, the longest period of under-ice Arctic surface water ΩAr undersaturation reported. Following Bates et al. (2009), and given the typical inorganic carbon properties in CB, if the anthropogenic CO_2 component of DIC (~40±5 µmol/kg) were subtracted from our calculated DIC values, ΩAr would be 0.33±0.02 higher (Tanhua et al., 2009). This means that it is likely during pre-industrial times ΩAr undersaturation would probably not have occurred in under-ice surface waters in CB if there was no change in all other observed environmental conditions of the 2016-2017 deployment (e.g. temperature, salinity, primary production, sea ice thickness and growth duration). This estimate leads us to conclude that the observed seasonal ΩAr undersaturation is likely caused by the biologically induced seasonality of ΩAr (described previously), superimposed on a decline in ΩAr due to long-term ocean acidification similar to Bates et al. (2009) (Δ ΩAr = 0.4).

7.0. Conclusions

The deployment of a pCO_2 and pH sensor on an underwater cabled observatory in the Arctic is, to the best of our knowledge, unique in the world. The Cambridge Bay Ocean Networks Canada Undersea Community Observatory offered data coverage during the most under-sampled Arctic marine seasons of fall and winter, in a seasonally ice covered Arctic estuary over three consecutive nearly yearlong deployments. A Satlantic SeaFET Ocean pH Sensor was first deployed on the platform in 2016, along with a Pro-Oceanus CO2-Pro CV sensor first deployed a year before in 2015. We set out to validate these pH/ pCO_2 sensor measurements using discrete samples, and provide a post-deployment data correction method to produce final sensor time-series data products. In order to evaluate and calibrate the deployed *in situ* carbon system sensors onboard the platform we collected discrete samples at the site through all three deployments (2015-2016, 2016-2017, and 2017-2018) measuring dissolved inorganic carbon, and total alkalinity. We tested methods of correction from raw factory single point calibration for the SeaFET and factory multipoint for the CO2-Pro against: factory end point calibrations, single point *in situ* calibrations, and multi-point *in situ* calibrations.

A SeaFET sensor correction was deemed necessary for both deployments as there were noted discrepancies between the sensors two independent reference electrodes, as well as temperature discrepancies in the SeaFET thermistor response. The *in situ* multipoint calibration method was determined to be the most robust and applicable given the long deployment intervals, and was used for both deployments to maintain consistency. There was no

distinguishable trend between *in situ* single point calibrations improving sensor performance taken at any particular time during deployment. The final pH data set produced over both deployments was within the realm of “weather level” data quality but not “climate level.”

The two Pro-Oceanus CO2-Pro CV sensors deployed in rotation had varied factory calibrated results. During the 2015-2016 deployment, the sensor had issues with power outages related to equilibration rebounding with surrounding seawater following an automatic zero point calibration. However, the sensor still performed quite well relative to discrete samples. During the 2016-2017 deployment of a separate sensor, there was no indication of significant drift or offset, but a correction was warranted based on variability in over and under-estimation of pCO_2 compared to discrete samples. In 2017-2018 the first sensor was factory recalibrated and redeployed, with the sensor significantly consistently overestimating pCO_2 through the entirety of the deployment. All deployments were corrected utilizing the inferred sensor offset from the mean sensor difference compared to *in situ* multipoint discrete sample references. Following correction, final pCO_2 data sets were close to “weather level” data quality but not “climate level.”

Given our carbon system sensor evaluation results, it is clear these sensors cannot be left unattended for long under-ice deployments without any independent reference to validate the sensor. However, based on our results the prospect of future autonomous marine observing platforms equipped with onboard carbon system sensors in the Arctic's shelf seas are encouraging. Recommendations for long term Arctic deployments include: allowing for appropriate pre-deployment sensor conditioning periods, the collection of frequent reference

discrete samples throughout the deployment interval, and deployment of co-located biogeochemical sensors (if feasible an oxygen and argon sensor to better constrain net ecosystem production). Another point of recommendation for deployment location and depth includes consideration of use. If air-sea gas exchange is of interest, near surface deployments are recommended being mindful of sea ice growth in the winter, isolation due to freshwater input in the spring/ early summer, potential sea surface warming into the late summer, and regional wind speed climatology to ensure the surface mixed layer is in fact well mixed.

Using CTD measurements and expanded spatial discrete sampling, the spatial and temporal representation of the platform relative to the greater oceanography of Cambridge Bay was assessed. Given the platform depth and location, based on our results the site is very representative of the greater sea surface mixed layer in the bay following sea ice formation, and development of a deep winter mixed layer. Physical and chemical forcing in the spring isolated the platform from the air-sea interface, making the platform incapable of estimating air-sea CO_2 flux for approximately eight weeks. Following melt and surface warming, it appears that by summer the platform is again representative of the surface due to wind driven mixing. Despite its near-shore location, the platform was representative of carbon cycling processes further off shore year round.

In our analysis of biogeochemical processes driving the inorganic carbon cycle over a complete cycle of sea ice growth and melt in Cambridge Bay, we made use of a diagnostic box model with five identified processes including: air–sea exchange, vertical diffusion, entrainment, brine rejection from sea ice growth, and net ecosystem production. Through the fall as pCO_2 was

undersaturated with respect to the atmosphere, air-sea gas exchange and biological respiration/ remineralization are the dominant drivers of increasing pCO_2 and decreasing pH. pCO_2 steadily increased, while pH continued to decrease through the early winter following sea ice freeze up, as brine rejection drove pCO_2 at the platform to seasonal supersaturation with respect to the atmosphere, and undersaturation in the aragonite saturation state. These are the first observations of prolonged seasonal aragonite undersaturation in surface waters of the Arctic, with the duration of the undersaturation period (~130 days) long enough to warrant future investigation of biological impacts. Shortly after the sun rose in the late winter under the ice, the ecosystem at the platform changed from net heterotrophic to net autotrophic at very low light levels, driving pCO_2 to return to undersaturation well before sea ice had begun to melt. During this late winter period, ice algae, pelagic phytoplankton and benthic microalgae were ruled out as potential communities driving the biologic "sunrise" DIC draw down. Biologic processes reported in the literature at this time of the year are scarce prompting reason for further investigation. As sea ice melted in the spring and light penetration increased in the underlying water column, biology was able to effectively drawdown a significant amount of carbon before the open water season, increasing pH. The biologic uptake through the spring was large enough to return the aragonite saturation state to supersaturation, and for pCO_2 to enter the open water season significantly undersaturated with respect to the atmosphere.

References

AMAP. (2013). AMAP Assessment 2013: Arctic Ocean Acidification. In *Arctic Monitoring and Assessment Programme (AMAP)* (p. viii + 99 pp). Oslo, Norway.

AMAP. (2018). AMAP Assessment 2018: Arctic Ocean Acidification. In *Arctic Monitoring and Assessment Programme (AMAP)* (p. vi+187pp). Tromsø, Norway. https://doi.org/10.1016/j.techfore.2013.08.036

Anderson, L. G., Falck, E., Jone, E. P., Jutterström, S., & Swift, J. H. (2004). Enhanced uptake of atmospheric CO2 during freezing of seawater: A field study in Storfjorden, Svalbard. *Journal of Geophysical Research C: Oceans*, *109*(6), 4–11. https://doi.org/10.1029/2003JC002120

Arrhenius, S. (1897). On the Influence of Carbonic Acid in the Air upon the Temperature of the Earth. *Publications of the Astronomical Society of the Pacific*, *9*, 14. https://doi.org/10.1086/121158

Arrigo, K. R., & Sullivan, C. W. (1992). The influence of salinity and temperature covariation on the photophysiological characteristics of Antarctic sea ice microalgae. *Journal of Phycology*, *28*, 746–756. https://doi.org/10.1111/j.0022-3646.1992.00746.x

Arrigo, Kevin R., Mock, T., & Lizotte, M. P. (2010). Primary Producers and Sea Ice. In *Sea Ice: Second Edition*. https://doi.org/10.1002/9781444317145.ch8

Arrigo, Kevin R., & van Dijken, G. L. (2015). Continued increases in Arctic Ocean primary production. *Progress in Oceanography*, *136*, 60–70. https://doi.org/10.1016/j.pocean.2015.05.002

Arrigo, Kevin R, Perovich, D. K., Pickart, R. S., Brown, Z. W., Dijken, G. L. Van, Lowry, K. E., … Swift, J. H. (2012). Massive Phytoplankton Blooms Under Arctic Sea Ice. *Science*, *336*(June). https://doi.org/10.1126/science.1215065

Aßmann, S., Frank, C., & Ḱrtzinger, A. (2011). Spectrophotometric high-precision seawater pH determination for use in underway measuring systems. *Ocean Science*. https://doi.org/10.5194/os-7-597-2011

Atamanchuk, D., Tengberg, A., Thomas, P. J., Hovdenes, J., Apostolidis, A., Huber, C., & Hall, P. O. J. (2014). Performance of a lifetime-based optode for measuring partial pressure of carbon dioxide in natural waters. *Limnology and Oceanography: Methods*, *12*(FEB), 63–73. https://doi.org/10.4319/lom.2014.12.63

Azetsu-Scott, K., Clarke, A., Falkner, K., Hamilton, J., Jones, E. P., Lee, C., … Yeats, P. (2010). Calcium carbonate saturation states in the waters of the Canadian Arctic Archipelago and the Labrador Sea. *Journal of Geophysical Research: Oceans*, *115*(11), 1–18. https://doi.org/10.1029/2009JC005917

Bates, N. R., & Mathis, J. T. (2009). The Arctic Ocean marine carbon cycle: evaluation of air-sea CO2 exchanges, ocean acidification impacts and potential feedbacks. *Biogeosciences*, *6*(4), 2433–2459. https://doi.org/10.5194/bgd-6-6695-2009

Bates, Nicholas R., Moran, S. B., Hansell, D. A., & Mathis, J. T. (2006). An increasing CO2 sink in the Arctic Ocean due to sea-ice loss. *Geophysical Research Letters*. https://doi.org/10.1029/2006GL027028

Bates, Nicholas R, Mathis, J. T., & Cooper, L. W. (2009). Ocean acidification and biologically induced seasonality of carbonate mineral saturation states in the western Arctic Ocean. *Journal of Geophysical Research*, *114*(November), 1–21. https://doi.org/10.1029/2008JC004862

Berge, J., Renaud, P. E., Darnis, G., Cottier, F., Last, K., Gabrielsen, T. M., … Falk-Petersen, S. (2015). In the dark: A review of ecosystem processes during the Arctic polar night. *Progress in Oceanography*, *139*, 258–271. https://doi.org/10.1016/j.pocean.2015.08.005

Bresnahan, P. J., Martz, T. R., Takeshita, Y., Johnson, K. S., & LaShomb, M. (2014). Best practices for autonomous measurement of seawater pH with the Honeywell Durafet. *Methods in Oceanography*, *9*(August), 44–60. https://doi.org/10.1016/j.mio.2014.08.003

Brix, H., Gruber, N., & Keeling, C. D. (2004). Interannual variability of the upper ocean carbon cycle at station ALOHA near Hawaii. *Global Biogeochemical Cycles*, *18*(4), 1–18. https://doi.org/10.1029/2004GB002245

Buck, R. P., Rondinini, S., Covington, A. K., Baucke, F. G. K., Brett, C. M. A., Camoes, M. F., … Wilson, G. S. (2002). Measurement of pH. Definition, standards, and procedures (IUPAC Recommendations 2002). *Pure and Applied Chemistry*. https://doi.org/10.1351/pac200274112169

Butterworth, B. J., & Else, B. G. T. (2018). Dried , closed-path eddy covariance method for measuring carbon dioxide flux over sea ice, 6075–6090. https://doi.org/10.5194/amt-11-6075-2018

Butterworth, B. J., & Miller, S. D. (2016). Air-sea exchange of carbon dioxide in the Southern Ocean and Antarctic marginal ice zone. https://doi.org/10.1002/2016GL069581.Received

Cai, W. J., Hu, X., Huang, W. J., Jiang, L. Q., Wang, Y., Peng, T. H., & Zhang, X. (2010). Alkalinity distribution in the western North Atlantic Ocean margins. *Journal of Geophysical Research: Oceans*, *115*(8). https://doi.org/10.1029/2009JC005482

Campbell, K., Mundy, C. J., Landy, J. C., Delaforge, A., Michel, C., & Rysgaard, S. (2016). Community dynamics of bottom-ice algae in Dease Strait of the Canadian Arctic. *Progress in Oceanography*, *149*, 27–39. https://doi.org/10.1016/j.pocean.2016.10.005

Campbell, K., Mundy, C. J., Rysgaard, S., Landy, J. C., Gosselin, M., & Delaforge, A. (2017). Net community production in the bottom of first-year sea ice over the Arctic spring bloom.

Geophysical Research Letters, *44*(17), 8971–8978. https://doi.org/10.1002/2017gl074602

Carmack, E. C. (1986). The Geophysics of Sea Ice. In N. Untersteiner (Ed.), *Circulation and mixing in ice-covered waters* (pp. 641–712). New York: Plenum.

Chen, B., Cai, W. J., & Chen, L. (2015). The marine carbonate system of the Arctic Ocean: Assessment of internal consistency and sampling considerations, summer 2010. *Marine Chemistry*, *176*, 174–188. https://doi.org/10.1016/j.marchem.2015.09.007

Chierici, M, & Fransson, A. (2009). Calcium carbonate saturation in the surface water of the Arctic Ocean: undersaturation in freshwater influenced shelves. *Biogeosciences Discussions*, *6*(3), 4963–4991. https://doi.org/10.5194/bgd-6-4963-2009

Chierici, Melissa, Fransson, A., Lansard, B., Miller, L. A., Mucci, A., Shadwick, E., … Papakyriakou, T. N. (2011). Impact of biogeochemical processes and environmental factors on the calcium carbonate saturation state in the Circumpolar Flaw Lead in the Amundsen Gulf, Arctic Ocean. *Journal of Geophysical Research: Oceans*, *116*(12). https://doi.org/10.1029/2011JC007184

Clayton, T. D., & Byrne, R. H. (1993). Spectrophotometric seawater pH measurements: total hydrogen ion concentration scale calibration of m-cresol purple and at-sea results. *Deep-Sea Research Part I*. https://doi.org/10.1016/0967-0637(93)90048-8

Coombs, A. (2014). Defining the anthropocene. *Frontiers in Ecology and the Environment*. https://doi.org/10.1890/1540-9295-12.4.204

DeGrandpre, M. D., Hammar, T. R., Smith, S. P., & Sayles, F. L. (1995). In situ measurements of seawater pCO2. *Limnology and Oceanography*. https://doi.org/10.4319/lo.1995.40.5.0969

Dickson, A. G. (1984). pH scales and proton-transfer reactions in saline media such as sea water. *Geochimica et Cosmochimica Acta*. https://doi.org/10.1016/0016-7037(84)90225-4

Dickson, Andrew G. (1990). Standard potential of the reaction: AgCl(s) + 1 2H2(g) = Ag(s) + HCl(aq), and and the standard acidity constant of the ion HSO4-in synthetic sea water from 273.15 to 318.15 K. *The Journal of Chemical Thermodynamics*, *22*(2), 113–127. https://doi.org/10.1016/0021-9614(90)90074-Z

Dickson, Andrew G., Sabine, C. L., & Christian, J. R. (2007). Guide to Best Practices for Ocean CO2 Measurements. *PICES Spec. Publ.* Sidney: North Pacific Marine Science Organization.

Dickson, Andrew G, & Goyet, C. (1997). Handbook of methods for the analysis of the various parameters of the carbon dioxide system in sea water. *Handbook of Methods for the Analysis of the Various Parameters of the Carbon Dioxide System in Sea Water*. https://doi.org/ORNL/CDIAC-74

Else, B. G T, Papakyriakou, T. N., Galley, R. J., Drennan, W. M., Miller, L. A., & Thomas, H. (2011). Wintertime CO2 fluxes in an Arctic polynya using eddy covariance: Evidence for enhanced air-sea gas transfer during ice formation. *Journal of Geophysical Research*, *116*(9), 1–15.

https://doi.org/10.1029/2010JC006760

Else, B. G T, Papakyriakou, T. N., Galley, R. J., Mucci, A., Gosselin, M., Miller, L. A., … Thomas, H. (2012). Annual cycles of pCO2sw in the southeastern Beaufort Sea: New understandings of air-sea CO2 exchange in arctic polynya regions. *Journal of Geophysical Research: Oceans*, *117*(4), 1–16. https://doi.org/10.1029/2011JC007346

Else, Brent G T, Whitehead, J. J., Galindo, V., Ferland, J., Mundy, C. J., Gonski, S. F., … Babin, M. (2019). Response of the Arctic marine inorganic carbon system to ice algae and under-ice phytoplankton blooms: A case study along the fast-ice edge of Baffin Bay. *Journal of Geophysical Research: Oceans Key*. https://doi.org/10.1029/2018JC013899

Environment and Natural Resources Canada. (2019). Water Survey of Canada. Retrieved from https://wateroffice.ec.gc.ca/index_e.html

Fabry, V. J., McClintock, J. B., Mathis, J. T., & Grebmeier, J. M. (2009). Ocean Acidification at High Latitudes: The Bellweather. *Oceanography*, *22*(4), 160–171. https://doi.org/10.5670/oceanog.2009.105

Falkowski, P. G., & LaRoche, J. (1991). Acclimation to spectral irradiance in algae. *Journal of Phycology*. https://doi.org/10.1111/j.0022-3646.1991.00008.x

Fassbender, A. J., Sabine, C. L., & Palevsky, H. I. (2017). Nonuniform ocean acidification and attenuation of the ocean carbon sink. *Geophysical Research Letters*, *44*(16), 8404–8413. https://doi.org/10.1002/2017GL074389

Fortier, M., Fortier, L., Michel, C., & Legendre, L. (2002). Climatic and biological forcing of the vertical flux of biogenic particles under seasonal Arctic sea ice. *Marine Ecology Progress Series*. https://doi.org/10.3354/meps225001

Fritzsche, E., Gruber, P., Schutting, S., Fischer, J. P., Strobl, M., Müller, J. D., … Klimant, I. (2017). Highly sensitive poisoning-resistant optical carbon dioxide sensors for environmental monitoring. *Analytical Methods*, *9*(1), 55–65. https://doi.org/10.1039/c6ay02949c

Fritzsche, E., Staudinger, C., Fischer, J. P., Thar, R., Jannasch, H. W., Plant, J. N., … Klimant, I. (2018). A validation and comparison study of new, compact, versatile optodes for oxygen, pH and carbon dioxide in marine environments. *Marine Chemistry*, *207*(October), 63–76. https://doi.org/10.1016/j.marchem.2018.10.009

Gade, H. G., Lake, R. A., Lewis, E. L., & Walker, E. R. (1974). Oceanography of an Arctic bay. *Deep-Sea Research and Oceanographic Abstracts*, *21*(7), 547–571. https://doi.org/10.1016/0011-7471(74)90012-6

Garneau, M. È., Vincent, W. F., Alonso-Sáez, L., Gratton, Y., & Lovejoy, C. (2006). Prokaryotic community structure and heterotrophic production in a river-influenced coastal arctic ecosystem. *Aquatic Microbial Ecology*. https://doi.org/10.3354/ame042027

Gasol, J. M., & Kirchman, D. L. (2018). *Microbial Ecology of the Oceans* (3rd Edition). Wiley-

Blackwell.

Geilfus, N. X., Carnat, G., Papakyriakou, T., Tison, J. L., Else, B., Thomas, H., … Delille, B. (2012). Dynamics of pCO2 and related air-ice CO2 fluxes in the Arctic coastal zone (Amundsen Gulf, Beaufort Sea). *Journal of Geophysical Research: Oceans*, *117*(2), 1–15. https://doi.org/10.1029/2011JC007118

Gonski, S. F., Cai, W. J., Ullman, W. J., Joesoef, A., Main, C. R., Pettay, D. T., & Martz, T. R. (2018). Assessment of the suitability of Durafet-based sensors for pH measurement in dynamic estuarine environments. *Estuarine, Coastal and Shelf Science*, *200*, 152–168. https://doi.org/10.1016/j.ecss.2017.10.020

Gosselin, M., Legendre, L., Rochet, M., Demers, S., & Therriault, J.-C. (1986). Physical control of the horizontal patchiness of sea-ice microalgae. *Marine Ecology Progress Series*, *29*, 289–298. https://doi.org/10.3354/meps029289

Gradinger, R. (2009). Sea-ice algae: Major contributors to primary production and algal biomass in the Chukchi and Beaufort Seas during May/June 2002. *Deep Sea Research Part II: Topical Studies in Oceanography*, *56*(17), 1201–1212. https://doi.org/https://doi.org/10.1016/j.dsr2.2008.10.016

Gran, G. (1950). Determination of the equivalent point in potentiometric titrations. *Acta Chemica Scandinavica*. https://doi.org/10.3891/acta.chem.scand.04-0559

Gran, G. (1952). Determination of the equivalence point in potentiometric titrations. Part II. *The Analyst*, *77*(920), 661. https://doi.org/10.1039/an9527700661

Grossmann, S., & Dieckmann, G. S. (1994). Bacterial Standing Stock , Activity , and Carbon Production during Formation and Growth of Sea Ice in the Weddell Sea , Antarcticat, *60*(8), 2746–2753.

Gruber, N., Keeling, C. D., & Bates, N. R. (2002). Interannual Variability in the North Atlantic Ocean Carbon Sink. *Science*, *298*(5602), 2374–2378. https://doi.org/10.1126/science.1077077

Gruber, N., Keeling, C. D., & Stocker, T. F. (1998). Carbon-13 constraints on the seasonal inorganic carbon budget at the BATS site in the northwestern Sargasso Sea. *Deep-Sea Research Part I: Oceanographic Research Papers*, *45*(4–5), 673–717. https://doi.org/10.1016/S0967-0637(97)00098-8

Hansson, I. (1973). A new set of pH-scales and standard buffers for sea water. *Deep-Sea Research and Oceanographic Abstracts*. https://doi.org/10.1016/0011-7471(73)90101-0

Haraldsson, C., Anderson, L. G., Hassellöv, M., Hulth, S., & Olsson, K. (1997). Rapid, high-precision potentiometric titration of alkalinity in ocean and sediment pore waters. *Deep-Sea Research Part I: Oceanographic Research Papers*. https://doi.org/10.1016/S0967-0637(97)00088-5

Hoegh-Guldberg, O., D. Jacob, M. Taylor, M. Bindi, S. Brown, I. Camilloni, A. Diedhiou, R. Djalante, K.L. Ebi, F. Engelbrecht, J. Guiot, Y. Hijioka, S. Mehrotra, A. Payne, S.I. Seneviratne, A. Thomas, R. Warren, and G. Z. (2018). *Impacts of 1.5°C Global Warming on Natural and Human Systems*. *Global Warming of 1.5°C. An IPCC Special Report on the impacts of global warming of 1.5°C above pre-industrial levels and related global greenhouse gas emission pathways, in the context of strengthening the global response to the threat of climate change,*.

Horner, R., & Schrader, G. C. (1982). Relative Contributions of Ice Algae, Phytoplankton, and Benthic Microalgae to Primary Production in Nearshore Regions of the Beaufort Sea. *Arctic*, *35*(4), 485–503. https://doi.org/10.14430/arctic2356

IPCC. (2013). *IPCC, 2013: Climate Change 2013: The Physical Science Basis. Contribution of Working Group I to the Fifth Assessment Report of the Intergovernmental Panel on Climate Change*. *IPCC* (Vol. AR5). https://doi.org/10.1017/CBO9781107415324

IPCC. (2014). *Climate Change 2014: Mitigation of Climate Change*. *Working Group III Contribution to the Fifth Assessment Report of the Intergovernmental Panel on Climate Change*. https://doi.org/10.1017/CBO9781107415416

Iversen, K. R., & Seuthe, L. (2011). Seasonal microbial processes in a high-latitude fjord (Kongsfjorden, Svalbard): I. Heterotrophic bacteria, picoplankton and nanoflagellates. *Polar Biology*. https://doi.org/10.1007/s00300-010-0929-2

Jiang, X., Jin, X., Yao, Y., Li, L., & Wu, F. (2008). Effects of biological activity, light, temperature and oxygen on phosphorus release processes at the sediment and water interface of Taihu Lake, China. *Water Research*, *42*(8–9), 2251–2259. https://doi.org/10.1016/j.watres.2007.12.003

Jiang, Z., Hydes, D. J., Hartman, S. E., Hartman, M. C., Campbell, J. M., Johnson, B. D., … Cosca, C. (2014). Application and assessment of a membrane-based pCO 2 sensor under field and laboratory conditions. *Limnology and Oceanography: Methods*, *12*, 264–280. https://doi.org/10.4319/lom.2014.12.264

Johnson, K. M., Wills, K. D., Butler, D. B., Johnson, W. K., & Wong, C. S. (1993). Coulometric total carbon dioxide analysis for marine studies: maximizing the performance of an automated gas extraction system and coulometric detector. *Marine Chemistry*. https://doi.org/10.1016/0304-4203(93)90201-X

Kapsenberg, L., Bockmon, E. E., Bresnahan, P. J., Kroeker, K. J., Gattuso, J.-P., & Martz, T. R. (2017). Advancing Ocean Acidification Biology Using Durafet® pH Electrodes. *Frontiers in Marine Science*, *4*(October), 1–9. https://doi.org/10.3389/fmars.2017.00321

Keeling, C. D., Brix, H., & Gruber, N. (2004). Seasonal and long-term dynamics of the upper ocean carbon cycle at Station ALOHA near Hawaii. *Global Biogeochemical Cycles*, *18*(4), 1–26. https://doi.org/10.1029/2004GB002227

King, A. D., Donat, M. G., Fischer, E. M., Hawkins, E., Alexander, L. V, Karoly, D. J., … Perkins, S. E. (2015). The timing of anthropogenic emergence in simulated climate extremes. *Environmental Research Letters*, *10*(9), 94015. https://doi.org/10.1088/1748-9326/10/9/094015

Körtzinger, A., Thomas, H., Schneider, B., Gronau, N., Mintrop, L., & Duinker, J. C. (1996). At-sea intercomparison of two newly designed underway pCO2systems - Encouraging results. *Marine Chemistry*. https://doi.org/10.1016/0304-4203(95)00083-6

Laxon, S. W., Giles, K. A., Ridout, A. L., Wingham, D. J., Willatt, R., Cullen, R., … Davidson, M. (2013). CryoSat-2 estimates of Arctic sea ice thickness and volume. *Geophysical Research Letters*, *40*(4), 732–737. https://doi.org/10.1002/grl.50193

Le Quéré, C., Takahashi, T., Buitenhuis, E. T., Rödenbeck, C., & Sutherland, S. C. (2010). Impact of climate change and variability on the global oceanic sink of CO2. *Global Biogeochemical Cycles*, *24*(4), 1–10. https://doi.org/10.1029/2009GB003599

Lee, K., Kim, T. W., Byrne, R. H., Millero, F. J., Feely, R. A., & Liu, Y. M. (2010). The universal ratio of boron to chlorinity for the North Pacific and North Atlantic oceans. *Geochimica et Cosmochimica Acta*, *74*(6), 1801–1811. https://doi.org/10.1016/j.gca.2009.12.027

Leu, E., Mundy, C. J., Assmy, P., Campbell, K., Gabrielsen, T. M., Gosselin, M., … Gradinger, R. (2015). Arctic spring awakening - Steering principles behind the phenology of vernal ice algal blooms. *Progress in Oceanography*, *139*, 151–170. https://doi.org/10.1016/j.pocean.2015.07.012

Lewis, E L, & Walker, E. R. (1970). The water structure under a growing ice sheet. *Journal of Geophysical Research*, *75 (33)*, 6836–6845.

Lewis, EL, & Jones, E. (2000). *The freshwater budget of the Arctic Ocean*. (Edward Lyn Lewis, E. P. Jones, P. Lemke, T. D. Prowse, & P. Wadhams, Eds.) (Series 2.). Springer Netherlands. https://doi.org/10.1007/978-94-011-4132-1

Lewis, Ernie, Wallace, D., & Allison, L. J. (1998). Program developed for CO2 system calculations. *Tennessee: Carbon Dioxide Information Analysis Center, Managed by Lockheed Martin Energy Research Corporation for the US Department of Energy*. https://doi.org/4735

Lichtschlag, A., James, R. H., Stahl, H., & Connelly, D. (2015). Effect of a controlled sub-seabed release of CO 2 on the biogeochemistry of shallow marine sediments , their pore waters , and the overlying water column. *International Journal of Greenhouse Gas Control*, *38*, 80–92. https://doi.org/10.1016/j.ijggc.2014.10.008

Liu, X., Patsavas, M. C., & Byrne, R. H. (2011). Purification and characterization of meta-cresol purple for spectrophotometric seawater ph measurements. *Environmental Science and Technology*. https://doi.org/10.1021/es200665d

Loose, B., Miller, L. A., Elliott, S., & Papakyriakou., T. (2011). Sea ice biogeochemistry and

material transport across the frozen interface. *Oceanography*, *24*(3), 202–218. https://doi.org/10.5670/oceanog.2011.65

Loose, B., Schlosser, P., Perovich, D., Ringelberg, D., Ho, D. T., Takahashi, T., … Tison, J. L. (2011). Gas diffusion through columnar laboratory sea ice: Implications for mixed-layer ventilation of CO2 in the seasonal ice zone. *Tellus, Series B: Chemical and Physical Meteorology*, *63*(1), 23–39. https://doi.org/10.1111/j.1600-0889.2010.00506.x

Lovett, G. M., Cole, J. J., & Pace, M. L. (2006). Is net ecosystem production equal to ecosystem carbon accumulation? *Ecosystems*, *9*(1), 152–155. https://doi.org/10.1007/s10021-005-0036-3

Lueker, T. J., Dickson, A. G., & Keeling, C. D. (2000). Ocean pCO_2 calculated from dissolved inorganic carbon, alkalinity, and equations for K_1 and K_2: validation based on laboratory measurements of CO_2 in gas and seawater at equilibrium. *Marine Chemistry*, *70*(1), 105–119. https://doi.org/10.1016/S0304-4203(00)00022-0

Macintyre, H. L., Kana, T. M., & Geider, R. J. (2000). The effect of water motion on short-term rates of photosynthesis by marine phytoplankton. *Trends in Plant Science*. https://doi.org/10.1016/S1360-1385(99)01504-6

Martz, T. R., Connery, J. G., & Johnson, K. S. (2010). Testing the Honeywell Durafet® for seawater pH applications. *Limnology and Oceanography: Methods*, *8*(MAY), 172–184. https://doi.org/10.4319/lom.2010.8.172

Maslanik, J. A., Fowler, C., Stroeve, J., Drobot, S., Zwally, J., Yi, D., & Emery, W. (2007). A younger, thinner Arctic ice cover: Increased potential for rapid, extensive sea-ice loss. *Geophysical Research Letters*, *34*(24). https://doi.org/10.1029/2007GL032043

McLaughlin, K., Dickson, A., Weisberg, S. B., Coale, K., Elrod, V., Hunter, C., … Weis, K. R. (2017). An evaluation of ISFET sensors for coastal pH monitoring applications. *Regional Studies in Marine Science*, *12*, 11–18. https://doi.org/10.1016/j.rsma.2017.02.008

McPhee, M. G., & Stanton, T. P. (1996). Turbulence in the statically unstable oceanic boundary layer under Arctic leads. *Journal of Geophysical Research C: Oceans*. https://doi.org/10.1029/95JC03842

Melling, H., Lake, R. A., Topham, D. R., & Fissel, D. B. (1984). Oceanic thermal structure in the western Canadian Arctic. *Continental Shelf Research*, *3*(3), 233–358.

Miller, C. A., Pocock, K., Evans, W., & Kelley, A. L. (2018). An evaluation of the performance of Sea-Bird Scientific's SeaFET(tm) autonomous pH sensor: Considerations for the broader oceanographic community. *Ocean Science*, *14*(4), 751–768. https://doi.org/10.5194/os-14-751-2018

Miller, L. A., Carnat, G., Else, B. G. T., Sutherland, N., & Papakyriakou, T. N. (2011). Carbonate system evolution at the Arctic Ocean surface during autumn freeze-up. *Journal of*

Geophysical Research: Oceans, *116*(10). https://doi.org/10.1029/2011JC007143

Miller, L. A., Papakyriakou, T. N., Collins, R. E., Deming, J. W., Ehn, J. K., MacDonald, R. W., … Sutherland, N. (2011). Carbon dynamics in sea ice: A winter flux time series. *Journal of Geophysical Research: Oceans*, *116*(2), 1–20. https://doi.org/10.1029/2009JC006058

Mundy, C. J., Gosselin, M., Ehn, J., Gratton, Y., Rossnagel, A., Barber, D. G., … Papakyriakou, T. (2009). Contribution of under-ice primary production to an ice-edge upwelling phytoplankton bloom in the Canadian Beaufort Sea. *Geophysical Research Letters*, *36*(17), 1–5. https://doi.org/10.1029/2009GL038837

Mundy, C. J., Gosselin, M., Gratton, Y., Brown, K., Galindo, V., Campbell, K., … Bélanger, S. (2014). Role of environmental factors on phytoplankton bloom initiation under landfast sea ice in Resolute Passage, Canada. *Marine Ecology Progress Series*. https://doi.org/10.3354/meps10587

Neale, P. J., & Priscu, J. C. (2013). Fluorescence Quenching in Phytoplankton of the Mcmurdo Dry Valley Lakes (Antarctica): Implications for The Structure and Function Of The Photosynthetic Apparatus. In *Ecosystem Dynamics in a Polar Desert: the Mcmurdo Dry Valleys, Antarctica* (pp. 241–253). American Geophysical Union (AGU). https://doi.org/10.1029/AR072p0241

Newton, J. A., Feely, R. A., Jewett, E. B., Williamson, P., & Mathis, J. (2015). Global Ocean Acidification Observing Network: Requirements and Governance Plan, (September), 57 pp. Retrieved from http://goa-on.org/docs/GOA-ON_Plan_final_Sept_2014.pdf

Niemi, A., Michel, C., Hille, K., & Poulin, M. (2011). Protist assemblages in winter sea ice: Setting the stage for the spring ice algal bloom. *Polar Biology*. https://doi.org/10.1007/s00300-011-1059-1

Nummelin, A., Ilicak, M., Li, C., & Smedsrud, L. H. (2016). Consequences of future increased Arctic runoff on Arctic Ocean stratification, circulation, and sea ice cover. *Journal of Geophysical Research: Oceans*, *121*(1), 617–637. https://doi.org/10.1002/2015JC011156

Ocean Networks Canada. (2011). *Canadian Arctic Cabled Marine Observatory Feasibility Study*. Victoria, BC Canada.

Papakyriakou, T., & Miller, L. (2011). Springtime CO₂ exchange over seasonal sea ice in the Canadian Arctic Archipelago. *Annals of Glaciology*, *52*(57), 215–224. https://doi.org/10.3189/172756411795931534

Peltzer, E. (2007). Model II least squares fit: lsqfitma.m. Retrieved from http://www.mbari.org/staff/ etp3/regress/lsqfitma.m

Peralta-Ferriz, C., & Woodgate, R. A. (2015). Seasonal and interannual variability of pan-Arctic surface mixed layer properties from 1979 to 2012 from hydrographic data, and the dominance of stratification for multiyear mixed layer depth shoaling. *Progress in*

Oceanography, *134*, 19–53. https://doi.org/10.1016/j.pocean.2014.12.005

Pereira, E., Schuster, U., Rérolle, V., Brown, P., Gkritzalis, T., Downing, B., … Spaulding, R. (2017). Biogeochemical Parameters: pCO2. In: A user's guide for selected autonomous biogeochemical sensors. An outcome from the 1st IOCCP International Sensors Summer Course [Lorenzoni, L., M. Telszewski, H. Benway, A. P. Palacz (eds.)]. *IOCCP Report No. 2*, 31–42.

Perovich, D. K., Light, B., Eicken, H., Jones, K. F., Runciman, K., & Nghiem, S. V. (2007). Increasing solar heating of the Arctic Ocean and adjacent seas, 1979-2005: Attribution and role in the ice-albedo feedback. *Geophysical Research Letters*, *34*(19). https://doi.org/10.1029/2007GL031480

Pierrot, D., Lewis, E., & Wallace, D. W. R. (2006). CO2SYS DOS Program developed for CO2 system calculations. *ORNL/CDIAC-105*.

Qi, D., Chen, L., Chen, B., Gao, Z., Zhong, W., Feely, R. A., … Cai, W.-J. (2017). Increase in acidifying water in the western Arctic Ocean. *Nature Climate Change*, *7*(3), 195–199. https://doi.org/10.1038/nclimate3228

Rérolle, V., Ruiz-Pino, D., Rafizadeh, M., Loucaides, S., Papadimitriou, S., Mowlem, M., & Chen, J. (2016). Measuring pH in the Arctic Ocean: Colorimetric method or SeaFET? *Methods in Oceanography*, *17*, 32–49. https://doi.org/10.1016/j.mio.2016.05.006

Riedel, A., Michel, C., & Gosselin, M. (2006). Seasonal study of sea-ice exopolymeric substances on the Mackenzie shelf: Implications for transport of sea-ice bacteria and algae. *Aquatic Microbial Ecology*. https://doi.org/10.3354/ame045195

Rivest, E. B., O'Brien, M., Kapsenberg, L., Gotschalk, C. C., Blanchette, C. A., Hoshijima, U., & Hofmann, G. E. (2016). Beyond the benchtop and the benthos: Dataset management planning and design for time series of ocean carbonate chemistry associated with Durafet®-based pH sensors. *Ecological Informatics*, *36*, 209–220. https://doi.org/10.1016/j.ecoinf.2016.08.005

Rogelj, J., D. Shindell, K. Jiang, S. Fifita, P. Forster, V. Ginzburg, C. Handa, H. Kheshgi, S. Kobayashi, E. Kriegler, L. Mundaca, R. Séférian, and M. V. V. (2018). Mitigation Pathways Compatible with 1.5°C in the Context of Sustainable Development. *Global Warming of 1.5°C. An IPCC Special Report on the Impacts of Global Warming of 1.5°C above Pre-Industrial Levels and Related Global Greenhouse Gas Emission Pathways, in the Context of Strengthening the Global Response to the Threat of Climate Change,*.

Rudels, B., Anderson, L. G., & Jones, E. P. (1996). Formation and evolution of the surface mixed layer and halocline of the Arctic Ocean. *Journal of Geophysical Research*, *101*, 8807–8821. https://doi.org/10.1029/96JC00143

Rysgaard, S., Glud, R. N., Sejr, M. K., Bendtsen, J., & Christensen, P. B. (2007). Inorganic carbon transport during sea ice growth and decay: A carbon pump in polar seas. *Journal of*

Geophysical Research, *112*(3), 1–8. https://doi.org/10.1029/2006JC003572

Rysgaard, Soren, Bendtsen, J., Delille, B., Dieckmann, G. S., Glud, R. N., Kennedy, H., … Tison, J. L. (2011). Sea ice contribution to the air-sea CO2 exchange in the Arctic and Southern Oceans. *Tellus, Series B: Chemical and Physical Meteorology*, *63*(5), 823–830. https://doi.org/10.1111/j.1600-0889.2011.00571.x

Sabine, C. L. (2004). The Oceanic Sink for Anthropogenic CO2. *Science*, *305*(5682), 367–371. https://doi.org/10.1126/science.1097403

Sarmiento, J. L., & Gruber, N. (2006). *Ocean Biogeochemical Dynamics* (Illustrate). Princeton: Princeton University Press.

Semiletov, I. P., Pipko, I. I., Repina, I., & Shakhova, N. E. (2007). Carbonate chemistry dynamics and carbon dioxide fluxes across the atmosphere-ice-water interfaces in the Arctic Ocean: Pacific sector of the Arctic. *Journal of Marine Systems*, *66*(1–4), 204–226. https://doi.org/10.1016/j.jmarsys.2006.05.012

Shadwick, E. H., Thomas, H., Chierici, M., Else, B., Fransson, A., Michel, C., … Tremblay, J.-É. (2011). Seasonal variability of the inorganic carbon system in the Amundsen Gulf region of the southeastern Beaufort Sea. *Limnology and Oceanography*, *56*(1), 303–322. https://doi.org/10.4319/lo.2011.56.1.0303

Shadwick, E. H., Trull, T. W., Thomas, H., & Gibson, J. A. E. (2013). Vulnerability of polar oceans to anthropogenic acidification: comparison of Arctic and Antarctic seasonal cycles. *Scientific Reports* , *3*, 2339. https://doi.org/10.1038/srep02339

Sherr, B. F., & Sherr, E. B. (2003). Community respiration/production and bacterial activity in the upper water column of the central Arctic Ocean. *Deep-Sea Research Part I: Oceanographic Research Papers*. https://doi.org/10.1016/S0967-0637(03)00030-X

Steele, M., Ermold, W., & Zhang, J. (2008). Arctic Ocean surface warming trends over the past 100 years. *Geophysical Research Letters*, *35*(2). https://doi.org/10.1029/2007GL031651

Steinacher, M., Joos, F., Frölicher, T. L., Plattner, G.-K., & Doney, S. C. (2008). Imminent ocean acidification projected with the NCAR global coupled carbon cycle-climate model. *Biogeosciences Discussions*, *5*(6), 4353–4393. https://doi.org/10.5194/bgd-5-4353-2008

Steinacher, M., Joos, F., Frölicher, T. L., Plattner, G. K., & Doney, S. C. (2009). Imminent ocean acidification in the Arctic projected with the NCAR global coupled carbon cycle-climate model. *Biogeosciences*. https://doi.org/10.5194/bg-6-515-2009

Subba Rao, D. V., & Platt, T. (1984). Primary production of arctic waters. *Polar Biology*, *3*(4), 191–201. https://doi.org/10.1007/BF00292623

Sundquist, E. T. (1985). Geological Perspectives on Carbon Dioxide and the Carbon Cycle. In *The Carbon Cycle and Atmospheric CO: Natural Variations Archean to Present* (pp. 55–59). Washington, D. C.: American Geophysical Union. https://doi.org/10.1029/GM032p0005

Takahashi, T., Olafsson, J., Goddard, J. G., Chipman, D. W., & Sutherland, S. C. (1993). Seasonal variation of CO2 and nutrients in the high-latitude surface oceans: A comparative study. *Global Biogeochemical Cycles*. https://doi.org/10.1029/93GB02263

Tanhua, T., Jones, E. P., Jeansson, E., Jutterstro, S., Jr, W. M. S., Wallace, D. W. R., & Anderson, L. G. (2009). Ventilation of the Arctic Ocean : Mean ages and inventories of anthropogenic CO2 and CFC-11. *Journal of Geophysical Research*, *114*(January), 1–11. https://doi.org/10.1029/2008JC004868

Terrado, R., Vincent, W. F., & Lovejoy, C. (2009). Mesopelagic protists: Diversity and succession in a coastal Arctic ecosystem. *Aquatic Microbial Ecology*. https://doi.org/10.3354/ame01327

Toole, J. M., Timmermans, M. L., Perovich, D. K., Krishfield, R. A., Proshutinsky, A., & Richter-Menge, J. A. (2010). Influences of the ocean surface mixed layer and thermohaline stratification on Arctic Sea ice in the central Canada Basin. *Journal of Geophysical Research: Oceans*, *115*(10). https://doi.org/10.1029/2009JC005660

Ulfsbo, A., Hannides, A., Atamanchuk, D., Poteau, A., Hartman, S., Bittig, H., … Bresnahan, P. (2017). Biogeochemical Parameters: pH. In: A user's guide for selected autonomous biogeochemical sensors. An outcome from the 1st IOCCP International Sensors Summer Course [Lorenzoni, L., M. Telszewski, H. Benway, A. P. Palacz (eds.)]. *IOCCP Report No. 2*, 43–59.

Van Heuven, S., Pierrot, D., Rae, J. W. B., Lewis, E., & Wallace, D. W. R. (2011, January 1). MATLAB Program Developed for CO2 System Calculations. ORNL/CDIAC-105b. Oak Ridge, Tennessee.: Carbon Dioxide Information Analysis Center, Oak Ridge National Laboratory, U.S. Department of Energy. https://doi.org/10.3334/CDIAC/OTG.CO2SYS_MATLAB_V1.1

Volk, T., & Hoffert, M. I. (1985). Ocean carbon pumps: Analysis of relative strengths and efficiencies in ocean-driven atmospheric CO2 changes. *Geophysical Monograph Series*, *32*, 99–110. https://doi.org/10.1029/GM032p0099

Vonk, J. E., & Gustafsson, Ö. (2013). Permafrost-carbon complexities. *Nature Geoscience*, *6*(9), 675–676. https://doi.org/10.1038/ngeo1937

Wanninkhof, R. (2014). Relationship between wind speed and gas exchange over the ocean revisited. *Limnology and Oceanography: Methods*, *12*(JUN), 351–362. https://doi.org/10.4319/lom.2014.12.351

Weiss, R. F. (1974). Carbon dioxide in water and seawater: the solubility of a non-ideal gas. *Marine Chemistry*, *2*(3), 203–215. https://doi.org/10.1016/0304-4203(74)90015-2

Weslawski, J. M., Szymelfenig, M., Zajaczkowski, M., & Keck, A. (1999). Influence of salinity and suspended matter on benthos of an Arctic tidal flat. In *ICES Journal of Marine Science*. https://doi.org/10.1006/jmsc.1999.0620

Yamamoto-Kawai, M., McLaughlin, F., & Carmack, E. (2013). Ocean acidification in the three oceans surrounding northern North America. *Journal of Geophysical Research: Oceans*, *118*(11), 6274–6284. https://doi.org/10.1002/2013JC009157

Yamamoto-Kawai, M., McLaughlin, F. A., Carmack, E. C., Nishino, S., Shimada, K., & Kurita, N. (2009). Surface freshening of the Canada Basin, 2003–2007: River runoff versus sea ice meltwater. *Journal of Geophysical Research*, *114*(C1), C00A05. https://doi.org/10.1029/2008JC005000

Zeebe, R. E. R. E., & Wolf-Gladrow, D. A. (2001). CO2 in seawater: equilibrium, kinetics, isotopes. *Elsevier Oceanography Series*, *65*(65), 346. https://doi.org/10.1016/S0924-7963(02)00179-3

Appendix

Appendix 1 All ONC platform carbon system sensor evaluation discrete samples collected during 2015-2016, 2016-2017, and 2017-2018 deployments. An asterisk denotes collection of 250 mL samples analyzed at Institute of Ocean Sciences (Sydney, British Columbia, Canada), the remaining are collected 125 mL samples analyzed at the University of Calgary (Calgary, Alberta, Canada).

Sample Dates	**Lab Salinity [PSU]**	**TA [µmol/kg]**	**DIC [µmol/kg]**
8/28/2015*	19.98	1246.18	1218.11
2/16/2016*	29.76	2082.84	2063.49
3/13/2016*	30.90	2089.00	2073.53
5/15/2016*	29.75	2076.54	2012.48
5/22/2016*	29.68	2070.25	2008.72
5/28/2016*	29.64	2071.93	2001.03
6/8/2016*	29.20	2063.27	1985.15
8/25/2016*	29.18	1925.09	1826.58
1/28/2017	28.50	2062.42	1993.10
2/2/2017*	28.55	2055.85	1999.96
2/27/2017	29.00	2106.28	2040.79
3/4/2017	28.70	2079.72	2021.70
3/11/2017	28.90	2092.21	2032.29
3/18/2017	28.90	2077.16	2026.16
3/28/2017	30.70	2181.53	2154.16
4/1/2017	28.80	2086.92	2028.67
4/14/2017	29.80	2141.14	2082.83
4/24/2017	29.20	2065.42	2023.33
4/30/2017*	29.47	2062.36	2007.55
5/3/2017	28.70	2078.30	1998.98
5/16/2017	28.60	2070.85	1998.05
5/24/2017	29.00	2057.63	2020.17
6/3/2017	28.50	2058.40	1943.57
6/9/2017	28.57	2054.52	1939.32
6/12/2017*	28.04	2025.82	1930.79
6/17/2017	28.70	2036.07	1911.84
6/24/2017	28.40	2038.19	1888.59
7/3/2017	28.40	2071.11	1899.13
7/10/2017	28.50	2029.70	1903.65
7/20/2017*	28.49	2040.36	1922.36
8/1/2017	27.10	2017.87	1872.11
9/14/17*	26.52	1932.85	1827.43

10/10/2017	26.00	1912.98	1809.32
10/31/2017	26.70	1935.05	1842.32
11/24/2017	26.80	1960.41	1879.03
2/5/2018	27.90	2022.62	1973.79
5/18/2018	28.70	2058.97	1989.43
6/4/2018	28.70	2044.40	1968.75
6/18/2018	28.47	2034.43	1958.82

Appendix 2 Discrete sample uncertainty. 2015-2016 discrete sample uncertainty determined through comparison of triplicate collected 250 mL in situ *discrete samples analyzed at Institute of Ocean Sciences. 2016-2017 discrete sample uncertainty determined through inter-lab comparison between 125 mL samples analyzed at the University of Calgary, and 250 mL bottles analyzed at Institute of Ocean Sciences. 2017-2018 discrete sample uncertainty determined through comparison of triplicate collected 125 mL* in situ *discrete samples analyzed at the University of Calgary.*

	Uncertainty in DIC [µmol/kg]	**Uncertainty in TA [µmol/kg]**	**Uncertainty in pK_1 pK_2 (Lueker et al., 2000)**	**Uncertainty in pCO_{2sys} [µatm]**	**Uncertainty in pH_{sys} [pH units]**
2015-2016	1.5	4.9	1.9%	14.51	0.0134
2016-2017	13.40	11.13	>1.9%	10.60	0.0086
2017-2018	3.7	3.1	1.9%	2.73	0.0024

Appendix 3 Mean and standard deviation (where applicable) difference between final multi-point in situ calibration corrected carbon system sensor time-series data and raw factory single-point calibrated carbon system sensor time-series data.

	ΔpH SeaFET|INT [pH units]	**ΔpH SeaFET|EXT [pH units]**	**ΔpCO_2 CO2-Pro [µatm]**
2015-2016	NA	NA	14.95
2016-2017	0.0591±0.0016	-0.0016±0.0129	-24.56
2017-2018	0.0288±0.0015	-0.0028±0.0134	-88.25

ELSEVIER LICENSE
TERMS AND CONDITIONS

Apr 26, 2019

This Agreement between University of Calgary ("You") and Elsevier ("Elsevier") consists of your license details and the terms and conditions provided by Elsevier and Copyright Clearance Center.

License Number	4576571432104
License date	Apr 26, 2019
Licensed Content Publisher	Elsevier
Licensed Content Publication	Elsevier Books
Licensed Content Title	Elsevier Oceanography Series
Licensed Content Author	Richard E. Zeebe
Licensed Content Date	Jan 1, 2001
Licensed Content Pages	84
Start Page	1
End Page	84
Type of Use	reuse in a thesis/dissertation
Intended publisher of new work	other
Portion	figures/tables/illustrations
Number of figures/tables/illustrations	1
Format	both print and electronic
Are you the author of this Elsevier chapter?	No
Will you be translating?	No
Original figure numbers	Figure 1.1.3 Effect of various processes on DIC and TA.
Title of your thesis/dissertation	Describing Seasonal Marine Carbon System Processes in Cambridge Bay Nunavut using an Innovative Sensor Platform
Expected completion date	Jun 2019
Estimated size (number of pages)	146
Requestor Location	University of Calgary 2500 University Drive NW Calgary, AB T2N 1N4 Canada Attn: University of Calgary
Publisher Tax ID	GB 494 6272 12
Total	0.00 USD
Terms and Conditions	

INTRODUCTION

1. The publisher for this copyrighted material is Elsevier. By clicking "accept" in connection with completing this licensing transaction, you agree that the following terms and conditions apply to this transaction (along with the Billing and Payment terms and conditions established by Copyright Clearance Center, Inc. ("CCC"), at the time that you opened your Rightslink account and that are available at any time at http://myaccount.copyright.com).

GENERAL TERMS

2. Elsevier hereby grants you permission to reproduce the aforementioned material subject to the terms and conditions indicated.

3. Acknowledgement: If any part of the material to be used (for example, figures) has appeared in our publication with credit or acknowledgement to another source, permission must also be sought from that source. If such permission is not obtained then that material may not be included in your publication/copies. Suitable acknowledgement to the source must be made, either as a footnote or in a reference list at the end of your publication, as follows:

"Reprinted from Publication title, Vol /edition number, Author(s), Title of article / title of chapter, Pages No., Copyright (Year), with permission from Elsevier [OR APPLICABLE SOCIETY COPYRIGHT OWNER]." Also Lancet special credit - "Reprinted from The Lancet, Vol. number, Author(s), Title of article, Pages No., Copyright (Year), with permission from Elsevier."

4. Reproduction of this material is confined to the purpose and/or media for which permission is hereby given.

5. Altering/Modifying Material: Not Permitted. However figures and illustrations may be altered/adapted minimally to serve your work. Any other abbreviations, additions, deletions and/or any other alterations shall be made only with prior written authorization of Elsevier Ltd. (Please contact Elsevier at permissions@elsevier.com). No modifications can be made to any Lancet figures/tables and they must be reproduced in full.

6. If the permission fee for the requested use of our material is waived in this instance, please be advised that your future requests for Elsevier materials may attract a fee.

7. Reservation of Rights: Publisher reserves all rights not specifically granted in the combination of (i) the license details provided by you and accepted in the course of this licensing transaction, (ii) these terms and conditions and (iii) CCC's Billing and Payment terms and conditions.

8. License Contingent Upon Payment: While you may exercise the rights licensed immediately upon issuance of the license at the end of the licensing process for the transaction, provided that you have disclosed complete and accurate details of your proposed use, no license is finally effective unless and until full payment is received from you (either by publisher or by CCC) as provided in CCC's Billing and Payment terms and conditions. If full payment is not received on a timely basis, then any license preliminarily granted shall be deemed automatically revoked and shall be void as if never granted. Further, in the event that you breach any of these terms and conditions or any of CCC's Billing and Payment terms and conditions, the license is automatically revoked and shall be void as if never granted. Use of materials as described in a revoked license, as well as any use of the materials beyond the scope of an unrevoked license, may constitute copyright infringement and publisher reserves the right to take any and all action to protect its copyright in the materials.

9. Warranties: Publisher makes no representations or warranties with respect to the licensed material.

10. Indemnity: You hereby indemnify and agree to hold harmless publisher and CCC, and their respective officers, directors, employees and agents, from and against any and all claims arising out of your use of the licensed material other than as specifically authorized pursuant to this license.

11. No Transfer of License: This license is personal to you and may not be sublicensed, assigned, or transferred by you to any other person without publisher's written permission.

12. No Amendment Except in Writing: This license may not be amended except in a writing signed by both parties (or, in the case of publisher, by CCC on publisher's behalf).
13. Objection to Contrary Terms: Publisher hereby objects to any terms contained in any purchase order, acknowledgment, check endorsement or other writing prepared by you, which terms are inconsistent with these terms and conditions or CCC's Billing and Payment terms and conditions. These terms and conditions, together with CCC's Billing and Payment terms and conditions (which are incorporated herein), comprise the entire agreement between you and publisher (and CCC) concerning this licensing transaction. In the event of any conflict between your obligations established by these terms and conditions and those established by CCC's Billing and Payment terms and conditions, these terms and conditions shall control.
14. Revocation: Elsevier or Copyright Clearance Center may deny the permissions described in this License at their sole discretion, for any reason or no reason, with a full refund payable to you. Notice of such denial will be made using the contact information provided by you. Failure to receive such notice will not alter or invalidate the denial. In no event will Elsevier or Copyright Clearance Center be responsible or liable for any costs, expenses or damage incurred by you as a result of a denial of your permission request, other than a refund of the amount(s) paid by you to Elsevier and/or Copyright Clearance Center for denied permissions.

LIMITED LICENSE

The following terms and conditions apply only to specific license types:
15. **Translation**: This permission is granted for non-exclusive world **English** rights only unless your license was granted for translation rights. If you licensed translation rights you may only translate this content into the languages you requested. A professional translator must perform all translations and reproduce the content word for word preserving the integrity of the article.
16. **Posting licensed content on any Website**: The following terms and conditions apply as follows: Licensing material from an Elsevier journal: All content posted to the web site must maintain the copyright information line on the bottom of each image; A hyper-text must be included to the Homepage of the journal from which you are licensing at http://www.sciencedirect.com/science/journal/xxxxx or the Elsevier homepage for books at http://www.elsevier.com; Central Storage: This license does not include permission for a scanned version of the material to be stored in a central repository such as that provided by Heron/XanEdu.
Licensing material from an Elsevier book: A hyper-text link must be included to the Elsevier homepage at http://www.elsevier.com . All content posted to the web site must maintain the copyright information line on the bottom of each image.

Posting licensed content on Electronic reserve: In addition to the above the following clauses are applicable: The web site must be password-protected and made available only to bona fide students registered on a relevant course. This permission is granted for 1 year only. You may obtain a new license for future website posting.
17. **For journal authors:** the following clauses are applicable in addition to the above:
Preprints:
A preprint is an author's own write-up of research results and analysis, it has not been peer-reviewed, nor has it had any other value added to it by a publisher (such as formatting, copyright, technical enhancement etc.).
Authors can share their preprints anywhere at any time. Preprints should not be added to or enhanced in any way in order to appear more like, or to substitute for, the final versions of articles however authors can update their preprints on arXiv or RePEc with their Accepted Author Manuscript (see below).
If accepted for publication, we encourage authors to link from the preprint to their formal publication via its DOI. Millions of researchers have access to the formal publications on ScienceDirect, and so links will help users to find, access, cite and use the best available

version. Please note that Cell Press, The Lancet and some society-owned have different preprint policies. Information on these policies is available on the journal homepage.
Accepted Author Manuscripts: An accepted author manuscript is the manuscript of an article that has been accepted for publication and which typically includes author-incorporated changes suggested during submission, peer review and editor-author communications.
Authors can share their accepted author manuscript:

- immediately
  - via their non-commercial person homepage or blog
  - by updating a preprint in arXiv or RePEc with the accepted manuscript
  - via their research institute or institutional repository for internal institutional uses or as part of an invitation-only research collaboration work-group
  - directly by providing copies to their students or to research collaborators for their personal use
  - for private scholarly sharing as part of an invitation-only work group on commercial sites with which Elsevier has an agreement
- After the embargo period
  - via non-commercial hosting platforms such as their institutional repository
  - via commercial sites with which Elsevier has an agreement

In all cases accepted manuscripts should:

- link to the formal publication via its DOI
- bear a CC-BY-NC-ND license - this is easy to do
- if aggregated with other manuscripts, for example in a repository or other site, be shared in alignment with our hosting policy not be added to or enhanced in any way to appear more like, or to substitute for, the published journal article.

Published journal article (JPA): A published journal article (PJA) is the definitive final record of published research that appears or will appear in the journal and embodies all value-adding publishing activities including peer review co-ordination, copy-editing, formatting, (if relevant) pagination and online enrichment.
Policies for sharing publishing journal articles differ for subscription and gold open access articles:
Subscription Articles: If you are an author, please share a link to your article rather than the full-text. Millions of researchers have access to the formal publications on ScienceDirect, and so links will help your users to find, access, cite, and use the best available version.
Theses and dissertations which contain embedded PJAs as part of the formal submission can be posted publicly by the awarding institution with DOI links back to the formal publications on ScienceDirect.
If you are affiliated with a library that subscribes to ScienceDirect you have additional private sharing rights for others' research accessed under that agreement. This includes use for classroom teaching and internal training at the institution (including use in course packs and courseware programs), and inclusion of the article for grant funding purposes.
Gold Open Access Articles: May be shared according to the author-selected end-user license and should contain a CrossMark logo, the end user license, and a DOI link to the formal publication on ScienceDirect.
Please refer to Elsevier's posting policy for further information.
18. **For book authors** the following clauses are applicable in addition to the above:
Authors are permitted to place a brief summary of their work online only. You are not allowed to download and post the published electronic version of your chapter, nor may you scan the printed edition to create an electronic version. **Posting to a repository:** Authors are permitted to post a summary of their chapter only in their institution's repository.

19. **Thesis/Dissertation**: If your license is for use in a thesis/dissertation your thesis may be submitted to your institution in either print or electronic form. Should your thesis be published commercially, please reapply for permission. These requirements include permission for the Library and Archives of Canada to supply single copies, on demand, of the complete thesis and include permission for Proquest/UMI to supply single copies, on demand, of the complete thesis. Should your thesis be published commercially, please reapply for permission. Theses and dissertations which contain embedded PJAs as part of the formal submission can be posted publicly by the awarding institution with DOI links back to the formal publications on ScienceDirect.

Elsevier Open Access Terms and Conditions

You can publish open access with Elsevier in hundreds of open access journals or in nearly 2000 established subscription journals that support open access publishing. Permitted third party re-use of these open access articles is defined by the author's choice of Creative Commons user license. See our open access license policy for more information.

Terms & Conditions applicable to all Open Access articles published with Elsevier:

Any reuse of the article must not represent the author as endorsing the adaptation of the article nor should the article be modified in such a way as to damage the author's honour or reputation. If any changes have been made, such changes must be clearly indicated.

The author(s) must be appropriately credited and we ask that you include the end user license and a DOI link to the formal publication on ScienceDirect.

If any part of the material to be used (for example, figures) has appeared in our publication with credit or acknowledgement to another source it is the responsibility of the user to ensure their reuse complies with the terms and conditions determined by the rights holder.

Additional Terms & Conditions applicable to each Creative Commons user license:

CC BY: The CC-BY license allows users to copy, to create extracts, abstracts and new works from the Article, to alter and revise the Article and to make commercial use of the Article (including reuse and/or resale of the Article by commercial entities), provided the user gives appropriate credit (with a link to the formal publication through the relevant DOI), provides a link to the license, indicates if changes were made and the licensor is not represented as endorsing the use made of the work. The full details of the license are available at http://creativecommons.org/licenses/by/4.0.

CC BY NC SA: The CC BY-NC-SA license allows users to copy, to create extracts, abstracts and new works from the Article, to alter and revise the Article, provided this is not done for commercial purposes, and that the user gives appropriate credit (with a link to the formal publication through the relevant DOI), provides a link to the license, indicates if changes were made and the licensor is not represented as endorsing the use made of the work. Further, any new works must be made available on the same conditions. The full details of the license are available at http://creativecommons.org/licenses/by-nc-sa/4.0.

CC BY NC ND: The CC BY-NC-ND license allows users to copy and distribute the Article, provided this is not done for commercial purposes and further does not permit distribution of the Article if it is changed or edited in any way, and provided the user gives appropriate credit (with a link to the formal publication through the relevant DOI), provides a link to the license, and that the licensor is not represented as endorsing the use made of the work. The full details of the license are available at http://creativecommons.org/licenses/by-nc-nd/4.0.

Any commercial reuse of Open Access articles published with a CC BY NC SA or CC BY NC ND license requires permission from Elsevier and will be subject to a fee.

Commercial reuse includes:

- Associating advertising with the full text of the Article
- Charging fees for document delivery or access
- Article aggregation
- Systematic distribution via e-mail lists or share buttons

Posting or linking by commercial companies for use by customers of those companies.

20. **Other Conditions**:

v1.9

Questions? customercare@copyright.com or +1-855-239-3415 (toll free in the US) or +1-978-646-2777.

ELSEVIER LICENSE TERMS AND CONDITIONS

Apr 26, 2019

This Agreement between University of Calgary ("You") and Elsevier ("Elsevier") consists of your license details and the terms and conditions provided by Elsevier and Copyright Clearance Center.

License Number	4576580268387
License date	Apr 26, 2019
Licensed Content Publisher	Elsevier
Licensed Content Publication	Deep Sea Research Part I: Oceanographic Research Papers
Licensed Content Title	Carbon-13 constraints on the seasonal inorganic carbon budget at the BATS site in the northwestern Sargasso Sea
Licensed Content Author	Nicolas Gruber,Charles D Keeling,Thomas F Stocker
Licensed Content Date	Apr 1, 1998
Licensed Content Volume	45
Licensed Content Issue	4-5
Licensed Content Pages	45
Start Page	673
End Page	717
Type of Use	reuse in a thesis/dissertation
Intended publisher of new work	other
Portion	figures/tables/illustrations
Number of figures/tables/illustrations	1
Format	both print and electronic
Are you the author of this Elsevier article?	No
Will you be translating?	No
Original figure numbers	Fig. 2. Schematic representation of the one-dimensional, two box ocean model employed in the diagnostic study of the seasonal carbon cycle at station BATS near Bermuda.
Title of your thesis/dissertation	Describing Seasonal Marine Carbon System Processes in Cambridge Bay Nunavut using an Innovative Sensor Platform
Expected completion date	Jun 2019
Estimated size (number of pages)	146
Requestor Location	University of Calgary 2500 University Drive NW Calgary, AB T2N 1N4 Canada Attn: University of Calgary

Publisher Tax ID	GB 494 6272 12
Total	0.00 USD

Terms and Conditions

INTRODUCTION

1. The publisher for this copyrighted material is Elsevier. By clicking "accept" in connection with completing this licensing transaction, you agree that the following terms and conditions apply to this transaction (along with the Billing and Payment terms and conditions established by Copyright Clearance Center, Inc. ("CCC"), at the time that you opened your Rightslink account and that are available at any time at http://myaccount.copyright.com).

GENERAL TERMS

2. Elsevier hereby grants you permission to reproduce the aforementioned material subject to the terms and conditions indicated.
3. Acknowledgement: If any part of the material to be used (for example, figures) has appeared in our publication with credit or acknowledgement to another source, permission must also be sought from that source. If such permission is not obtained then that material may not be included in your publication/copies. Suitable acknowledgement to the source must be made, either as a footnote or in a reference list at the end of your publication, as follows:
"Reprinted from Publication title, Vol /edition number, Author(s), Title of article / title of chapter, Pages No., Copyright (Year), with permission from Elsevier [OR APPLICABLE SOCIETY COPYRIGHT OWNER]." Also Lancet special credit - "Reprinted from The Lancet, Vol. number, Author(s), Title of article, Pages No., Copyright (Year), with permission from Elsevier."
4. Reproduction of this material is confined to the purpose and/or media for which permission is hereby given.
5. Altering/Modifying Material: Not Permitted. However figures and illustrations may be altered/adapted minimally to serve your work. Any other abbreviations, additions, deletions and/or any other alterations shall be made only with prior written authorization of Elsevier Ltd. (Please contact Elsevier at permissions@elsevier.com). No modifications can be made to any Lancet figures/tables and they must be reproduced in full.
6. If the permission fee for the requested use of our material is waived in this instance, please be advised that your future requests for Elsevier materials may attract a fee.
7. Reservation of Rights: Publisher reserves all rights not specifically granted in the combination of (i) the license details provided by you and accepted in the course of this licensing transaction, (ii) these terms and conditions and (iii) CCC's Billing and Payment terms and conditions.
8. License Contingent Upon Payment: While you may exercise the rights licensed immediately upon issuance of the license at the end of the licensing process for the transaction, provided that you have disclosed complete and accurate details of your proposed use, no license is finally effective unless and until full payment is received from you (either by publisher or by CCC) as provided in CCC's Billing and Payment terms and conditions. If full payment is not received on a timely basis, then any license preliminarily granted shall be deemed automatically revoked and shall be void as if never granted. Further, in the event that you breach any of these terms and conditions or any of CCC's Billing and Payment terms and conditions, the license is automatically revoked and shall be void as if never granted. Use of materials as described in a revoked license, as well as any use of the materials beyond the scope of an unrevoked license, may constitute copyright infringement and publisher reserves the right to take any and all action to protect its copyright in the materials.
9. Warranties: Publisher makes no representations or warranties with respect to the licensed material.
10. Indemnity: You hereby indemnify and agree to hold harmless publisher and CCC, and their respective officers, directors, employees and agents, from and against any and all

claims arising out of your use of the licensed material other than as specifically authorized pursuant to this license.
11. No Transfer of License: This license is personal to you and may not be sublicensed, assigned, or transferred by you to any other person without publisher's written permission.
12. No Amendment Except in Writing: This license may not be amended except in a writing signed by both parties (or, in the case of publisher, by CCC on publisher's behalf).
13. Objection to Contrary Terms: Publisher hereby objects to any terms contained in any purchase order, acknowledgment, check endorsement or other writing prepared by you, which terms are inconsistent with these terms and conditions or CCC's Billing and Payment terms and conditions. These terms and conditions, together with CCC's Billing and Payment terms and conditions (which are incorporated herein), comprise the entire agreement between you and publisher (and CCC) concerning this licensing transaction. In the event of any conflict between your obligations established by these terms and conditions and those established by CCC's Billing and Payment terms and conditions, these terms and conditions shall control.
14. Revocation: Elsevier or Copyright Clearance Center may deny the permissions described in this License at their sole discretion, for any reason or no reason, with a full refund payable to you. Notice of such denial will be made using the contact information provided by you. Failure to receive such notice will not alter or invalidate the denial. In no event will Elsevier or Copyright Clearance Center be responsible or liable for any costs, expenses or damage incurred by you as a result of a denial of your permission request, other than a refund of the amount(s) paid by you to Elsevier and/or Copyright Clearance Center for denied permissions.

LIMITED LICENSE

The following terms and conditions apply only to specific license types:
15. **Translation**: This permission is granted for non-exclusive world **English** rights only unless your license was granted for translation rights. If you licensed translation rights you may only translate this content into the languages you requested. A professional translator must perform all translations and reproduce the content word for word preserving the integrity of the article.
16. **Posting licensed content on any Website**: The following terms and conditions apply as follows: Licensing material from an Elsevier journal: All content posted to the web site must maintain the copyright information line on the bottom of each image; A hyper-text must be included to the Homepage of the journal from which you are licensing at http://www.sciencedirect.com/science/journal/xxxxx or the Elsevier homepage for books at http://www.elsevier.com; Central Storage: This license does not include permission for a scanned version of the material to be stored in a central repository such as that provided by Heron/XanEdu.
Licensing material from an Elsevier book: A hyper-text link must be included to the Elsevier homepage at http://www.elsevier.com . All content posted to the web site must maintain the copyright information line on the bottom of each image.

Posting licensed content on Electronic reserve: In addition to the above the following clauses are applicable: The web site must be password-protected and made available only to bona fide students registered on a relevant course. This permission is granted for 1 year only. You may obtain a new license for future website posting.
17. **For journal authors:** the following clauses are applicable in addition to the above:
Preprints:
A preprint is an author's own write-up of research results and analysis, it has not been peer-reviewed, nor has it had any other value added to it by a publisher (such as formatting, copyright, technical enhancement etc.).
Authors can share their preprints anywhere at any time. Preprints should not be added to or enhanced in any way in order to appear more like, or to substitute for, the final versions of

articles however authors can update their preprints on arXiv or RePEc with their Accepted Author Manuscript (see below).
If accepted for publication, we encourage authors to link from the preprint to their formal publication via its DOI. Millions of researchers have access to the formal publications on ScienceDirect, and so links will help users to find, access, cite and use the best available version. Please note that Cell Press, The Lancet and some society-owned have different preprint policies. Information on these policies is available on the journal homepage.
Accepted Author Manuscripts: An accepted author manuscript is the manuscript of an article that has been accepted for publication and which typically includes author-incorporated changes suggested during submission, peer review and editor-author communications.
Authors can share their accepted author manuscript:

- immediately
  - via their non-commercial person homepage or blog
  - by updating a preprint in arXiv or RePEc with the accepted manuscript
  - via their research institute or institutional repository for internal institutional uses or as part of an invitation-only research collaboration work-group
  - directly by providing copies to their students or to research collaborators for their personal use
  - for private scholarly sharing as part of an invitation-only work group on commercial sites with which Elsevier has an agreement
- After the embargo period
  - via non-commercial hosting platforms such as their institutional repository
  - via commercial sites with which Elsevier has an agreement

In all cases accepted manuscripts should:

- link to the formal publication via its DOI
- bear a CC-BY-NC-ND license - this is easy to do
- if aggregated with other manuscripts, for example in a repository or other site, be shared in alignment with our hosting policy not be added to or enhanced in any way to appear more like, or to substitute for, the published journal article.

Published journal article (JPA): A published journal article (PJA) is the definitive final record of published research that appears or will appear in the journal and embodies all value-adding publishing activities including peer review co-ordination, copy-editing, formatting, (if relevant) pagination and online enrichment.
Policies for sharing publishing journal articles differ for subscription and gold open access articles:
Subscription Articles: If you are an author, please share a link to your article rather than the full-text. Millions of researchers have access to the formal publications on ScienceDirect, and so links will help your users to find, access, cite, and use the best available version.
Theses and dissertations which contain embedded PJAs as part of the formal submission can be posted publicly by the awarding institution with DOI links back to the formal publications on ScienceDirect.
If you are affiliated with a library that subscribes to ScienceDirect you have additional private sharing rights for others' research accessed under that agreement. This includes use for classroom teaching and internal training at the institution (including use in course packs and courseware programs), and inclusion of the article for grant funding purposes.
Gold Open Access Articles: May be shared according to the author-selected end-user license and should contain a CrossMark logo, the end user license, and a DOI link to the formal publication on ScienceDirect.
Please refer to Elsevier's posting policy for further information.

18. **For book authors** the following clauses are applicable in addition to the above: Authors are permitted to place a brief summary of their work online only. You are not allowed to download and post the published electronic version of your chapter, nor may you scan the printed edition to create an electronic version. **Posting to a repository:** Authors are permitted to post a summary of their chapter only in their institution's repository.
19. **Thesis/Dissertation**: If your license is for use in a thesis/dissertation your thesis may be submitted to your institution in either print or electronic form. Should your thesis be published commercially, please reapply for permission. These requirements include permission for the Library and Archives of Canada to supply single copies, on demand, of the complete thesis and include permission for Proquest/UMI to supply single copies, on demand, of the complete thesis. Should your thesis be published commercially, please reapply for permission. Theses and dissertations which contain embedded PJAs as part of the formal submission can be posted publicly by the awarding institution with DOI links back to the formal publications on ScienceDirect.

Elsevier Open Access Terms and Conditions

You can publish open access with Elsevier in hundreds of open access journals or in nearly 2000 established subscription journals that support open access publishing. Permitted third party re-use of these open access articles is defined by the author's choice of Creative Commons user license. See our open access license policy for more information.

Terms & Conditions applicable to all Open Access articles published with Elsevier:

Any reuse of the article must not represent the author as endorsing the adaptation of the article nor should the article be modified in such a way as to damage the author's honour or reputation. If any changes have been made, such changes must be clearly indicated.

The author(s) must be appropriately credited and we ask that you include the end user license and a DOI link to the formal publication on ScienceDirect.

If any part of the material to be used (for example, figures) has appeared in our publication with credit or acknowledgement to another source it is the responsibility of the user to ensure their reuse complies with the terms and conditions determined by the rights holder.

Additional Terms & Conditions applicable to each Creative Commons user license:

CC BY: The CC-BY license allows users to copy, to create extracts, abstracts and new works from the Article, to alter and revise the Article and to make commercial use of the Article (including reuse and/or resale of the Article by commercial entities), provided the user gives appropriate credit (with a link to the formal publication through the relevant DOI), provides a link to the license, indicates if changes were made and the licensor is not represented as endorsing the use made of the work. The full details of the license are available at http://creativecommons.org/licenses/by/4.0.

CC BY NC SA: The CC BY-NC-SA license allows users to copy, to create extracts, abstracts and new works from the Article, to alter and revise the Article, provided this is not done for commercial purposes, and that the user gives appropriate credit (with a link to the formal publication through the relevant DOI), provides a link to the license, indicates if changes were made and the licensor is not represented as endorsing the use made of the work. Further, any new works must be made available on the same conditions. The full details of the license are available at http://creativecommons.org/licenses/by-nc-sa/4.0.

CC BY NC ND: The CC BY-NC-ND license allows users to copy and distribute the Article, provided this is not done for commercial purposes and further does not permit distribution of the Article if it is changed or edited in any way, and provided the user gives appropriate credit (with a link to the formal publication through the relevant DOI), provides a link to the license, and that the licensor is not represented as endorsing the use made of the work. The full details of the license are available at http://creativecommons.org/licenses/by-nc-nd/4.0.

Any commercial reuse of Open Access articles published with a CC BY NC SA or CC BY NC ND license requires permission from Elsevier and will be subject to a fee.

Commercial reuse includes:

- Associating advertising with the full text of the Article
- Charging fees for document delivery or access
- Article aggregation
- Systematic distribution via e-mail lists or share buttons

Posting or linking by commercial companies for use by customers of those companies.

20. **Other Conditions**:

v1.9